Investigating cellular responses to growth factors presentation with a biomimetic approach

Elisa Migliorini

Université Grenoble Alpes
Ecole Doctorale ISCE

Demande d'Habilitation à Diriger des Recherches

présentée par

Elisa Migliorini, PhD

Chercheur CNRS

Investigating cellular responses to growth factors presentation with a biomimetic approach

soutenue le 15 décembre 2023 devant le jury composé de

Dr. Philippe LAVALLE (Directeur INSERM, Université de Strasbourg)	rapporteur
Prof. Gerhard SENGLE (Université de Cologne, Allemagne)	rapporteur
Dr Stephanie DESCROIX (Directeur CNRS, Institute Curie, Paris)	rapporteuse
Dr. Hugues LORTAT JACOB (Directeur CNRS, IBS, Grenoble)	examinateur
Dr. Delphine DEBARRE (Chercheur CNRS, Liphy, Grenoble)	examinatrice
Dr. Karine ANSELME (Directeur CNRS, Institut de Science des Matériaux de Mulhouse)	examinatrice

Équipe CNRS EMR 5000 Biomimetism and Regenerative Medicine (BRM), INSERM U1292 Biosanté

Institut de Recherche Interdisciplinaire de Grenoble (IRIG)

Centre CEA de Grenoble

Contents

ABBREVIATION TABLE

b-Atto : biotin-Atto565

b-HS: biotinylated heparan sulfate

b-BMP2: biotinylated bone morphogenetic protein 2

BLI: bio-layer interpherometry

BMP: bone morphogenetic protein

CHO WT cells: Chinese hamster ovary wild-type cells

CHO HS KO: CHO pgsD-677 lacking the EXT1 enzyme responsible for HS chain elongation

CHO CS/HS KO: pgsA-745 lacking the xylotransferase responsible for catalyzing the first sugar transfer in GAG synthesis

CS: chondroitin sulfate

cRAD: cyclic arginine-alanine-aspartic acid

cRGD: cyclic arginine-glycin-aspartic acid

DS: dermatan sulfate

EXT-1, EXT-2: glycosyltransfserases of the exostin family

FGF: fibroblast growth factor

fl-SAv: SAv-Atto565

GAGs: glycosaminoglycans

HA: hyaluronic acid

HS-dps: HS-derived oligosaccharides with a degree of polymerization

hMSCs : primary human mesenchymal stromal cells

iBMP2: immobilized/biotinylated BMP2

ICAM-1: intercellular adhesion molecule 1

IFNγ : Interferon γ

iHH: indian hedgehog

iHS: immobilized/biotinylated heparan sulfate

iPEG: biotinylated PEG

SAv: streptavidin

SAv-Atto565: streptavidin labeled with the Atto565 fluorophore

SAv-Alexa: streptavidin Alexa 555

SLB : supported lipid bilayer

PEG: poly-ethylen-glycol

QCM-D: quartz crystal microbalance with dissipation monitoring

SE: spectroscopic ellipsometry

CURRICULUM VITAE

Personal details	
Name and first name:	Migliorini Elisa
Personal Webpage :	https://biosante-lab.fr/en/Pages/BRM/migliorini-elisa.aspx

Current position[1]

Since 2017- CNRS researcher (section 11), in 2020 changed affectation from LMGP, Grenoble-INP, UMR 5628 to **Biosanté U1292 (UGA, INSERM, CEA), équipe EMR BRM 5000 CNRS**, 38016 Grenoble

Previous positions

2015–2017 Marie-Curie postdoc fellow at Max Planck Institute for intelligent system, Stuttgart, Germany

2014–2015 Postdoc, CIC biomaGUNE, San Sebastian, Spain

2012–2014 Postdoc, Département de chimie moléculaire UGA, Grenoble, France (Fondation Nanosciences)

2009–2012 PhD, IOM-CNR, Trieste, Italy

Education

2009–2012: PhD in nanotechnology at Trieste University, Italy

2010–2011: MCA-SISSA, master in complex actions, Italy

2006–2008: Master in medical biotechnology, Trieste, Italy

2003–2006: Bachelor in medical biotechnology, Ferrara, Italy

Obtained Grants as coordinator

Period	Funding agency	Subject	Amounts
2022–2024	CEA_ Focus Organ on Chip	Development of metastatic trap on chip: “MetasTrap”:	120 k€

2022–2024	CNRS_International Exploratory Action (CNRS-IEA)	Polymer brushes carrying BMPs to drive osteogenic differentiation OsteoBrush Collaboration with Queen Mary University of London	30 k€
2021–2022	UGA_IRGA exploratory project	Engineering of platforms to mimic the elasticity and the chemical composition of the brain extracellular matrix	20 k€
2021–2024	Fondation recherche medicale (FRM)_maladie rares	Study of rare neuronal pathologies with biomimetic materials	PhD fellowship (120 k€)
2020–2024	ANR_PRCI with Germany	Deciphering the biophysical basis by which Glycosaminoglycans CONtrol growth factor signaling during development: a biomimetic approach: GlyCON	500 k€
2018–2021	UGA_IDEXIRS	Engineered Biomimetic platforms to analyse the molecular and cellular role of Heparan Sulfate on bone morphogenetic protein 2 bioactivity: BioPlat	160 k€
2015–2017	UE_ Marie Sklodowska-Curie Individual fellowship	Spatial nanoscale control of growth and adhesion factors to enhance the osteogenic differentiation of mesenchymal stem cells: Osteonano	200 k€
2015–2017	Heidelberg University_CellNetworks cluster	Same as Osteonano	30 k€

Other activities

SUPERVISION:

- **4 PhD students**. 2 graduated, 1 ongoing and one died in August 2023
- **2 Postdocs:** one finished in 2021 and one from 2022 to 2024
- **2 bachelor and 10 master students**

TEACHING:

- **Theoretical courses** of physical chemistry to Master 2 student and Engineering school PHELMA and **University of Grenoble Alps**.
- **Theoretical and practical courses** of biophysics to undergraduate molecular biology students at the **University of Heidelberg**

COLLECTIVE RESPONSABILITIES:

- Elected member of the Biosanté unit council
- HAL correspondent for Biosanté unit
- **Scientific responsible** of the axis Bioinspired Materials of the international research cluster (GDR) 2088 BIOMIM (CNRS)
- **Steering committee** of the CNRS organization “federation physique et vivant”
- **PhD defense jury** of Nathan LAGNEU (2022), Mathilde RODRIGUEZ (2023), Alexandre EPALLE (2023)
- Member of 5 individual **follow-up PhD committees** (CSI)
- **Reviewer** for Acta Biomaterialia, Biomaterials, Carbohydrate polymers, Bioengineering, Health Care Materials, Chinese Chemical Letters, Molecular Science, Materials Today, Colloid interfaces…
- Organizing committee of the Leeds-Grenoble workshop, 2021
- Organizing committee of the 10th NaMiECeB workshop 2017

MATERNITY LEAVES:

- March – September 2020
- January – May 2023

LIST OF THE SCIENTIFIC ARTICLES

Until now I have published 28 research articles,2 are under submission and one is in open access. 11 of them I wrote as first author, 5 as last author and 8 as corresponding author.
The publications from the CNRS CRCN position are written in green.
The ones from the postdoc positions in blue.
And the ones from the PhD position in pink.

PUBLISHED articles:

A.1 Sefkow-Werner J., Le Pennec J., Machillot P., Ndayishimiye B., Castro-Ramirez E., Lopes J., Licitra C., Wang I., Delon A., Picart C*., Migliorini. E*., Automated Fabrication of Streptavidin-Based Self-assembled Materials for High content Analysis of Cellular Response to Growth Factors. ACS Appl Mater. Interfaces. 2022. DOI: 10.1021/acsami.2c08272

A.2 Sefkow-Werner J., Migliorini E*., Picart C., Wahyuni D.,Wang I., Delon A*. Combining Fluorescence Fluctuations and Photobleaching to Quantify Surface Density. Anal. Chem Anal Chem. 2022 DOI: 10.1021/acs.analchem.1c05513

A.3 Sales, A., V. Khodr, P. Machillot, L. Chaar, L. Fourel, A. Guevara-Garcia, E. Migliorini, C. Albigès-Rizo and C. Picart. Differential bioactivity of four BMP-family members as function of biomaterial stiffness. Biomaterials 2022. DOI:10.1016/j.biomaterials.2022.121363

A.4 Khodr V., Machillot P., Migliorini E., Reiser J.P., Picart C. High-throughput measurements of bone morphogenetic protein/bone morphogenetic protein receptor interactions using biolayer interferometry. Biointerphases J. 2021. DOI: 10.1116/6.0000926.

A.5 Migliorini E, Cavalcanti-Adam E.A, Uva A.E, Fiorentino M, Gattullo M., Manghisi V.M, Vaiani L., Boccaccio A. Nanoindentation of mesenchymal stem cells using atomic force microscopy: effect of adhesive cell-substrate structures. Nanotechnology 2021. DOI: 10.1088/1361-6528/abe748

A.6 Vaiani L., Migliorini E., Cavalcanti-Adam E.A., Uva A.E., Fiorentino M., Gattullo M., Manghisi V.M., Boccaccio A. Coarse-grained elastic network modelling: A fast and stable numerical tool to characterize mesenchymal stem cells subjected to AFM nanoindentation measurements. MSEC. 2021. DOI: 10.1016/j.msec.2020.111860

A.7 Sefkow-Werner J.,Wang I., Picart C.,Migliorini E., Delon A. Photobleaching and correlation spectroscopy for in-situ quantification of multi-labelled molecules on surfaces 2021, Conference: Advances in Microscopic Imaging. DOI: 10.1117/12.2615697

A.8 Sefkow-Werner J., Machillot P., Sales A., Castro-Ramirez E., Degardin M., Boturyn D., Cavalcanti-Adam E.A., Albiges-Rizo C., Picart C.*, Migliorini E*. Heparan sulfate co-immobilized with cRGD ligands and BMP2 on biomimetic platforms promotes BMP2-mediated osteogenic differentiation. Acta Biomat. 2020. DOI:10.1016/j.actbio.2020.07.015

A.9 Migliorini E., Guevara-Garcia A., Albiges-Rizo C. and Picart C. Learning from BMPs and their biophysical extracellular matrix microenvironment for biomaterial design. Bone J. 2020. DOI: 10.1016/j.bone.2020.115540

A.10 Cavalcanti-Adam E.A. and Migliorini E. Comment on "Tuning the bioactivity of bone morphogenetic protein-2 with surface immobilization strategies" by Chen et al. Acta Biomat. 2019. DOI: 10.1016/j.actbio.2019.01.068

A.11 Migliorini E, Weidenhaupt M., Picart C. Practical guide to characterize biomolecule adsorption on solid surfaces (Review). Biointerphases J. 2018. DOI: 10.1116/1.5045122.

A.12 Migliorini E*, Horn P, Haraszti T, Wegner S.V, Hiepen C, Knaus P, Richter PR and Cavalcanti-Adam EA. Enhanced Biological Activity of BMP-2 Bound to Surface-Grafted Heparan Sulfate. Adv Biosys J. 2017. DOI: 10.1002/adbi.201600041

A.13 Thakar D, Dalonneau F, Migliorini E, Lortat-Jacob H, Boturyn D, Albiges-Rizo C, Coche-Guerente L, Picart C, Richter RP. Binding of the chemokine CXCL12α to its natural extracellular matrix ligand heparan sulfate enables myoblast adhesion and facilitates cell motility. Biomaterials. 2017. DOI: 10.1016/j.biomaterials

A.14 Dyer DP, Migliorini E, Salanga CL, Thakar D, Handel TM, Richter RP. Differential structural remodelling of heparan sulfate by chemokines: the role of chemokine oligomerization. Open Biol. 2017. DOI: 10.1098/rsob.160286

A.15 Migliorini E, Valat A, Picart C, Cavalcanti-Adam E.A. Tuning cellular responses to BMP-2 with material surfaces. CGFR Review. 2016 DOI: 10.1016/j.cytogfr.2015.11.008

A.16 Migliorini E, Thakar D, Kühnle J, Sadir R, Dyer DP, Li Y, Sun C, Volkman BF, Handel TM, Coche-Guerente L, Fernig DG, Lortat-Jacob H, Richter RP. Cytokines and growth factors cross-link heparan sulfate. Open Biol. 2015. DOI: 10.1098/rsob.150046.

A.17 Migliorini E, Thakar D, Sadir R, Pleiner T, Baleux F, Lortat-Jacob H, Coche-Guerente L, Richter RP. Well-defined biomimetic surfaces to characterize glycosaminoglycan-mediated interactions on the molecular, supramolecular and cellular levels. Biomaterials. 2014. DOI: 10.1016/j.biomaterials.2014.07.017

A.18 Thakar D, Migliorini E, Coche-Guerente L, Sadir R, Lortat-Jacob H, Boturyn D, Renaudet O, Labbe P, Richter RP. A quartz crystal microbalance method to study the terminal functionalization of glycosaminoglycans. Chem Commun. 2014 DOI: 10.1039/c4cc06905f

A.19 Andolfi L, Bourkoula E, Migliorini E, Palma A, Pucer A, Skrap M, Scoles G, Beltrami AP, Cesselli D, Lazzarino M. Investigation of adhesion and mechanical properties of human glioma cells by single cell force spectroscopy and atomic force microscopy Plos One 2014. DOI: 10.1371/journal.pone.0112582

A.20 Migliorini E*, Ban J, Grenci G, Andolfi L, Pozzato A, Tormen M, Torre V, Lazzarino M. Nanomechanics controls neuronal precursors adhesion and differentiation. Biotech and Bioeng. 2013. DOI: 10.1002/bit.24880

A.21 Lien TL, Ban J, Tormen M, Migliorini E, Grenci G, Pozzato A, Torre V. Can hippocampal neurites and growth cones climb over obstacles? PLoS One. 2013.

DOI: 10.1371/journal.pone.0073966

A.22 Amin L., Ercolini E, Shahapure R., Migliorini E. and Torre V. The role of membrane stiffness and actin turnover on the force exerted by DRG lamellipodia. Biophys J. 2012. doi: 10.1016/j.bpj.2012.04.036

A.23 Lasalvia M, Perna G, Mezzenga E, Migliorini E , Lazzarino M, L'Abbate N and Capozzi V. Atomic force microscopy investigation of morphological changes in living keratinocytes treated with HgCl(2) at not cytotoxic doses . J. of Micr. 2011. DOI: 10.1111/j.1365-2818.2010.03479

A.24 Migliorini E, Grenci G, Ban J, Pozzato A, Tormen M, Lazzarino M, Torre V, Ruaro ME. Acceleration of neuronal precursors differentiation induced by substrate nanotopography. Biotech and Bioeng. 2011. DOI: 10.1002/bit.23232

A.25 Migliorini E, Ban J, Di Foggia V, Ruaro ME, Torre V, Pozzato A, Grenci G, Tormen M, Lazzarino M. Eur Biophys .J. (Suppl 1) 2009. DOI: 10.1089/scd.2010.0217

A.26 Laishram J., Kondra S., Avossa D., Migliorini E., Lazzarino M., Torre V. A morphological analysis of growth cones of DRG neurons combining atomic force and confocal microscopy. Journal of Structural Biology. 2009. DOI: 10.1016/j.jsb.2009.09.005

A.27 Migliorini E, Ban J, Di Foggia V, Lazzarino M, Ruaro ME, Torre V. Fragmentation as a mechanism for growth cone pruning and degeneration. Stem Cells Dev. 2008 DOI: 10.1016/j.jneumeth.2008.09.034

A.28 Kondra S, Laishram J., J. Ban J.,Migliorini E., Di Foggia V., Lazzarino M., Torre V., Ruaro M.E. Integration of confocal and atomic force microscopy images; Journal of Neuroscience methods. 2009. DOI: 10.1016/j.jneumeth.2008.09.034

*****corresponding author

SUBMITTED publications:

S01 Le Pennec J, Picart C.*, Vivès R.R*, Migliorini E*. Sweet but challenging: tackling the complexity of GAGs with engineered tailor-made biomaterials. Review on Advanced Materials. Under second review

S02 Le Pennec J, Nevola P, Gout E, Machillot P, Friedel-Arboleas M, Picart C, Vortkamp A., Vivès R.R*, Migliorini E* Glycosaminoglycans exhibit distinct interactions and signaling with BMP2 according to their nature and localization. Carbohydrate polymers. Submitted

OPEN ACCESS papers

Op01 Le Pennec J, Guibert A, Vivès R.R*, Migliorini E*. BMP2 binds non-specifically to PEG-passivated biomaterials and induces substantial signaling. BioRxiv

COMMUNICATIONS at **international conferences**:

I took part in several international conferences during my career (at least one per year).The most important are:

- 13th annual conference of the European society for biomaterials: 4 – 8 September 2022, Bordeaux. ORAL presentation title: Automated fabrication of biomimetic platforms to present bone morphogenetic proteins
- Materials 2022: 18 – 20 April 2022, Boston. Hybrid meeting. ORAL INVITED presentation title: Biomimetic Approach to Investigate the Effect of Heparan Sulfate on BMP2-Mediated Osteogenic Differentiation
- INSERM workshop 256 GAG biology: 19 – 21 June 2019, Bordeaux. ORAL and POSTER presentation title: Biomimetic approach to investigate the effect of heparan sulfate on BMP2-mediated osteogenic differentiation
- 12th international BMP conference: 24 – 28 October 2018, Tokyo Japan. POSTER presentation title: Biomimetic approach to control BMP2¬–integrin crosstalk and the effect of heparan sulfate. Travel award
- 7 lake proteoglycan conference: 10 – 14 September 2017, Varese, Italy. ORAL and POSTER presentation title: Enhanced biological activity of BMP-2 bound to surface-grafted heparan sulfate. Best oral presentation price
- 11th international BMP conference: 26 – 30 October 2016, Boston USA. POSTER presentation title: Improving in vitro BMP-2 bioactivity with well-characterized biomimetic platforms
- FEBS advanced lecture: course “matrix pathology, signaling and molecular targets” 24 – 29 September 2015. Rhodes Island, Greece. POSTER presentation title: nanoscale control of growth factors to enhance osteogenic differentiation
- Proteoglycan meeting: 25 – 29 August 2014, Frankfurt, Germany. POSTER presentation title: Chemokines cross-link heparan sulfate. Poster prize
- FEBS meeting Biological surfaces and interfaces: 30 June – 05 July 2013. Sant Feliu de Guixols, Catalonia, Spain. POSTER title: Glycosaminoglycan-presenting surfaces to study lymphocyte trafficking during immune response
- Proteoglycan Gordon research seminar and conference: 05 – 11 July 2014. Andover NH, USA. ORAL and POSTER presentation title: Morphogens cross-link heparan sulfate. Best oral presentation: international Society for Matrix Biology Young Scientist
- European biophysical society meeting: 05 – 09 August 2011 Baltimore USA. POSTER presentation
- Tissue Engineering & Regenerative Medicine International Society: 7-11 June, 2011, Granada, Spain. ORAL presentation
- European biophysical society meeting: 11 – 15 July 2009, Genoa, Italy. POSTER presentation

SUPERVISION AND TEACHING

I have had the opportunity to supervise 4 PhD students since my CNRS position.

Julius Sefkow-Werner (defended in 2021) co-supervised with C. Picart,

Jean Le Pennec (defended in October 2023) co-supervised with Romain Vivès,

João Carlos (passed away in August 2023), co-supervised with C. Picart

Nathan Thibieroz (started in October 2023) co-direction with C. Picart

I am supervising a postdoc, Elisa Lambert who started in November 2022.

I have supervised several master students (10), other license students (2) and an engineer.

I am looking for funding to finance another PhD student next year to work on the continuation of the ANR GlyCON project and a postdoc to develop the 3D bone niche. To improve my supervision skills, I plan to follow trainings on “how to manage a team/a research project” and “ethical supervision of a PhD thesis”.

Regarding my teaching activities, in 2016 I gave theoretical and practical courses of biophysics to undergraduate students at the university of Heidelberg (20 hours)

Since 2017, I give theoretical courses (5 hours plus exams) of physical chemistry (QCM-D and ellipsometry) to Master 2 students and engineering school PHELMA at the University of Grenoble Alps.

ADMINISTRATIVE RESPONSABILITIES

In the last five years I have taken several responsibilities.

As coordinator of an ANR project I am in charge of writing reports, to control the financial reporting and to write and elaborate the data management plan.

I am one of the scientific animators of the GDR 2088 BIOMIM. In this context I animated monthly national webinars and, together with the other two scientific animators, we are organizing a summer school on biomimetic materials.

I am part of the steering committee of a "federation physique du vivant", a network of researcher at the interface between biology, chemistry and physics (120 researchers) which aims at promoting collaboration and scientific exchange between them in Grenoble. To this end, we have already organized two symposiums and we wrote a project that has been positively evaluated by CNRS, UGA and CEA.

I am one of the two elected members of the Biosanté Unit Council, so I represent all the researchers of the Biosanté Laboratory during the meetings of the Biosanté Unit Council.

I was part of the organization of several meetings such as the 10th NaMiECeB workshop 2017, the GDR BIOMIM annual meeting 2020, the University of Leeds – UGA online meeting in 2021.

I organize thematic meetings on BMPs at the Biosanté laboratory and I am the HAL correspondent for the laboratory. HAL is a web repository of scientific productions (papers, book chapters, theses...) where CNRS researchers (in particular) have to upload their papers and provide an open access version. My role is to help all Biosanté researchers to upload their work on HAL and to communicate any important information about the Open Access tools available at the University of Grenoble Alps.

I was part of the jury member of three PhD students of Nathan LAGNEU (2022), Mathilde RODRIGUEZ (2023), Alexandre EPALLE (2023) and member of 5 individual follow-up PhD committees.

I have reviewed several scientific articles on journals like Acta Biomaterialia, Biomaterials, Carbohydrate polymers, Bioengineering, Health Care Materials, Chinese Chemical Letters, Molecular Science, Materials Today, Colloid interfaces… with an average of one article per month.

REPORT ON THE SCIENTIFIC ACTIVITIES AFTER THE PHD

I have obtained my PhD degree in Italy at the University of Trieste in 2012. For that I worked at the **laboratory IOM-CNR** at the Area Science Park Trieste, under the supervision of Dr. **Marco Lazzarino** and in tight collaboration with the group of Vincent Torre at the SISSA institute in Trieste. I worked on the control of substrate stiffness and topography to guide neuronal differentiation. The same year I started my first **postdoc** under the supervision of Prof. **Ralf Richter** which was the PI of a chair of excellence project in Grenoble and a group leader at San Sebastian, Spain. In 2015 I have obtained a Marie-Sklodowska Curie individual fellowship to work on nanostructured materials with controlled chemical properties to enhance the osteogenic differentiation of stem cells. This work was done between the University of Heidelberg and the Max Planck Institute for Intelligent Systems in Stuttgart, Germany in the group of **Prof. Ada Cavalcanti** and **Prof. Joachim Spatz**. After that, I obtain the CNRS position in 2017 to work in the team of **Prof. Catherine Picart** on biomimetic materials to study BMP2 signaling.

The main objective of my scientific career is the study and the interpretation of the interface between cells and extracellular matrix (ECM). My research is multidisciplinary and is located in between physics, chemistry and biology. The *"file rouge"* connecting all my activities is the **biomimicry of the ECM by surface patterning and functionalization**, in such a way to guide and control cellular responses, in particular cellular differentiation. My research has been financed by fellowships and international grants and thanks to these funding I was able to enroll PhD students, master students and engineers in my group. In the following chapters, I describe the results obtained starting from my first postdoc position. Since I had the opportunity to follow my research and interests and to connect all my research activities from my first postdoc until now, I decided in this manuscript not to divide them on the base of the career positions but based on the scientific topics**.** For each scientific topic that is still under investigation, I present the perspectives for the coming years as well as the new directions of my research.

1. Biomimetic surfaces to interrogate glycosaminoglycan-mediated immune cell trafficking

PEOPLE INVOLVED: Dr. E. Migliorini, Mr. D. Thakar, Dr; R. Sadir, Prof. H. Lortat-Jacob, Dr. L. Guerente and Prof. R. P. Richter

FUNDING: Fondation Nanoscience "chair d'excellence" 2011-2014 (PI. Ralf Richter).

I joined the "chair of excellent project" directed by Dr. Ralf P. Richter and funded by Nanoscience Foundation (Grenoble, France) in 2012. This project was the result of a

collaboration between four different laboratories in Grenoble, including the group of Prof. Catherine Picart at LMGP.

During this postdoctoral project I developed new surface functionalization protocols and learned and applied surface sensitive techniques to quantify the adsorbed amount of molecules in a sample.

The aim of my project was to **develop** and to employ an ***in vitro* system as a platform for molecular and cellular studies**, able to mimic *in vivo* cues that are presented by the **blood vessel endothelium**. These cues elicit lymphocyte recruitment and activation during the immune response. The glycosaminoglycan heparan sulfate (HS), present at the cell surface of endothelial cells, is known to be fundamental to create a gradient of chemokines such as CXCL12α (Laguri, Sadir et al. 2007). To immobilize HS and other selected components of the blood vessel endothelium, such as cell adhesion ligands, two platforms were used: polyethylene glycol (PEG)-thiol monolayers on gold surfaces and supported lipid bilayers (SLBs) on silica surfaces **Figure *1*1**.

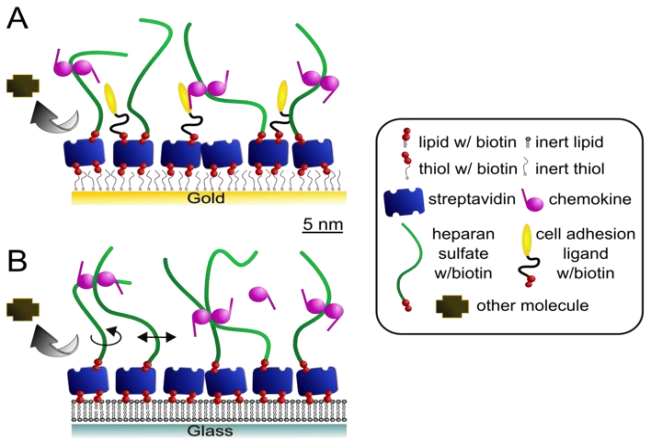

Figure 1: Design of biomimetic surfaces that reproduce the presentation of cell surface GAGs *(A17, A18).*

HS is biotinylated site-specifically at the reducing end (Thakar, Migliorini et al. 2014) and immobilized on a SAv monolayer with controlled orientation. a) Model surface based on a gold-supported PEG monolayer exposing biotin at the end of a fraction of the PEG molecules. Stable attachment to the gold is mediated by thiols. b) Model surface based on a silica-supported lipid bilayer (SLB) exposing biotin at the head of a fraction of the lipids.

Both platforms display biotin groups and thereby permit the stable binding of streptavidin (SAv) and the formation of a SAv monolayer. Gold platforms are based on a thin gold layer of 8 nm that is sputtered on glass surfaces with an evaporator machine in a clean room. The gold layer remains transparent so that the sputtered surface can be used as a standard glass coverslip for cellular culture and microscopy. Gold surfaces are passivated overnight by a mixture of thiol-PEG and thiol-PEG-biotin in a molar ratio of 95:5 on the top of which SAv forms a stable and fix monolayer. Biotin-functionalized supported lipid bilayers (SLBs) were prepared by the method of vesicle spreading through exposure of small unilamellar vesicles (SUVs) to glass surfaces. SUVs were prepared by sonication from mixtures of dioleoylphosphatidylcholine (DOPC) and dioleoylphosphatidylethanolamine-CAP-biotin (DOPE-CAP-b) in a molar ratio of 95:5, as previously described(van der Meulen, Dubacheva et al. 2014). The two platforms differ not only by the support but also since **SLBs molecules are laterally mobile on the contrary of PEG-thiol moieties that are stably bound to the gold**. On a SAv monolayer only biotinylated molecules can bind. In particular, to mimic the blood vessel endothelium, HS was grafted in an oriented manner on SAv

thanks to a site-specific biotinylation of its reducing end thanks to an oxime ligation as detailed in **A18** (Thakar, Migliorini et al. 2014). In this way, biotinylated HS (b-HS) is immobilized and oriented on SAv as on the core proteins of the proteoglycans. We used the chemokine CXCL12α (also known as SDF-1α) as a well-known chemoattractant for T-lymphocytes during the immune response.

SAv monolayer became a fundamental intermediate layer for all the following research projects that I pursued. The advantages of having this intermediate layer with respect to direct grafting of the molecules at the surface are multiples: (i) it is possible to graft on it all the desired biotinylated molecules or peptides (ii) biotin linkers are widely commercialized with different PEG spacers based on the needed application and several biotinylated molecules are already commercialized , (iii) it is possible to control the surface density of the biotinylated compounds since a limited number of free biotin pockets are available at the surface of the SAv and (iv) these platforms are compatible with surface sensitive techniques which permit the correct characterization of the adsorbed amount of molecules .

A specific control of the platforms functionalization is fundamental not only for the reproducibility of the results but also for the multiple information we can obtain, such as the binging kinetics of each molecule and their surface density. This characterization was done with surface sensitive techniques as we reviewed in **A11** (Migliorini, Weidenhaupt et al. 2018) such as quartz crystal microbalance with dissipation monitoring (**QCM-D**), spectroscopic ellipsometry (**SE**) and surface plasmon resonance (**SPR**). A brief explanation of these surface sensitives techniques is reported in ANNEX I: CHARACTERIZATION TECHNIQUES

1.1. Major scientific achievements

For this study, I have performed the majority of the experiments, wrote the first draft of the article and prepared the figures.

1.1.1. Several morphogens cross-link the heparan sulfate chains

By using these surface sensitive techniques, we tested the effect of several extracellular signaling molecules on HS model matrices, namely the α and γ isoforms of the chemokine CXCL12, the cytokine interferon-γ (IFNγ) and the growth factors fibroblast growth factor-2 (FGF-2) and FGF-9 (Migliorini, Thakar et al. 2015)(**A16**). These were selected based on their known affinity for HS and distinct structure of the HS binding-site. For that study we used SLB-coated glass platforms with a not-saturated monolayer of fluorescent SAv-Atto565 (fl-SAv) (**Figure 2A**). SAv molecules bound to the SLB were mobile, even with grafted biotinylated HS (b-HS) but they increased their immobile fraction upon HS cross-linking (**Figure 2C and D**).

We proved that CXCL12 α and γ, FGF-2 and in minor extend IFNγ but not FGF-9 cross-link HS film. The cross-linking has been proved by two complementary techniques: QCM-D and fluorescent recovery after photobleaching (FRAP) (**Figure 2**) (see ANNEX

I: CHARACTERIZATION TECHNIQUES). By QCM-D we measured the increased rigidity of the HS layer by applying the viscoelastic modelling (Domack, Prucker et al. 1997) which revealed a decrease in the elastic and viscous compliance upon chemokines binding which means film rigidification (data not shown). With the FRAP technique, we measured the time SAv needed to recover the fluorescence after bleaching. We proved that CXCL12α reduces the diffusion constant and the mobile fraction of fl-SAv carrying b-HS layer (**Figure 2a-d**).

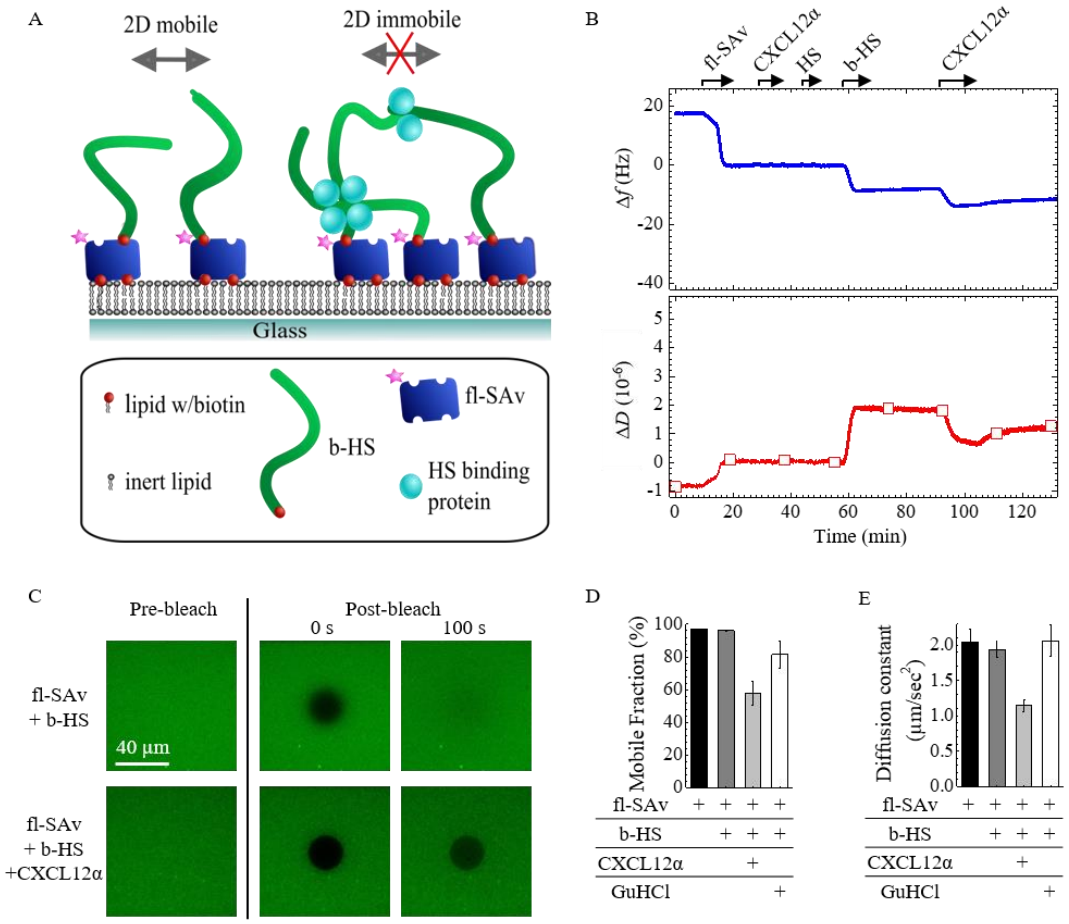

Figure 2: CXCL12a-mediated cross-linking of HS films. *a) Schematic representation of HS films used for FRAP experiments. b-HS, anchored to fl-SAv, can diffuse along the surface thanks to a fluid biotin-presenting supported lipid bilayer (left). Cross-linking, mediated by HS-binding proteins, is expected to lead to a reduction of HS (and hence SAv-Atto565) lateral mobility (right). b) Surface functionalization and CXCL12a binding followed by QCM-D. Start and duration of each incubation step with different samples are indicated by an arrow; during all other times, the surface was exposed to buffer. fl-SAv was incubated at 20 µg/ml until saturation; the low percentage of biotinylated lipids (0.5%) limits fl-SA binding to a sub-monolayer. CXCL12a (0.64 mM) and 50 µg/ml biotin-free HS produced no measurable response, confirming that the fluorescent label does not induce any non-specific binding. The QCM-D responses for b-HS (incubated at 50 µg/ml to saturation) and for CXCL12a (incubated at 0.64 mM) were comparable with the low-density HS films shown in figure 2b. c) Representative fluorescence micrographs demonstrating the FRAP assay to assess chemokine-mediated cross-linking. Recovery of the bleached spot is seen after 100 s for a bare HS film, but not for a CXCL12a-loaded HS film. d,e) Quantitative analysis of FRAP data in terms of the mobile fraction d) and its diffusion constant. e) Lateral mobility of fl-SAv was assessed in the absence of b-HS, after incubation with b-HS at saturation, after 15 min incubation of the HS film with chemokines (in the presence of 0.64 mM chemokines in solution) and after regeneration of the HS film by 2 M GuHCl. Data corresponds to mean and standard error of the mean for three independent experiments. Image taken from* ***A16***

We therefore demonstrated that **CXCL12α was a strong and unexpected HS cross-linker**, which has been shown to possess a single heparin binding site (Ziarek, Veldkamp et al. 2013). A minimal length of HS chain was however needed to assure an efficient cross-linking since hexa-oligosaccharides (dp6) were not long enough to permit the HS crosslinking. **FGF-2 which is known to have 2 HS binging sites also cross-linked the HS layer while FGF-9 with a single HS binding site did not cross-link the HS chains**. Interestingly, IFNγ with two distinct HS binding site at the C-terminus showed only a moderate HS cross-linking, suggesting that the two HS binding sites interact with the same HS chain. We proposed that the HS cross-linking is a common feature of several HS-binding chemokines and growth factors that might have important cellular readout such as signaling activation, changing in the glycocalyx stiffness and/or thickness resulting in the exposition of integrins normally hidden by the thick glycocalyx. These hypotheses are now under investigation at the cellular lever by different groups (Dr. R. Sadir, Dr. Douglas Dyer and Prof. R. Richter).

1.1.2. HS-presenting platforms for cellular adhesion studies

These well-characterized platforms have been adopted as support for cellular adhesion studies. We aimed to reconstitute the *in vivo* distribution of HS, chemokines and cell-adhesion ligands, such as the intercellular adhesion molecule 1 (ICAM-1) into tailor-made and multifunctional model surfaces (Migliorini, Thakar et al. 2014)(**A17**). ICAM-1 is known to be presented by the endothelial cell surface and to bind to the leucocyte function-associated antigen-1 (LFA-1; also called integrin αLβ2). This interaction is responsible for the attachment of T-lymphocytes to the vascular endothelium, a precursor step towards migration through the endothelial barrier (Hogg, Laschinger et al. 2003). We first analyzed the exact surface adsorbed amount of each component shown in **Figure 1a** by SE and we demonstrated that up to two CXCL12α dimers can bind to a single HS chain. By SPR we determined that the effective affinity of CXCL12α to HS was ~13μM which is close to the value obtained in literature with a different HS immobilization method (Laguri, Sadir et al. 2007). T-Lymphocytes (Jurkat cells) have been seeded on the top of the platforms (**Figure 3b** and **c**). We proved that these cells adhered specifically to surfaces presenting CXCL12α (called SDF-1 α in the image). The adhesion was improved on surfaces co-functionalized with HS-bound CXCL12α and ICAM-1 **A.17**. This assay thus demonstrates that the co-presentation of an integrin ligand and a GAG-bound chemokine elicits a cellular response that is distinct from the response to each individual cue alone.

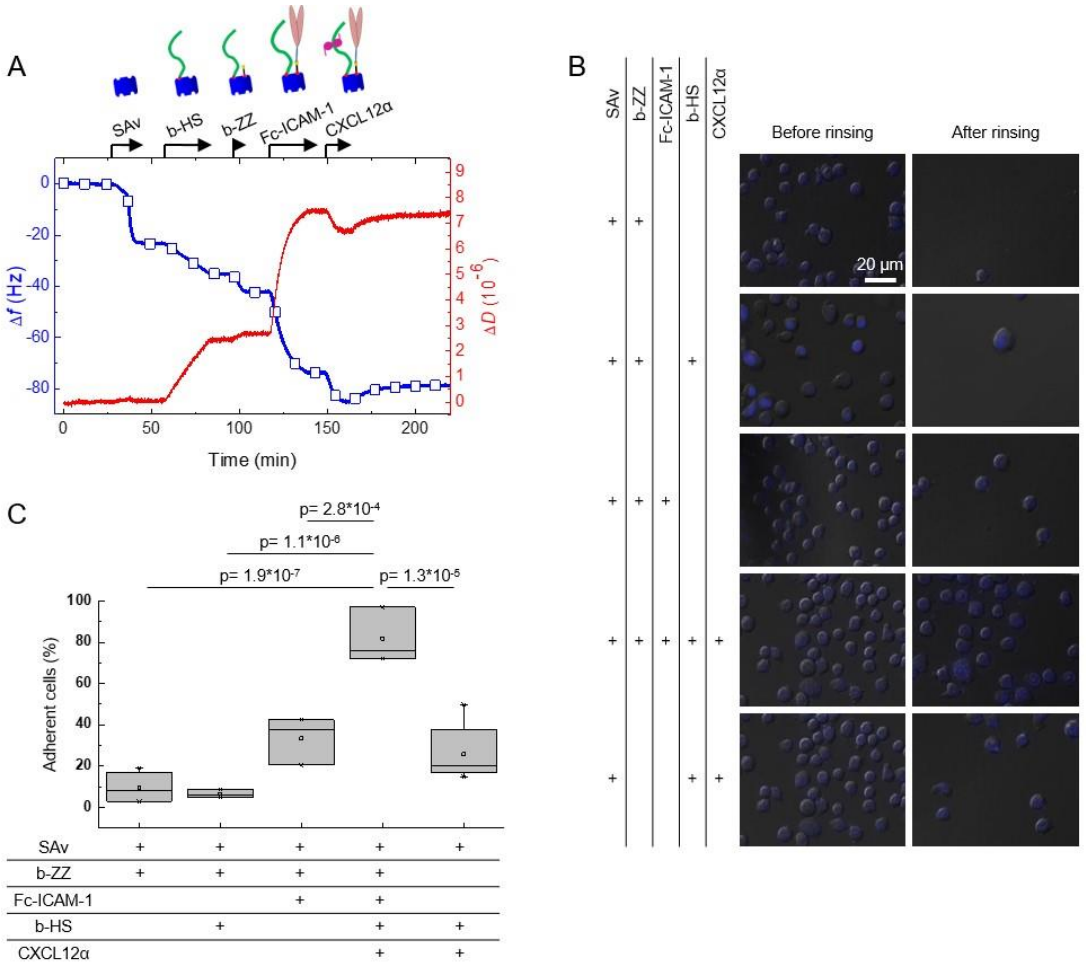

Figure 3: T-lymphocytes differentially respond to surfaces presenting HS-bound chemokine with an integrin ligand. *a) The assembly of a biomimetic surface displaying HS-bound SDF-1α together with the cell adhesion molecule ICAM-1 on a SAv-coated gold-supported PEG monolayer was demonstrated by QCM-D. b) Representative micrographs of Jurkat cells plated on surfaces presenting different surface functionalization. Cells were incubated, and their micrographs before and after rinsing are presented c) Box plot representing the distribution of the percentage of adherent cells that remain after rinsing as a function of surface functionalization. Image taken from* ***A17***

1.2. Conclusions

During my first postdoc I have implemented skills on surface functionalization and characterization. We designed biomimetic platforms that were adopted for molecular and for cellular studies. Thanks to that versatile tool we proved with independent techniques that some HS-binding chemokines and growth factors can cross-link the HS film. The biological role of HS film crosslinking is now studied in other groups such as SAGAG at IBS (Dr. R. Sadir). We also proved that the co-presentation of HS-bound chemokines and adhesion ligands enhanced cellular adhesion with respect of the single cue presented alone. This initial study opens the path to further research on the role of the cross-talk between adhesion ligands and chemokines/growth factors (**A13** and **A8**) (Thakar, Dalonneau et al. 2017, Sefkow-Werner, Machillot et al. 2020) .

2. Spatial nanoscale control of Bone Morphogenetic Protein 2 and heparan sulfate to enhance the osteogenic differentiation of stem cells

PEOPLE INVOLVED: Dr. E. Migliorini (Postdoc and CRCN), Mr. Julius Sefkow-Werner (M2 and PhD), Ms.Elaine Castro-Ramirez (M1 and M2), Prof. A. Cavalcanti-Adam (team leader) and Prof. C. Picart (team leader)

FUNDING: Marie-Sklodowska Curie IF and CellNetworks funding of Heidelberg University (PI: E. Migliorini) IDEX-IRS 2018 (PI: E. Migliorini), FRM (PI: C. Picart) and ANR CODECIDE (PI: C. Albiges-Rizo)

This new project aims at studying the **importance of the presentation of bone morphogenetic protein 2 (BMP2) by the extracellular matrix (ECM)** during the induction of osteogenic differentiation. BMP2 is a multifunctional growth factor belonging to the transforming growth factor β (TGF β) superfamily. It was identified in the 1970s as an essential molecule for *de novo* bone formation in adult animals (Urist 1965, Urist and Strates 1971). **BMP2 is one of the strongest osteoinductive factors known so far**: it initiates the differentiation of mesenchymal stem cells (MSCs) into osteoblasts and chondrocytes *in vivo* and *in vitro* (Ryoo, Lee et al. 2006), as well as the transdifferentiation of muscle cells into bone cells (Katagiri, Akiyama et al. 1997).

As well-detailed in the review **A15** (Migliorini, Valat et al. 2016), the mechanism of BMP2-mediated signaling and osteogenic differentiation is shown in **Figure 4.** BMP2 signals upon binding to two types of cell transmembrane serine/threonine kinase receptors, the BMP type I (BMPRI) and type II (BMPRII) receptors. The binding of BMP2 to BMPRI results in the **phosphorylation of SMAD1/5/8(9)**, which forms a complex with co-SMAD (SMAD4) and translocates to the nucleus. For transcriptional signaling, this shuttling leads to a subsequent expression of transcription factors such as Id1 and BMP2 responsive element, among them Osterix and RunX2, typical markers of osteogenic differentiation. At later time points, alkaline phosphatase (ALP) is expressed after several days, and mineralized matrix deposition is detected after several weeks of culture (Ryoo, Lee et al. 2006). Besides the SMAD pathway, gene transcription is induced by BMP2 *via* non-SMAD signaling as BMP induces the MAPK pathway, which leads to the expression of ALP, osteopontin and collagen (Sieber, Kopf

et al. 2009).

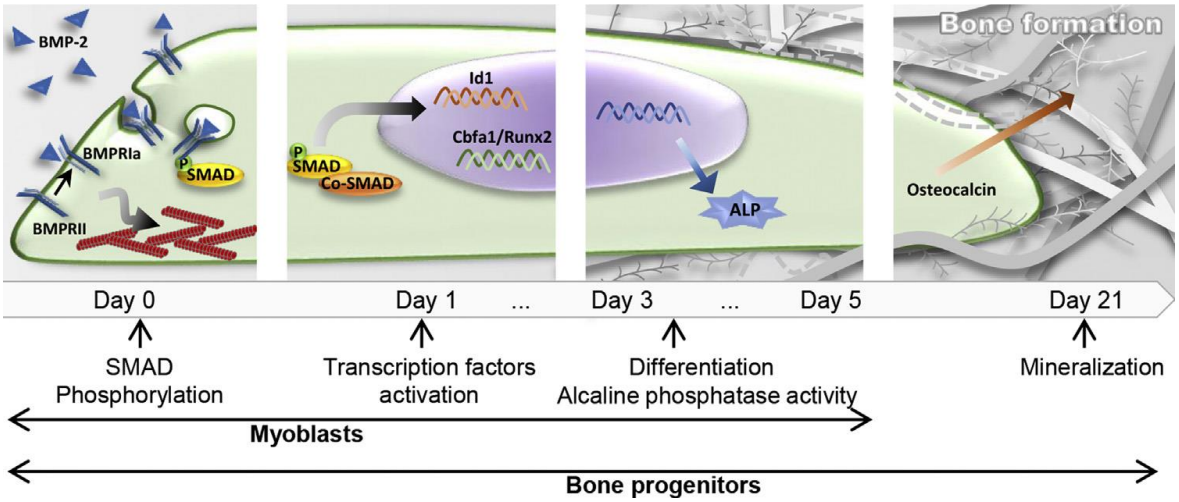

Figure 4: Schematic representation of the major steps in the differentiation *of bone progenitor cells and myoblasts over time. Note that the crosstalk with other signaling pathways and other relevant markers is omitted for simplicity. Adapted from A15.*

In view of its osteogenic potential, the clinical use of recombinant human BMP2 (here just named BMP2), first purified in 1988 by Wang et al. (Wang, Rosen et al. 1988), was approved in 2002 by the Food and Drug Administration (FDA) and validated by the European Medicines Agencies. The only FDA-approved material carrier is an absorbable collagen sponge to which a high amount of BMP2 (up to 2.1 mg/level) is applied in open tibial shaft fractures and in spinal fusion. The need of this high amount of BMP2 is due to its poor affinity for collagen (Kim and Valentini 2002). In clinical trials (spinal surgery) it has been reported that up to 23% of patients suffered complications, such as hematomas and swelling in the neck and throat regions (Carragee, Hurwitz et al. 2011), dysphagia and an increased risk of cancer (Fu, Selph et al. 2013). Nowadays there is therefore the growing socio-economic need for effective materials which allow the control of BMP2 delivery to improve bone therapies. In the same review **A15** we reported a timeline showing a few of the most important findings on BMP2 in biological and material sciences **Figure 5**. It is noteworthy that approval for the clinical use of BMP2 (2003) took place before the development of advanced materials able to control and reduce BMP2 release and before the discovery of new biological functions of BMP2 such as its influence on the whole human body**.** In view of future clinical applications, some critical questions regarding BMP2 presentation and functions remain to be solved in order to provide innovative solution for tissue engineering.

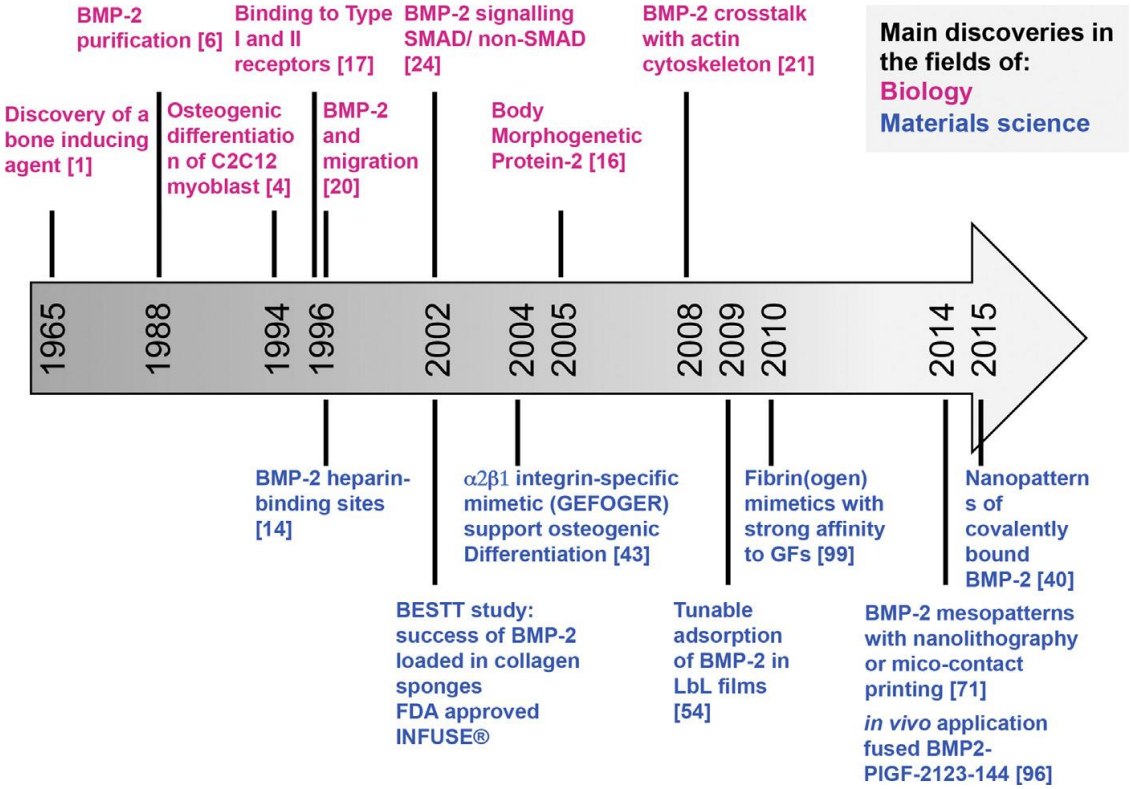

***Figure 5**: **Timeline** showing few of the most important findings on BMP2 in biology (in red) and in material sciences (in blue). Fundamental biological discoveries such as the influence of BMP2 in the whole human body and the development of advanced materials able to modulate the physicochemical presentation of BMP2 followed the approval for the in vivo use of BMP2 in 2002. (For interpretation of the references in this figure, please refer to the web version of this article A15).*

One of the objective of my research is therefore to design an advanced biomaterial which takes into consideration the physical and chemical complexity of the extracellular environmental where BMP2 is retained and released.

2.1. Major scientific achievements

To reach the scientific achievements reported below I wrote and obtained my own postdoc fellowships, I have performed the majority of the lab work, prepared the figure and wrote the papers. For the last part of the work, I supervised a Master student (Julius Sefkow-Werner) who continued the work as PhD.

2.1.1. Surface-immobilized heparan sulfate enhances BMP2 biological activity

Biomimetic materials could serve as a tool for biologists to reveal novel biological properties of BMP2 which could not be explored so far with standard culture methods (Migliorini, Guevara-Garcia et al. 2020) **(A.9)**.

For that, we investigated the **role of HS on the BMP2-mediated signaling and osteogenic differentiation**. To start this project, I obtained a Marie-Sklodowska Curie Individual fellowship to join **Ada Cavalcanti**'s team (expert on engineering surfaces presenting BMP2) at Max Planck Institute for intelligent systems, Stuttgart and the

University of Heidelberg, Germany. When I started this project, few papers showed the importance of HS on BMP2 signaling (Ruppert, Hoffmann et al. 1996, Murali, Rai et al. 2013), however all these studies were done with soluble HS and BMP2 while *in vivo* BMP2 is a growth factor bound to the ECM (**A9**) (Migliorini, Guevara-Garcia et al. 2020). For that, I initially adapted the SAv platforms to present BMP2 to murine myoblast cell line C2C12 cells (well-accepted cell model for BMP2 signaling studies) and to primary human mesenchymal stromal cells (hMSCs) which are involved in the osteogenic regeneration after injury. The growth factors were presented to cell surface either alone, immobilized to SAv *via* a biotin-SAv linker, or bound to biotinylated HS (here named b-HS and later iHS as immobilized HS) (**Figure 6a**). The results have been published in Advanced Biosystems Journal (**A12**) (Migliorini, Horn et al. 2017).

These platforms were characterized by SE and QCM-D (**Figure 6c and d**). We demonstrated that at saturation up to 13 BMP2 dimers can be immobilized on one HS chain – suggesting a possible oligomerisation of BMP2 on HS chains, which is so far complicated to be proved. We have also studied the capability of **BMP2 to cross-link the HS**. Indeed BMP2 presents a heparin-binding site at the N-terminus of the homodimer (Ruppert, Hoffmann et al. 1996) (**Figure 6b**). It has previously been predicted that the N-terminus of BMP2 might have a secondary HS-binding site since it is composed of two basic regions that impart electropositive character to both sides of BMP2 (Gandhi and Mancera 2012); this however has not been directly proved. We have shown that **BMP2 is a partial HS cross-linker**, since the diffusion constant was significantly reduced upon BMP2 binding to b-HS but the mobile fraction was only slightly reduced (**Figure 6e**). We propose that, at increased BMP2 concentration, more than one b-HS chain binds to each BMP2 dimer, consistent with the presence of two or more independent Hp/HS binding sites at the BMP2 dimer's N-terminus, which has previously been predicted (Gandhi and Mancera 2012).

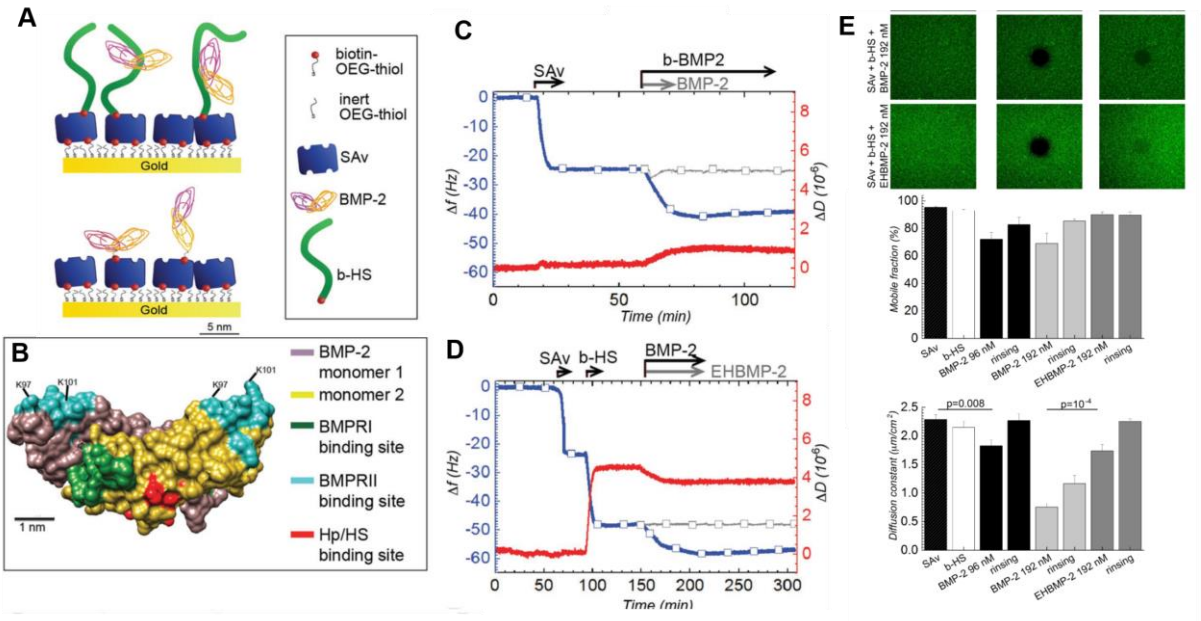

***Figure 6: HS film conformational changes upon BMP2 binding**. A) schematic representation of the BMP2*

presenting platforms. Here BMP2 is presented by HS (top image) or directly immobilized to SAv via a biotin-PEG linker. B: BMP-2 homodimer structure (PDB: 3BMP(Scheufler, Sebald et al. 1999)) showing the Heparin/HS binding site and the BMP receptors binding sites. C-D) QCM-D characterization of the C) bBMP2 bound to the Sav (blue and red line) and of BMP2 non-specific binding to Sav and D) BMP2 bound to b-HS compared with mutated BMP2 for the HS binding site (grey curve). The red line indicates the dissipation and blue line the frequency shift. Arrows indicate the start and the period of injection of one solution. In between, the platforms were rinsed with Hepes buffer. E) We implemented FRAP technique to evaluate the mobile fraction of HS molecules bound to SAv-Atto upon BMP2 binding. We used silica-supported fluid lipid bilayers containing biotinylated lipids instead of gold-based PEG monolayers as support. Fluorescently labelled SAv (SAv-Atto) was used for the attachment of b-HS and as a reporter for HS mobility. Crosslinking of two or more HS chains by BMP-2 dimers was expected to decrease HS mobility, whereas HS mobility should remain largely unchanged if each BMP2 dimer binds only a single HS chain. We quantified the mobile fraction and the diffusion constant of SAv-Atto with BMP2 or EHBMP2 bound to b-HS at different concentrations. P-values have been determined with the student T-test analysis. Figure adapted from ***A12****.*

In the same study we analyzed the responses of C2C12 cells and hMSCs on BMP2-presenting biomimetic platforms and the effect of BMP2 was quantified on early BMP2 signaling effectors SMAD 1/5/9 phosphorylation by western blot. It is important to notice that cells were not adhering on the platforms since there were no adhesion peptides. Due to that we were able to study only early signaling event of the BMP2 pathway. We proved a **significant sustained effect of BMP2 signaling when BMP2 was adsorbed to HS after 3 hours of cell culture, with respect to the soluble BMP2** on both cell types. On bBMP2 the p-SMAD 1/5/9 levels were lower than on HS for the C2C12 cells but not for the hMSCs (**Figure 7a, c**). We also analyzed the effect of the BMP2 antagonist noggin in presence of soluble and immobilized HS. Noggin binds to the BMP2 binding domains for the BMPRs with high affinity in the picomolar range (Zimmerman, De Jesús-Escobar et al. 1996). As shown in **Figure 7b, d** for both C2C12 cells and hMSCs, pre-mixing BMP2 with noggin inhibited the signal but when BMP2 was bound to b-HS, noggin did not inhibit the SMAD1/5/9 phosphorylation. We concluded that **b-HS–bound BMP2 reduces noggin's antagonistic activity**. This effect was not present with soluble HS (**Figure 7b, d**). Thus, **grafted HS positively affects BMP2 cellular activity.**

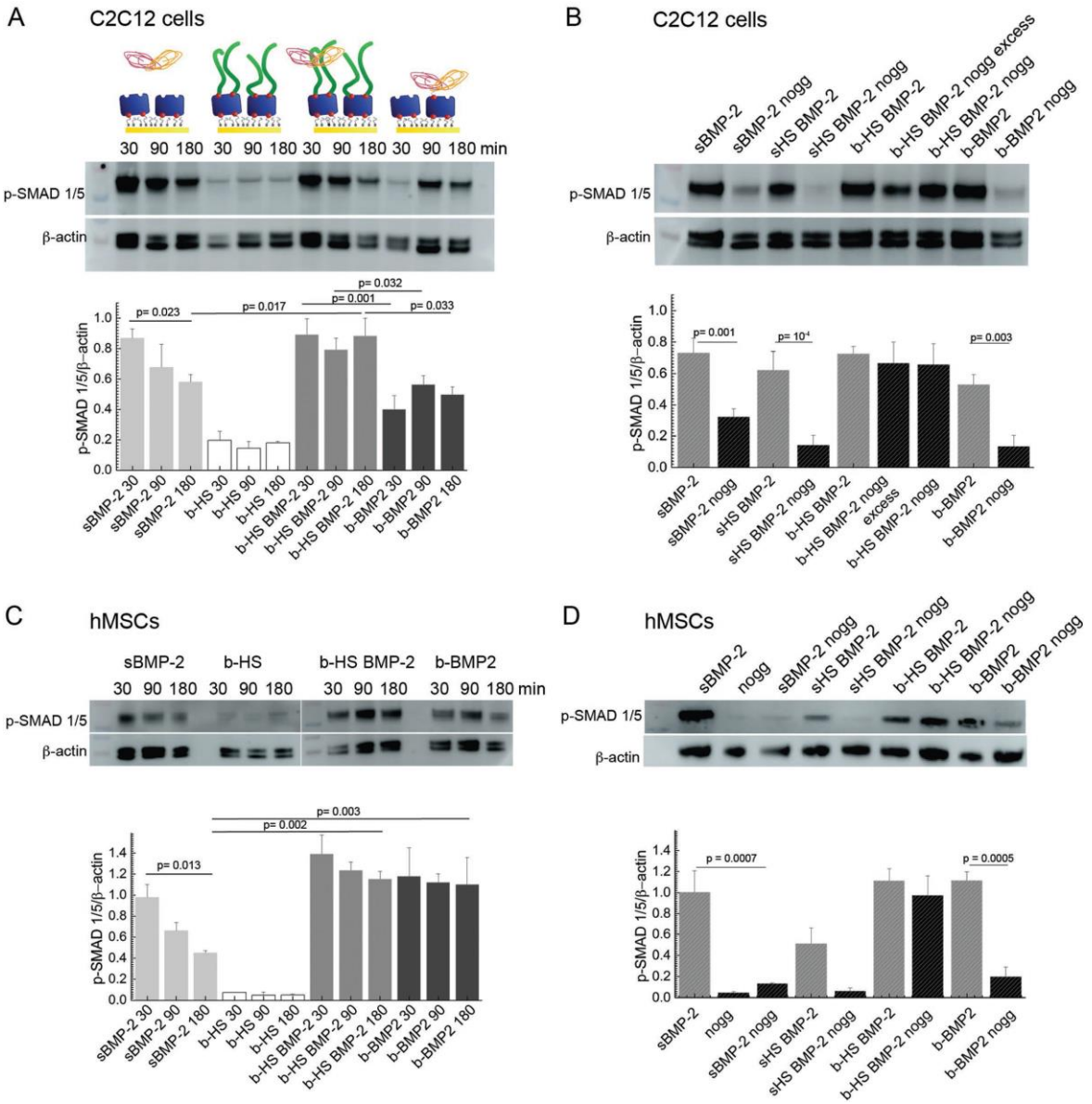

Figure 7: ***Effect of b-HS on BMP2-SMAD 1/5/9 signaling***. *A,B) C2C12 cells and C,D) hMSCs plated on functionalized surfaces. A,C) Cells lysed 30, 90 and 160 min after plating on surfaces functionalized with b-HS, BMP2 and bBMP2 or B, D) after 90 min on substrates incubated with or without noggin (200 nM). P-SMAD 1/5 expression was analyzed by western blot. The significance has been tested by parametric one-way analysis of variance (ANOVA). P-values are indicated in given figures with values of <0.05 being considered as statistically significant. Figure taken from* ***A12***

2.1.2. The bidirectional crosstalk between bone morphogenetic proteins receptors and integrins

I moved to the laboratory of **C. Picart** as a **CNRS researcher** to be able to continue this project by improving the biomimetic approach and further study the effect of HS on BMP2 bioactivity. For this project, I had the help of Master students and a PhD student (Julius Sefkow-Werner).

In the last years, the interplay between integrins and growth factors (GFs) receptors has been the topic of several studies (Ivaska and Heino 2011, Sawala, Scarcia et al.

2015, Fourel, Valat et al. 2016, Monteiro, Kollmetz et al. 2018), but **it remains unclear whether this crosstalk is bidirectional**. Moreover, **the role of HS on this crosstalk is unexplored**. The work related to the following results has been published in Acta Biomaterialia (Sefkow-Werner, Machillot et al. 2020) **A8.**

Integrins are transmembrane receptors consisting of α and β subunits which bind to cell adhesion ligands in the ECM (Barczyk, Carracedo et al. 2009) and allow cells to spread by developing focal adhesions. It has been shown that surface-presented BMP2 can induce cell spreading on LbL films with low cross-linking (named soft films) whereas cells did not spread on soft films without BMP2 (Fourel, Valat et al. 2016). In this particular context, β_3-integrins were needed for BMP2-induced cell spreading and controlled SMAD 1/5/8 phosphorylation and degradation. However, the type of integrins involved in GFs signaling might be context-dependent. As for example, experiments with vascular endothelial growth factor (VEGF) have shown that β_1-integrins upregulate VEGF-induced vascularization in hydrogels while β_3-integrins have no influence (Garcia, Clark et al. 2016). It has further been demonstrated on mesenchymal stem cells that increased lateral spacing of arginine-glycin-aspartic acid (RGD) containing-peptide ligands significantly decreases ALP activity and reveals a similar trend on Runx2 expression (Frith, Mills et al. 2012). *In vivo* studies with Drosophila have revealed that integrins are also necessary for a peak p-SMAD 1/5/9 signal (Sawala, Scarcia et al. 2015), indeed collagen IV mutants embryos present a reduced p-Mad (the equivalent of p-SMAD) signaling. To better understand the role of integrins recruitment on BMP2 signaling we designed a simple experiment by developing SAv platforms presenting an increasing concentration on cyclic RGD (cRGD) peptides (**Figure 8**) **A.8**. cRGD is known to bind and activate integrins β_1 and β_3 subunits (Pfaff, Tangemann et al. 1994). The surface density of cRGD peptide was quantified with the combined QCM-D/SE setup and it was of 2, 10 and 23 ng/cm^2. On these platforms we plated C2C12 cells and we stimulated them with soluble BMP2 (sBMP2) at a constant concentration (6 nM). We observed by western blot that the **phosphorylation of SMAD 1/5/9 was up-regulated by increasing the cRGD surface concentration**. This result shows that an increased recruitment of integrins at the cell membrane positively influences the BMP2 signaling pathway (Sefkow-Werner, Machillot et al. 2020). As control, we designed cRAD (cyclic arginine-alanine-aspartic acid) platforms with comparable peptide surface concentrations. It is known that cRAD peptide has 400 times less affinity for integrins with respect to cRGD (Pfaff, Tangemann et al. 1994). C2C12 cells exposed to sBMP2 (6 nM) on cRAD platforms slightly up-regulated p-SMAD 1/5/9 levels but no changes were observed on different cRAD surface concentrations (data not shown), **proving that the effect shown in Figure 8 c and d is truly integrin-mediated**.

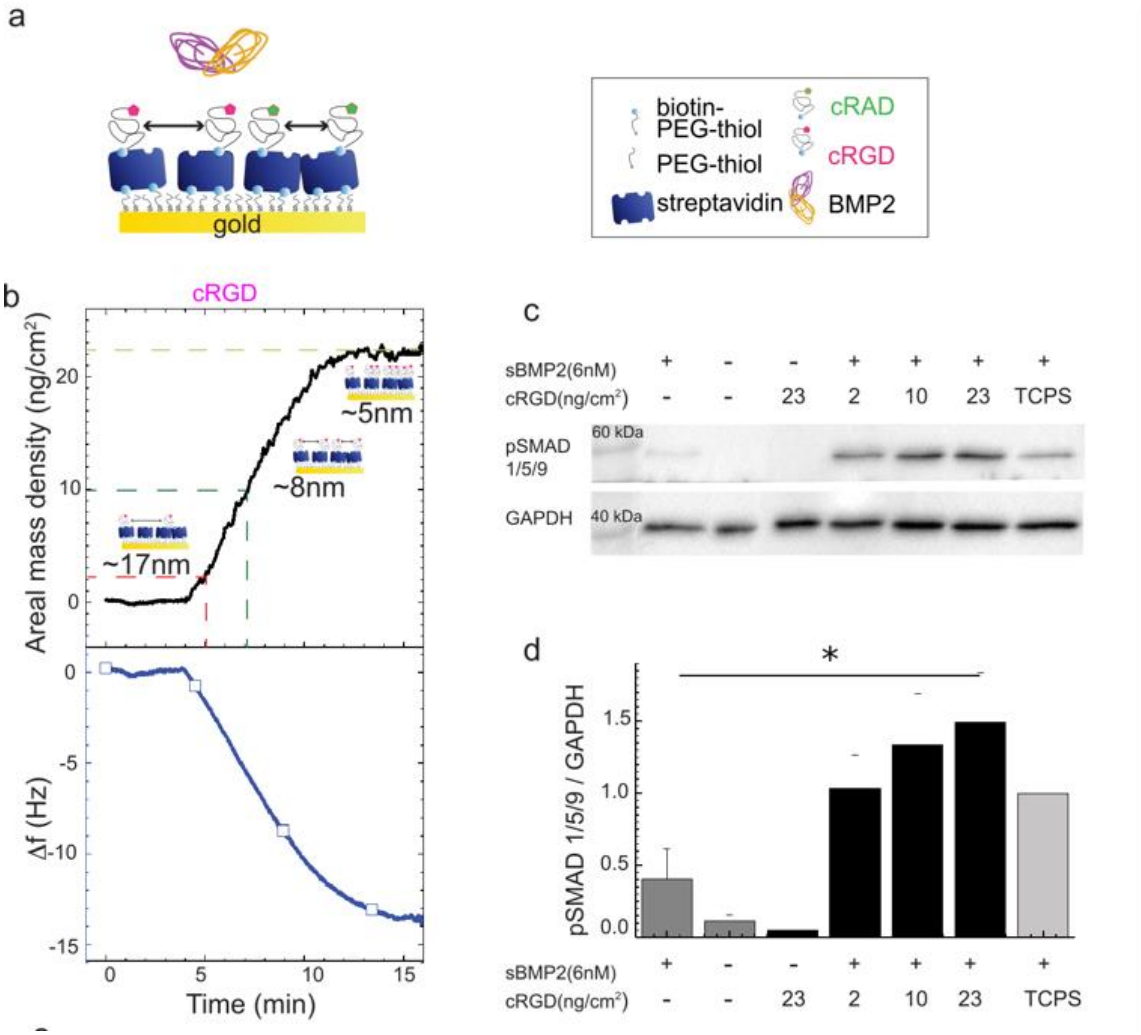

Figure 8: Increasing surface concentration of cRGD, and therefore the integrin engagement at the membrane, enhances cell response to sBMP2*. a) Schematic representation of the cRGD and cRAD platforms employed for this experiment, with variable inter-molecular distances between biotinylated cRGD and cRAD peptides immobilized on Streptavidin (SAv). b) Combined QCM-D / SE measurement of cRGD binding to SAv. The black curve corresponds to the spectroscopic ellipsometry data and the blue curve to the QCM-D binding of cRGD to SAv. The dashed lines mark the incubation times that we used to functionalize the platforms for cellular studies and correspond to the adsorbed masses of ~2, 10 and 23 ng/cm² of cRGD respectively. c) Western blot of p-SMAD1/5/9 levels in C2C12 cells plated on surfaces presenting three different cRGD surface concentrations and stimulated with sBMP2 (6 nM). As control, C2C12 cells have been plated on platforms presenting only SAv and on a plastic petri-dish (TCPS) with sBMP2. 1 hour after plating, cells were lysed and the level of p-SMAD1/5/9 plotted and normalized to the housekeeping gene GAPDH. d) Quantification of the western blot bands. Bars correspond to the mean ± SEM. Non-parametric Mann-Whitney test has been used for single comparisons. *p < 0.05. Image adapted from **A.8** (Sefkow-Werner, Machillot et al. 2020)*

We confirmed with these platforms that the adhesion of C2C12 cells was also improved in presence of BMP2 on low adhesive platforms, as it was previously shown on soft non-adherent polyelectrolytes films presenting bound BMP2 (Fourel, Valat et al. 2016). Thus, we designed low adhesive cRGD platforms to quantify the effect of BMP2 on cell adhesion. We mixed cRGD peptides with an inert ligand having the same binding kinetics: a biotinylated PEG (iPEG) molecule with a similar molecular weight of the cRGD. Mixing different ratios of these components diluted the cRGD concentration in

solution and reduced its final surface density down to physiological levels (Arnold, Cavalcanti-Adam et al. 2004).

For this experiment we wanted to study the effect of immobilized biotinylated BMP2 (here named iBMP2) and of sBMP2 on cellular adhesion and for that we co-functionalized the platforms with cRGD and iBMP2 (**Figure 9a, b)**.

The number of cells that remained adherent to the platforms 1 hour after plating, decreased with the reduction of cRGD surface concentration (**Figure 9d,** white bars). The density of 0.25 ng/cm^2 cRGD was at the limit to induce cell adhesion. In this condition the presence of sBMP2 or iBMP2 significantly increased the number of adherent cells (**Figure 9d**). However, the presence of BMP2 did not improve cell spreading since cell area was the same whatever the type of BMP2 presentation. The results shown here demonstrate that there is a **bidirectional crosstalk between integrins and BMP2 signaling**.

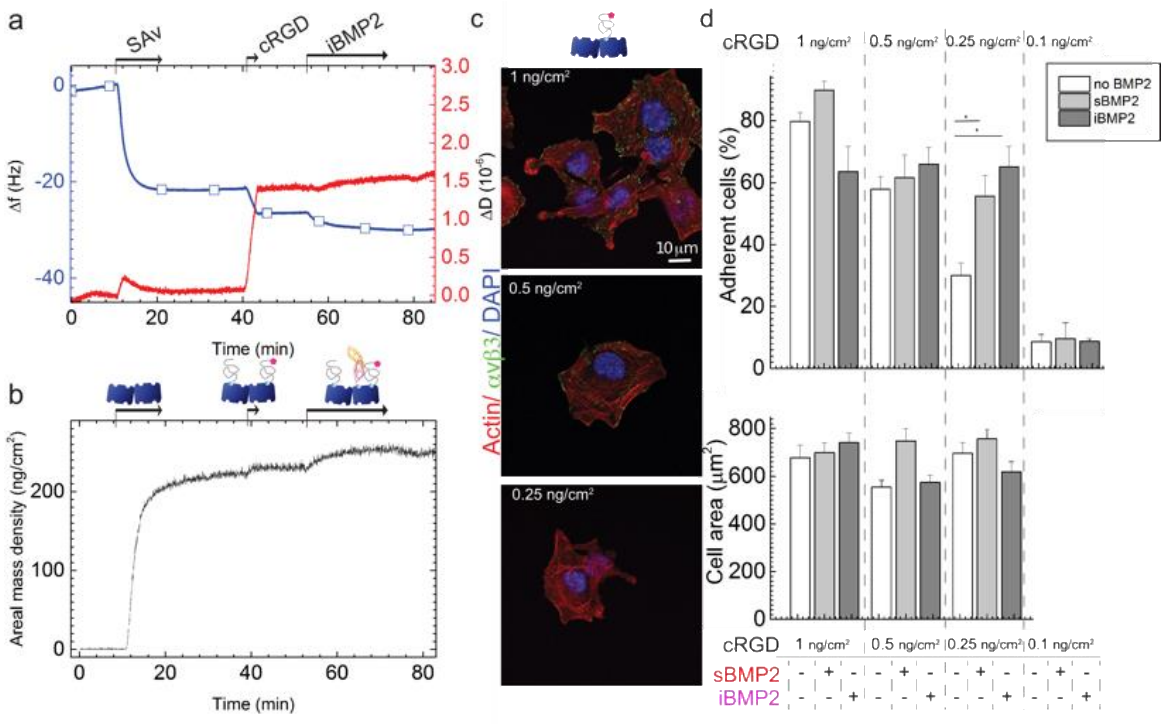

Figure 9: BMP2 improves the number of adherent cells on platforms presenting 0.25 ng/cm2 cRGD surface concentration. *a) QCM-D measurement shows the co-functionalization of Sav platforms with cRGD and iBMP2. The blue line shows frequency shifts and the red line dissipation shifts. Arrows indicate the start and the duration of the injections. In the remaining time, the surfaces were exposed to running buffer. b) SE measurement of the mass adsorption. The curve shows the increase of the adsorbed mass (measured in ng/cm2) during the molecular injections (indicated by arrows). c) Confocal immunofluorescence images of C2C12 cells plated on biomimetic platforms presenting different cRGD surface concentrations (from 1 to 0.25 ng/cm2) and fixed 1.5 hours after seeding. Non-adherent cells have been washed away by gentle pipetting and were fixed in 4% paraformaldehyde. Immunofluorescence staining was performed to reveal the presence of FAs positive for integrins β3 (labelled in green). Scale bar = 10 μm. d) Adherent cells and cell area of C2C12 cells 1 hour after plating. Cell number was quantified on five different images per condition and in three independent experiments. Cell area of isolated cells was measured (by Image J analysis, using the function "analyze particle") on decreasing cRGD surface concentrations: 1, 0.5 and 0.25 ng/cm2. This analysis has not been performed on 0.1 ng/cm2 since only a residual*

*number of cells remained adherent to the platforms. Bars correspond to the average value ± standard deviation. Non-parametric Mann-Whitney test has been used for single comparisons. *p < 0.05. Image taken from (A8) (Sefkow-Werner, Machillot et al. 2020)*

2.1.3. The role of heparan sulfate in the BMPRs – integrins crosstalk

It has been previously proposed that HS can bind integrins with a 2.02 μM affinity (Faye, Moreau et al. 2009). To understand the role of iHS on the BMP2 signaling, on its synergy with integrins activation and on BMP2-mediated osteogenic differentiation, we designed biomimetic platforms co-presenting cRGD and iHS with adsorbed BMP2 (here named aBMP2). These platforms were characterized with QCM-D and SE as previously in **Figure 9.** The surface amount of iBMP2 and aBMP2 was comparable.

C2C12 cells were plated on platforms presenting decreasing amounts of cRGD (**Figure 10a**) and with the same amount of sBMP2, iHS, iHS + aBMP2 and iBMP2. The p-SMAD 1/5/9 levels, one hour after plating, were quantified with western blot (**Figure 10a**) and the Osterix expression was quantified with qPCR after one day (**Figure 10b**). We observed that the levels of p-SMAD 1/5/9 decreased on lower cRGD surface concentration when BMP2 was presented in the soluble form sBMP2 and also immobilized on the platform **but not in the condition where BMP2 is adsorbed on iHS**. In the case of Osterix expression, we also observed that the osteogenic differentiation is not influenced by the cRGD surface concentration when BMP2 is adsorbed on iHS. Moreover, the Osterix expression is higher on iHS + aBMP2 with respect to iBMP2 and this was confirmed by the analysis of the other osteogenic marker Runx2.

We prove therefore that iHS has a positive effect on BMP2 signaling and on BMP2 mediated osteogenic differentiation and that this effect is **independent of the cRGD surface concentration**.

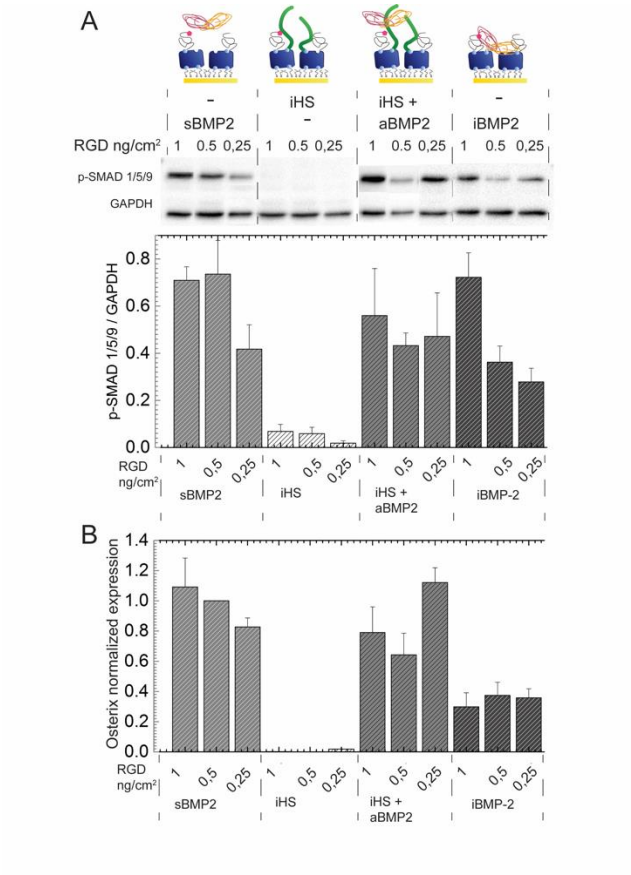

***Figure 10*: iHS has a positive effect on BMP2-mediated SMAD1/5/9 phosphorylation and on Osterix expression**

a) Western blot and quantification of p-SMAD1/5/9 in C2C12 cells plated on platforms functionalized with different cRGD surface concentrations and with sBMP2, iHS, iHS and aBMP2 and iBMP2 (as schematically represented). Cells were lysed 1 hour after plating and the phosphorylation of SMAD1/5/9 has been normalized to GAPDH (n=3). The triplicate experiment is available online http://dx.doi.org/10.17632/y8mscmkcxk.1. b) Osterix normalized expression in C2C12 which were let to differentiate for 1 day on platforms functionalized with different cRGD surface concentrations, sBMP2, iHS with or without aBMP2 and iBMP2. qPCR was used to study the expression of osteogenic transcription factors normalized to three housekeeping genes (n=5). Figure adapted from A8 (Sefkow-Werner, Machillot et al. 2020).

To further understand the importance of iHS on integrin-BMP signaling crosstalk, we changed the type of ligand on the surface (cRAD *vs* cRGD) and we knocked down β_1 and β_3 integrins by silencing RNA, known to be the integrins which mainly recognize cRGD peptides (Pfaff, Tangemann et al. 1994).

C2C12 cells were plated on cRGD co-presenting sBMP2 or iHS or iHS + aBMP2 or iBMP2. BMP2 signaling was analyzed either after 1.5 hours for p-SMAD1/5/9 staining (**Figure 11a**) or after 3 days for ALP staining (**Figure 11c**).

SMAD1/5/9 phosphorylation was down-regulated when either β_3 or β_1 integrins were silenced. The silencing of integrins reduced SMAD1/5/9 phosphorylation, independently of the type of BMP2 presentation (iHS + aBMP2 *vs* iBMP2). **Both integrins are therefore involved in p-SMAD1/5/9 signaling activation, independently of the presence of iHS.**

The silencing of β_3 and β_1 integrins also led to a down-regulated expression of ALP (**Figure 11d**) in particular on cRGD platforms presenting sBMP2 and aBMP2.

We prove that both integrins, β_3 and β_1, are important for p-SMAD1/5/9 signaling and later on for ALP expression. To notice is, that the presence of iHS + aBMP2 enhances ALP staining. However, the down-regulation of integrins decreases both p-SMAD1/5/9 and ALP on HS + aBMP2 conditions showing that **both, integrins and iHS, are fundamental actors to promote BMP2-mediated signaling pathway.**

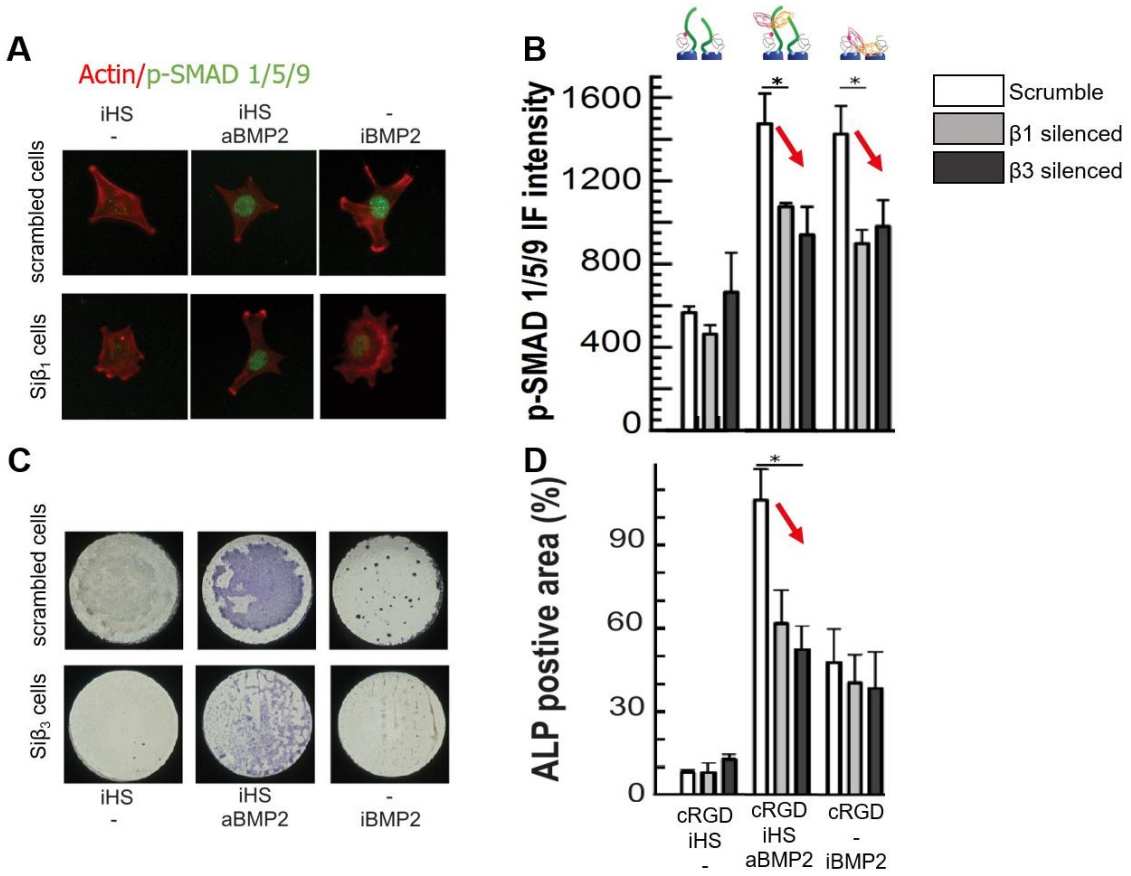

Figure 11: Effect of the ligand (cRAD vs cRGD) and the presence of specific integrins in the regulation of p-SMAD1/5/9 pathway and of the ALP expression.

*Cells were silenced for either β_1 or β_3 integrins and plated on cRGD platforms and fixed after 1.5 h for p-SMAD1/5/9 staining (a) or after 3 days for ALP staining (c). In graphics b,d, scrambled cells are represented with white bars, silenced β_1 cells (siβ_1) with grey and silenced β_3 cells (siβ_3) with dark grey bars. Bars represent the mean of three independent experiments ± SEM. a) Representative IF images of scrambled and siβ1 cells plated on cRGD platforms and stained for actin (red) and p-SMAD1/5/9 (green). Scale bar = 20 μm. Representative images of all the conditions are available online: DOI:10.17632/ip9m2nmpry.1 b) Immunofluorescence intensity of p-SMAD1/5/9 translocated into cell nuclei is plotted for each condition and cell type. Number of quantified cells was >50 for each experiment and condition. c) Representative wells after ALP staining for scrambled and siβ_3 cells plated on cRGD platforms. Representative images of all the conditions are available online: DOI:10.17632/ip9m2nmpry.1 d) ALP positive area normalized by the number of cells in each well (n=3). Non-parametric Mann-Whitney test has been used for single comparisons. *p < 0.05, **p < 0.01. Image taken from* ***A8***

2.2. Conclusions

After the second postdoc I developed the SAv-based platforms for cellular mechanistic assays to study the role of cRGD and HS on BMP2 signaling. We demonstrated the presence of a bidirectional crosstalk between integrins and BMP signaling meaning that the increased surface concentration of cRGD (but not cRAD) promoted BMP-mediated SMAD 1/5/9 phosphorylation in presence of the same quantity of soluble or immobilized BMP2. We also proved that both integrins β_3 and β_1 are important for p-SMAD1/5/9 signaling and later on for ALP expression. This result has been further

confirmed in a following study by another postdoc in the team (Sales, Khodr et al. 2022) **A3**. The presence of iHS supports p-SMAD 1/5/9, Osterix and RunX2 levels even at low cRGD surface concentration and promoted ALP expression, demonstrating a positive role of iHS on BMP2-mediated osteogenic differentiation. However, the mechanism of action of HS on BMP2 signaling is not yet clear, in particular, if the iHS film presented on the streptavidin platform works as a reservoir of BMPs or if there is a specific function of HS on the BMP2 signaling. Moreover, the contribution of the cell surface HS on the BMP ligand-receptor binding has not been investigated in this study.

To answer to these questions, I planned to compare the role of different GAGs on BMP2 bioactivity and to address the presence of cell surface HS on cellular adhesion.

3. Automated functionalization of streptavidin platform and *in situ* characterization

PEOPLE INVOLVED: Dr. Julius Sefkow-Werner (PhD), Mr. Jean Le Pennec (M2 and PhD), Mr. João Cardoso Filho Lopes (M2 and PhD), Ms. Elaine Castro-Ramirez (M2), Mr. Bertin Ndayishimiye (M2), Léa Aubert (L3), Mr. Paul Machillot (IE), Prof. Catherine Picart (team director) and Elisa Migliorini.

Collaborators: Prof. Antoine Delon (Liphy) and Christophe Licitra (CEA Leti)

FUNDING: ANR-DFG GlyCON (E. Migliorini) IDEX-IRS 2018 (E. Migliorini), équipe FRM (C. Picart)

To advance our understanding of the role of multiple extracellular or cell surface GAGs on BMP2 signaling, it was essential to increase the number of conditions that could be tested in parallel in the same experiment. Therefore, we needed to automatically functionalize multi-well plates in parallel, such as 96-well plates, using a liquid handling robot. The advantage of using 96-well plates is the drastic reduction in the volume needed to functionalize the plates (50 µl instead of 500 µl) and therefore the need for expensive reagents such as BMPs. The only disadvantage is that the number of cells per well is also limited (~30,000) and molecular biology assays such as Western blot and qPCR are generally performed with higher cell numbers. Another bottleneck was the *in situ* characterization of the surface density of the bound molecules upon the automated functionalization.

3.1. Major scientific achievements

The achievements on this technical project have been published in ACS Applied Materials and Interfaces (Sefkow-Werner J., Le Pennec J. et al. 2022) **A.1.** The experimental protocol to characterize the adsorbed amount of molecules *in situ* has been published in ACS Analytical Chemistry (Sefkow-Werner, Migliorini et al. 2022) **A.2.** This work was the second part of the PhD thesis of Julius Sefkow-Werner, who

carried out most of the experiments and wrote the first draft of the paper. Jean Le Pennec and João Lopes, two other PhD students that I supervised, helped in the realization of the graphical user interface for the manipulation of the liquid handling robot. Other Master students that I supervised during these years helped in the development of this project.

3.1.1. Functionalization of glass platforms

The main issue to use multi-wells plates was the fact that before, we adopted a functionalization routine that was based on a thiol-PEG/thiol-PEG-biotin passivated gold layer on which SAv forms a rigid monolayer (Migliorini, Thakar et al. 2014). On the contrary, 96-well plates are generally commercially available with glass or plastic bottom. So, we had to switch from gold to glass as a base substrate. This change was not immediate because we needed to find the right ligand that could bind glass on one side and present biotins on the other. We initially tested silane-PEG-biotin, but this gave us significant non-specific binding of BSA molecules. We tested the commercially available linker PLL(20)-g[3.5]-PEG(2)/PEGbiotin(3.4)50% (here after called PLL-g-PEGbiotin50%) which consists of a Poly(L-Lysine) backbone (~20 kDa, ~100 monomers) with one PEG chain (2 kDa) or one PEG biotin chain (3.4 kDa) grafted to one of 3.5 PLL monomers in a 50% ratio. The PLL binds with electrostatic interactions to the glass. Before choosing the final percentage of biotin, we tested PLL-g-PEGbiotin20% and different mixture between PLL-g-PEGbiotin50% with PLL-g-PEG. We finally proved that **PLL-g-PEGbiotin50%** generated a **SAv layer** with enough available biotin binding sites, in line with previous publications (Huang, Vörös et al. 2002). The quantity of cRGD that we could graft on the SAv monolayer was anyway almost 10 times less than on our gold standard platforms. As shown **in Figure 12b** and **c** the partial cRGD saturation of SAv monolayer on gold platforms generated a shift of -7 ± 0.5 Hz (**Figure 12b**) (Sefkow-Werner, Machillot et al. 2020)**A.8** while the same sub-saturation of SAv layer by cRGD on glass platforms generated a shift of only -0.8 ± 0.1 Hz (**Figure 12c**) (Sefkow-Werner, Le Pennec et al. 2022)**A.1**. The study of Zhen et al.(Zhen, Eggli et al. 2004) shows that the number of available biotin binding sites increases when SAv is pre-linked with a biotinylated molecule, probably due to improved layer organization. For that, we pre-coupled in solution SAv with cRGD at the molar ratio 3:4 for 30 min. This mixture injected to the PLL-g-PEGbiotin50% generated a higher frequency shift than the sum of single SAv and cRGD incubated one after each other (**Figure 12c**). Moreover, the pre-coupling increases the available binding sites for iHS (**Figure 12c, d**). Consequently, more BMP2 can be grafted on platforms functionalized by the pre-coupling of SAv and cRGD with respect to the sequential binding.

This **novel platform functionalization has been characterized by SE** thanks to the collaboration with C. Licitra at CEA Leti. To note is, that the liquid chamber (500 µL liquid cell from Quantum Design, Darmstadt, Germany) is not identical to the one used for the QCM-D experiment since the volume is 10 times higher while the microfluidics

connections are comparable. The substrate and the way of activation was also different since we adopted an UV-ozone cleaner at BRM to clean and activate the SiO_2 QCM-D crystals while at Leti we used a plasma O_2 to clean and activate silicon wafers covered with a 60 nm-thick thermal SiO_2 layer. These differences made the direct comparison of the binding kinetics between the two types of experiments difficult. However, we could extract information such as the optical mass adsorbed at saturation of each layer as shown in **Figure 12e**. PLL-g-PEGbiotin50% bound to glass with 119 ± 9 ng/cm^2, SAv then with 264 ± 6 ng/cm^2 (data not shown) and SAv/cRGDmix with 343 ± 25 ng/cm^2. iHS bound with 2.9 ± 1 ng/cm^2 and aBMP2 with 114 ± 10 ng/cm^2.

We conclude that the functionalization of glass supports with PLL-g-PEGbiotin50% is less precise than on gold supports since we cannot perform the sequential adsorption of molecule and therefore control the saturation level of cRGD on SAv monolayer. On the contrary, we proved that the frequency shifts of each molecule is overall reproducible. In addition, the **functionalization of glass platforms is convenient for scaling-up the functionalization protocol to commercially available multi-well plates**.

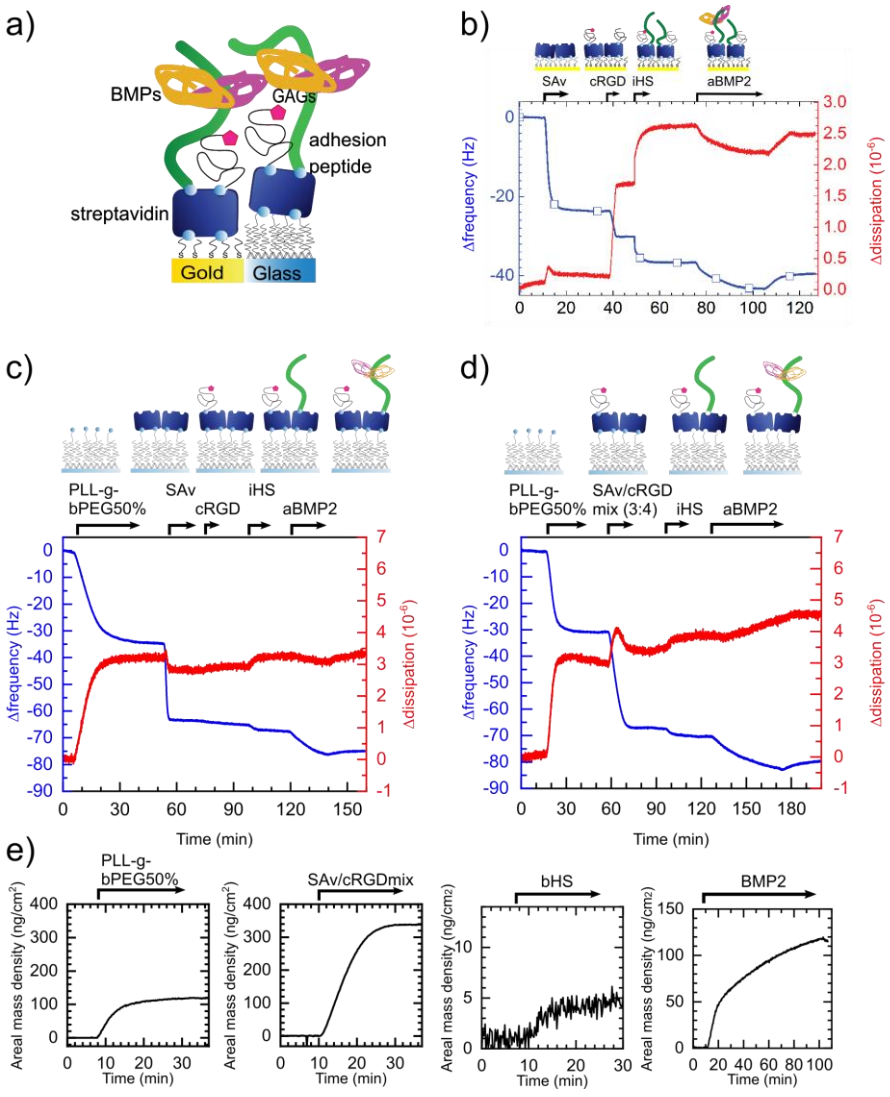

Figure 12 Functionalization of the biomimetic platforms on gold and on glass supports a) Schematic representation of the biomimetic platforms composition on the two different supports, gold and glass. b) QCM-D characterization of the platform building up on gold supports (Figure extracted from (Sefkow-Werner, Machillot et al. 2020). As for the other QCM-D graphs c and d the frequency is displayed in blue and the dissipation in red. The injection of each molecule is represented by an arrow, in between the surface is exposed to running Hepes buffer. c) Sequential functionalization of glass platforms. PLL-g-PEGbiotin50% adsorbed SAv bound to it. Then cRGD was incubated at a concentration of 0.25 µg/ml but incubation was intentionally interrupted before saturation to keep biotin-binding sites available for subsequent compounds. Interrupting the cRGD adsorption after four minutes led to a sub-monolayer with a barely visible frequency shift of -0.8 ± 0.1 Hz. iHS then saturated the remaining binding sites and increased further the dissipation. Finally, BMP2 with a concentration of 5 µg/ml adsorbed to iHS and saturated after 20 min with 6.1 ± 1.3 Hz of which some was partly removed by rinsing. D) Pre-coupled SAv and cRGD in molar ratio of 3:4 were incubated on PLL-g-PEGbiotin50%. The mix adsorbed more than the sum of single SAv and cRGD incubated one after each other. This also resulted in more available biotin-binding sites as seen by higher iHS adsorption and higher aBMP2 adsorption. e) Spectroscopic ellipsometry measurement of the areal mass density of molecules adsorbed on silicon wafers coated with a thin layer of SiO_2. Each panel corresponds to the injection of one molecule. We can observe that the binding kinetics of the SE measurement was different from the one on the QCM-D generally more rapid, in particular for the BMP2.

3.1.2. Automated biomimetic platforms functionalization

To scale up the functionalization process using multi-well plates, we decided to use a liquid handling robot available in the BRM team, as we could not functionalize more than 12 platforms manually with a high risk of experimental errors. This robot was already used in C. Picart's group for layer-by-layer assembly (Machillot, Quintal et al. 2018), but the software used allowed a cyclic deposition of three molecules on the whole plate. To functionalize the SAv platform, we needed a completely different protocol with more than three solutions and the ability to functionalize each well differently. To do this, we modified the macro and script created for layer-by-layer deposition to be able to **functionalize each well of the plate separately with an unlimited number of molecules**. **(Figure 13)**. This process has been used to test several GAGs and several BMPs in parallel, and in the future, it will be possible to adapt it to any type of surface functionalization for different types of approaches. We are currently trying to exploit this discovery and make it accessible to other laboratories by creating a start-up company. The upscale of surface functionalization is followed by an **automated workflow of image acquisition and analysis**. For that, we adopt an automatized imaging routine thanks to a high content microscope, to acquire multiple images per well and to run a macro to analyze the intensity of the transcription factors translocated into cell nuclei (Fitzpatrick, Fourel et al. 2017, Sales, Khodr et al. 2021) **A.3**. As shown in **Figure 13**, we can quantify the translocation of transcription factors to the cellular nuclei and the cell area by immunofluorescence. The high content microscope acquires multiple fields of view per well and the software can perform batch analysis of the intensity of the staining and/or of the cell area.

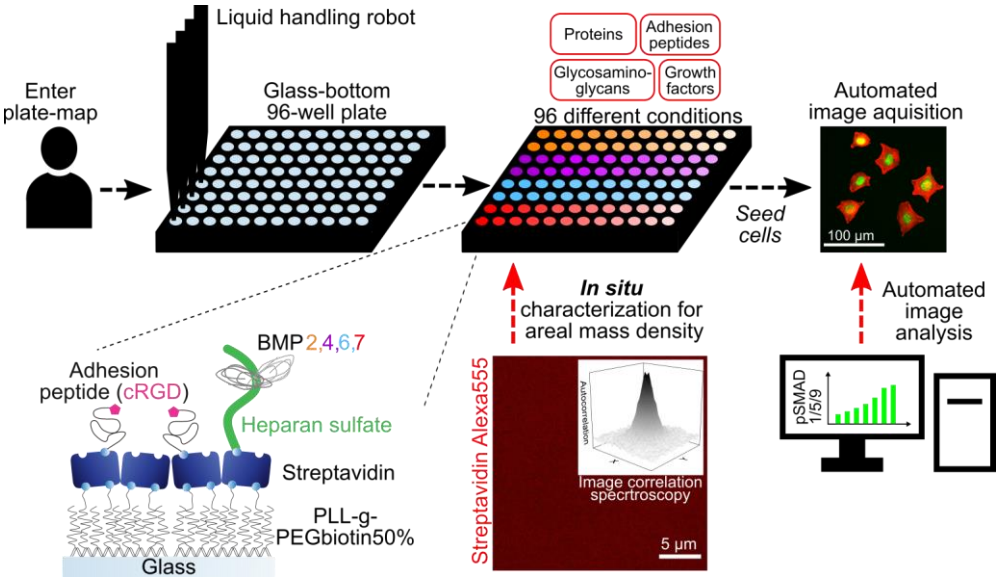

Figure 13 Schematic of automated platform fabrication, surface characterization and cellular studies. *The user communicates the plate-map corresponding to the experimental plan to the liquid handling robot. Glass bottom 96-well plates are then automatically functionalized with different biomimetic platforms co-presenting cellular adhesion ligands, glycosaminoglycans and GFs. In this work, streptavidin binds to the linker PLL-g-PEGbiotin50%. Then, biotinylated cRGD and biotinylated heparan sulfate bind to streptavidin and BMP2,4,6 or 7 adsorb to heparan sulfate. The areal mass density of fluorescence labelled molecules such as StreptavidinAlexa555 is characterized in situ using image correlation spectroscopy. Cells are seeded on the platforms for biophysical assays using automated image acquisition and automated image analysis to quantify for example BMP-mediated SMAD1/5/9 phosphorylation inside the nucleus.*

3.1.3. In situ characterization with image correlation spectroscopy

To characterize the areal mass density of the molecules deposited by the liquid handling robot into the 96-well plate we applied the optical technique of **image correlation spectroscopy** (ICS) (**A.2**) (Sefkow-Werner, Migliorini et al. 2022). The basic principle of that technique is that signal originating from a confined region within the image, corresponding to the Point Spread Function (PSF) of the microscope, exhibits statistical fluctuations, since this PSF region does not always include the same number of molecules due to spontaneous fluorescence intensity fluctuations of a sample. The relative amplitude of these fluctuations provides an estimation of the average number of molecules in the PSF region and hence the concentration or density. This technique is not novel but has been applied for the first time to characterize biomaterials. In collaboration with A. Delon at Liphy (UGA) we further developed ICS to **precisely measure the number of labelled molecules on 2D biomaterials**. The spatial autocorrelation of confocal images reveals intensity fluctuations and its amplitude indicates the number of molecules per point spread function.

With ICS we quantified the areal mass density of SAv-Alexa555 and biotin-Atto565 (b-Atto) since SAvAlexa binds as well as SAv to the PLL-g-PEGbiotin50% and the bAtto can bind to the free biotin pockets present on the SAv. Therefore, it simulated the cRGD sequentially bound to the SAv. Confocal images were analyzed using the principle of ICS as described elsewhere (Costas, López-Puente et al. 2015, Sefkow-

Werner, Migliorini et al. 2022). In summary, the confocal images were split up into 64 sub-images and the spatial autocorrelation function (ACF) was calculated for each sub-image. This ACF reveals **intensity fluctuations and its amplitude is inversely proportional to the number of molecules in the observation area** (Petersen, Höddelius et al. 1993). The observation was defined by the waist of the point spread function specific for each microscope, in our case around 230 nm. Since molecules usually carry an unknown number of labels following a distribution, the average number of labels per molecule needs to be determined. For that, an additional **photobleaching routine was applied**(**A.2**) (Sefkow-Werner, Migliorini et al. 2021) and the result was used to correct the number of molecules by the factor 1.2 for SAvAlexa and 1.09 for bAtto.

Confocal images were acquired to quantify the mass density *in situ* using ICS (**Figure 14**). Representative 63x confocal images showed no systematic defect at the microscale and a **homogeneous functionalization** of the platforms (**Figure 14a**). The absolute quantification of the adsorbed mass with ICS *in situ* gave a value for SAvAlexa of 336 ± 34 ng/cm^2 and of 334 ± 45 ng/cm^2 for SAvAlexa/cRGDmix condition. Then, 0.79 ± 0.19 ng/cm^2 bAtto bound to SAv. To note: bAtto binding could not be measured by QCM-D and neither SE due to its low molecular weight and hence low adsorbed mass.

We can conclude that **the ICS provides comparable areal mass density with respect to the SE measurement** (**Figure 12e**)(343 ± 25 ng/cm^2), therefore validating this technique for future characterization of biomaterials.

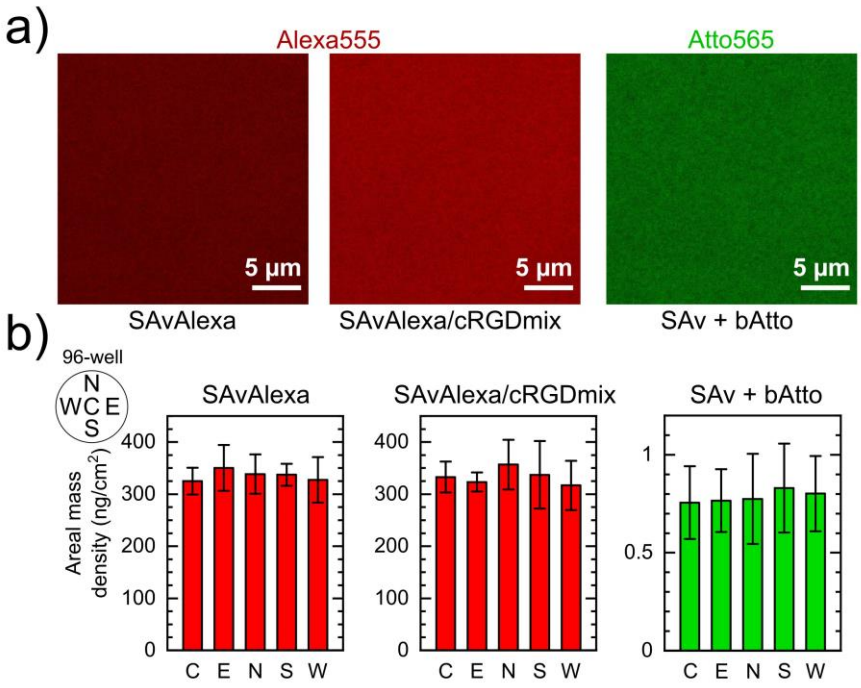

Figure 14: In situ characterization for areal mass density of SAvAlexa, SAvAlexa/cRGDmix and SAvAlexa + bAtto*. a) Representative 63x confocal images taken inside a single well. b) Graphs*

showing the areal mass density measured via ICS at five different positions per well (n=3 wells, 2 replicates, error bars = SD)

3.1.4. Comparison of cellular responses when treated with different BMPs

Thanks to the help of a M2 student supervised by J. Le Pennec and J. Sefkow-Werner (Bertin Ndayishimiye) we adopted the high content fabrication protocol to study the dose response of C2C12 cells to four different BMPs in parallel by comparing the EC_{50} values. With the liquid handling robot, we functionalized a 96-well plate with 42 different conditions in technical duplicates presenting the BMPs either in solution (sBMP2,4,6,7) or adsorbed on iHS (aBMP2,4,6,7). We quantified SMAD1/5/9 phosphorylation by immunofluorescence with automated microscopy and image analysis (**Figure 15a**).

For all sBMP2,4,6,7 and aBMP2,4,6,7 conditions, we observed a BMP dose-dependent response in C2C12 cells (**Figure 15c**). The sBMP2,4,6,7 concentration of 1 µg/ml, which in all cases represented an upper plateau p-SMAD1/5/9 signal, was significantly higher than the negative control. Also, when comparing the aBMP2,4,6,7 conditions, the comparable concentration of 3, 5, 10 and 5 µg/ml respectively induced a plateau of p-SMAD1/5/9 signal, which was significantly higher than the negative control and comparable to the plateau induced by corresponding sBMP2,4,6 and 7.

EC_{50} was calculated from these curves, which corresponded to the BMP concentration for which the p-SMAD1/5/9 signal was about 50% of the plateau value. The results of the fits are summarized in **Table 1: EC50 values for sBMP2,4,6 and 7** and **aBMP2,4,6 and 7 on cRGD platforms compared to values of a similar study with C2C12 cells on tissue culture plates** (Hammers, Merscham-Banda et al. 2017). Values are given as mean ± SD over three replicates.**sBMP2 thus was more potent to induce SMAD1/5/9 phosphorylation** than sBMP4,6 and 7 which were comparable to each other. In addition, aBMP2 was more bioactive than aBMP4 and aBMP7 but for aBMP6 the fit for the dose response curve failed because at high aBMP6 concentrations the plateau of the p-SMAD1/5/9 response was not reached. Hammers et al. measured in a similar experiment with soluble BMPs EC_{50} values for sBMP2,4,6 and 7 **Table 1** (Hammers, Merscham-Banda et al. 2017).

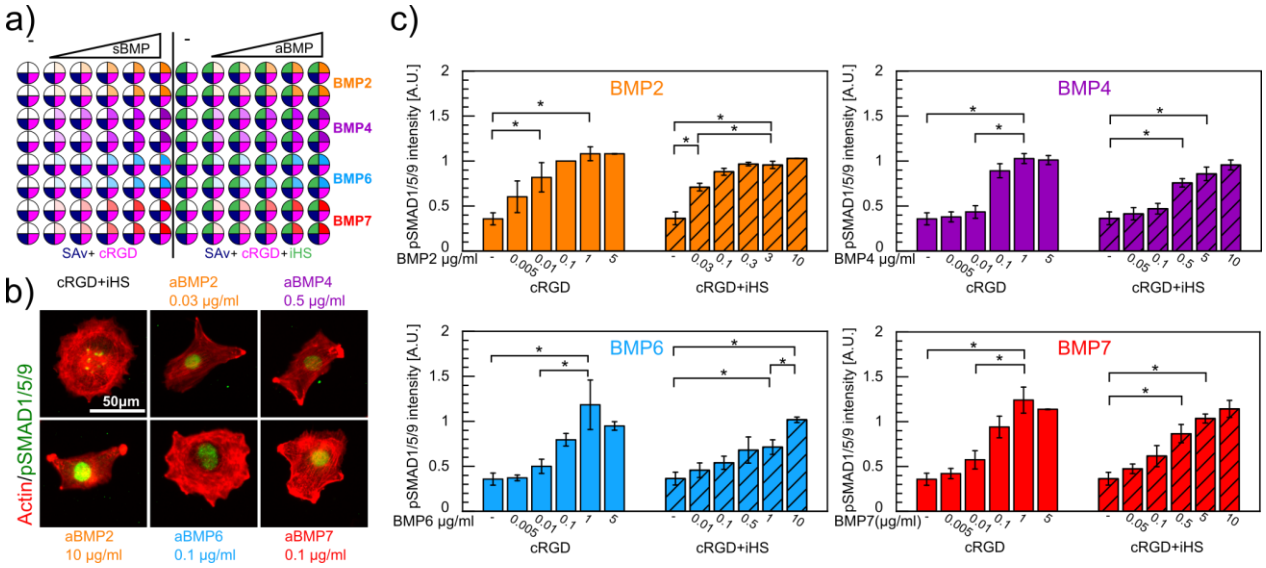

Figure 15: Automated high content study of C2C12 cell response to sBMP2,4,6,7 and aBMP2,4,6,7. *a) Schematic of a 96-well plate with 42 different conditions in duplicates fully functionalized by the robot. sBMP2,4,6 and 7 in different concentrations were added by hand into the cell media when cells were plated. b) Representative and equally treated images of C2C12 cells plated inside the 96-well plate functionalized by the robot, fixed after 90 min and labelled for actin and pSAMD1/5/9 translocated into the nucleus. BMP concentrations were chosen to represent a condition close to the EC_{50} concentration c) Graphs show the quantification of p-SMAD1/5/9 translocated into the nucleus. Values were normalized to the sBMP2 condition at 0.1 µg/ml. Each experiment was the average of two wells and the error bars represent the SEM. Significance was tested with Mann-Whitney and p <0.05 for n = 3. The aBMP2,4,6 and 7 concentrations represent the concentrations used for the incubation on iHS and don't permit a quantitative conclusion on the amount of aBMP2/4/6/7 eventually adsorbed on iHS.*

Table 1: EC_{50} values for sBMP2,4,6 and 7 and aBMP2,4,6 and 7 on cRGD platforms compared to values of a similar study with C2C12 cells on tissue culture plates *(Hammers, Merscham-Banda et al. 2017). Values are given as mean ± SD over three replicates.*

	EC50 (µg/ml)		*EC50 (nM)*		*EC50 (nM)*
	sBMP	*aBMP*	*sBMP*	*aBMP*	*sBMP*
BMP2 (26 kDa)	0.007 ± 0.001	0.028 ± 0.007	0.269 ± 0.038	1.08 ± 0.27	0.033 ± 0.002
BMP4 (24 kDa)	0.027 ± 0.003	0.227 ± 0.033	1.13 ± 0.13	9.46 ± 1.38	0.010 ± 0.0004
BMP6 (30 kDa)	0.035 ± 0.022	fit failed	1.12 ± 0.73	fit failed	1.3 ± 0.032
BMP7 (26 kDa)	0.042 ± 0.011	0.294 ± 0.150	1.62 ± 0.42	11.3 ± 5.77	5.9 ± 0.22

3.2. Conclusions

The automation of the platforms functionalization with liquid handling robot drastically improved our experimental routine since it is now possible to functionalize in parallel 3 entire 96-well plates with different conditions and therefore to present different peptides, GAGs or GFs to cells and to reveal cellular responses. The automated functionalization is providing comparable mass adsorption to what we expect by SE measurements (revealed by ICS technique) and the platforms coating is homogeneous. Automated analysis of the cellular responses is today based on immunofluorescence and in particular on the translocation of transcription factors to cellular nuclei. In the future, there will be the need to improve the type of readouts that

can be performed on 96-well plates such as immunofluorescence of proteins in the cytoplasm or at the cell membrane, cellular protrusion or even qPCR and western blot.

3.3. Perspective for the coming years

In collaboration with Prof. Antoine Delon at Liphy in Grenoble we aim at further improving the applications of the photobleaching ICS technique to characterize the surface amount of molecules adsorbed on biomaterials. This technique can be further developed and transferred to different applications. Simplification of the analysis software to facilitate a user-friendly toolbox would help to propagate these methods to research facilities not specialized on ICS methods. For biomimetic streptavidin platforms, quantification of labelled PLL-g-PEGbiotin50% would allow comparison of this basal layer formation between *in situ* and *ex situ* surfaces as well as with values found in the literature (Morgenthaler et al., 2006). Consequently, quantification of labelled aBMP2 adsorbed on iHS is of great interest, since the low surface concentrations identified as critical for aBMP2-mediated SMAD1/5/9 phosphorylation in C2C12 cells (**Figure 15**) could not be detected by SE or QCM-D. However, this information is key to draw absolute conclusions about the influence of aBMP2 dose.

4. Deciphering the role of heparan sulfate and chondroitin sulfate on BMP2 bioactivity

PEOPLE INVOLVED: Dr. Jean Le Pennec (PhD), Dr. Julius Sefkow-Werner (PhD), Mr. Amaury Guibert (L1, L2 bachelor student), Ms. Lea Aubert (L3 bachelor student) and Dr. Elisa Migliorini.

Collaborators: Dr. Romain Vivès, Dr. Anne-Christine Severmann (Postdoc) and Prof. Andrea Vortkamp

FUNDING: ANR-GlyCON (E.Migliorini), IDEX-IRS 2018 (E. Migliorini)

Heparan sulfate (HS) carrying proteoglycans (HSPGs) are present at the cellular surface and at the pericellular matrix (here called for simplicity ECM) of all vertebrate cells (Iozzo and Schaefer 2015). They play critical roles in regulating the distribution and activity of many extracellular proteins including GFs like BMPs. Mutations in HS synthesizing enzymes lead to severe developmental defects in mice and distinct genetic disorders in human (Wuyts, Van Hul et al. 1998) supporting the importance of HS as a regulator of development and tissue homeostasis. One of the best investigated HS related human disorders is multiple osteochondroma (MO), which is caused by clonal loss of HS in single chondrocytes leading to the formation of the osteochondromas (Bovee, Cleton-Jansen et al. 1999, Legeai-Mallet, Rossi et al. 2000, Hall, Cole et al. 2002, Reijnders, Waaijer et al. 2010). Genetic alteration of the glycosyltransferases of the exostosin family (EXT1 and EXT2) enzymes, which elongate HS chains, are responsible for the MO disease. In mice models, heterozygote mutants of EXT2 develop exostoses (like in MO) and homozygote mutants of EXT1

and EXT2 fail to gastrulate (Lin, Wei et al. 2000). Skeletal dysplasia is another pathology induced by mutations in the proteoglycans/glycosaminoglycan biosynthesis (Superti-Furga and Unger 1993). One hypothesis well investigated to explain the link between GAGs and these diseases is their involvement **in finely regulating the signaling and the spatial distribution of morphogens.** Relevant morphogens involved in the skeletal developments are hedgehogs (Hh), Wingless-related integration site (Wnt), fibroblast growth factor (FGF) and BMPs. While Hh signaling is negatively regulated by the level of HS in chondrocytes (Koziel, Kunath et al. 2004), results on how the loss of HS affects BMP signaling (up-regulation in osteochondromas, down-regulation at chondrocyte condensation stages) are contradictory (Matsumoto, Matsumoto et al. 2010, Huegel, Enomoto-Iwamoto et al. 2015). The **role of cell surface *vs* extracellular HS may therefore be different,** but this hypothesis needs a systematic investigation by adopting cells with and without cell surface HS on supports presenting HS.

Besides HS, CS is highly abundant in the ECM of chondrocytes. Although often considered as a structural component, CS binds different GFs like BMP2 (Hintze, Samsonov et al. 2014). **However, the function of CS as a regulator of growth factor signaling** in particular in relation to HS **is, so far, little understood**. Our collaborators at the University of Duisburg-Essen have characterized the composition of GAGs on mice with reduced level of HS ($Ext^{gt/gt}$) and on 6-O HS sulfotransferases ($Hs2st1^{-/-}$) mutants. They have shown an **increase on the CS levels** on both mutant mice. This demonstrates that not only a reduced HS synthesis but also an altered HS structure leads to increased levels of CS in mammalian tissues and suggests a compensation of the HS compromised activity by CS (Bachvarova, Dierker et al. 2020).

The understanding of GAG-protein interactions is a key step to comprehend the full picture of the GAG-mediated regulation of proteins bioactivity. BMP2 has a well-demonstrated high affinity for HS (Kisiel, Klar et al. 2013, Migliorini, Horn et al. 2017, Billings, Yang et al. 2018) and Hep (Ruppert, Hoffmann et al. 1996), which could be related to the important functions of HSPGs in the regulation of bone development *in vivo*. However, the **affinity values** reported in the literature **deserve to be clarified**, as they are subject to variations of several orders of magnitude, possibly related to different experimental setups or GAG sources. Furthermore, the binding affinities between different GAGs have not been directly compared within the same study.

4.1. Major scientific achievements

This topic was the major subject of my research in the last 3 years. To realize it, I obtained an ANR-DFG grant in 2020 in collaboration with Andrea Vortkamp in Essen, Germany. Two PhD students, Julius Sefkow-Werner (until 2021) and Jean Le Pennec contributed to this work and to the supervision of master and bachelor students. Here, the reported PhD work of Jean Le Pennec, is part of a publication titled “Glycosaminoglycans exhibit distinct interactions and signaling with BMP2 according

to their nature and localization" under submission to Carbohydrate Polymers. The method he developed to avoid the non-specific binding of BMP2 to our biomimetic platforms will be published in BioRXiv. The results obtained by Julius Sefkow-Werner on the role of HS localization on cell adhesion will be part of a common publication with the group of A. Vortkamp.

4.1.1. BMP2 binding to different GAGs: determination of the binding affinities

It has been previously proposed that BMP2 binds *via* its Hp/HS binding site to other sulfated GAGs such as chondroitin sulfate (Hintze, Samsonov et al. 2014). The CS disaccharide unit differs from HS, as the disaccharide unit comprises an N-acetyl galactosamine and a glucuronic acid. CS can also be sulfated in different positions, as shown in **Figure 16a**, giving rise to different CS namely CS-A, B (or DS), C, D and E. In literature, we noticed a lack of information on the binding affinities between GAGs and BMP2 and a huge variation on the reported biding affinities due to the different methods used or immobilization strategies.

We therefore decided to study the binding of BMP2 to CS and to Hyaluronic Acid (HA), a non-sulfated GAG used as negative control, using surface sensitive techniques. Specifically with QCM-D we study the binding efficiency of each GAG and its ability to immobilize BMP2. Using SE, we measured the total amount of BMP2 bound to each GAG and the binding affinities using biolayer interpherometry (BLI).

The GAGs HS, CS-A, D, E, DS and HA are biotinylated at their reducing end by oxime ligation as previously reported (Thakar, Migliorini et al. 2014)**A.18**. QCM-D measurement showed that all the GAGs were successfully biotinylated since they bind to the SAv monolayer (**Figure 16b**). The different frequency shift decreased proportionally to the molecular weight of each GAG, HS being the shortest and HA the longest GAG. The binding of BMP2 at 5 µg/mL was varying depending on the GAGs, as indicated by the distinct frequency shifts. BMP2 bound more to CS-D followed by CS-E, DS, HS and then CS-A. On the contrary, BMP2 did not bind to the non-sulfated HA (**Figure 16c**). BMP2 dissociated more during rinsing on CS and DS with respect to HS (**Figure 16d**). As previously observed, the binding of BMP2 to HS triggered a negative shift of the dissipation, likely indicating a cross-linking of HS chains mediated by BMP2 (Migliorini, Thakar et al. 2015, Migliorini, Horn et al. 2017)**A.16, A.12**. Here, we showed that the BMP2 binding on CS and DS triggered the same effect (**Figure 16f**).

The areal mass density of GAGs adsorbed on SAv measured by SE was small compared to the QCM-D mass. In fact, GAG layers are highly hydrated and with QCM-D we measured the hydrated mass, whereas with SE we calculated the optical mass of the molecule (**Figure 16g**). At saturation, an **equal amount of BMP2 was adsorbed to the different GAGs** apart to HA where the binding was small but detectable in comparison to QCM-D measurement. We finally measured the binding affinities between immobilized GAGs and BMP2 by using BLI technique (**Figure 16h, i**). Further

details on the BLI technique can be found in ANNEX I: CHARACTERIZATION TECHNIQUES. BMP2 bound to HS with the highest affinity (KD of 57±7 nM) followed by CS-D (KD of 400±43 nM). The other CS types and DS exhibited affinities in the low µM range (2.5±0.4 µM and 1.4±0.4 µM for CS-E and DS, respectively), or above 70 µM for CS-A (**Figure 16j**).

QCM-D, SE and BLI data gave different results, with respect to BMP2 adsorption to HS and the other GAGs. It was less pronounced on QCM-D and SE compared to BLI. There are several differences between the techniques based on the different functionalization of the sensors : i) The GAG layer on the BLI biosensor was less dense compared to the quartz crystal of the QCM-D and the SiO_2 coated silicon wafer of the SE. Surface density may be critical for GF binding and capture – the role of GAG density on BMP binding will be addressed in future studies. (ii) the BLI biosensor was immersed into a BMP2 solution, while the solution of BMP2 passed from an Eppendorf tube to a surface inside the fluid chambers of the QCMD and SE and therefore interacted with other plastic components that may promote protein aggregation. (Chouchane, Frachon et al. 2022). In the future, we may try to compare the two immobilization strategies to better understand the reason for the difference between the three techniques.

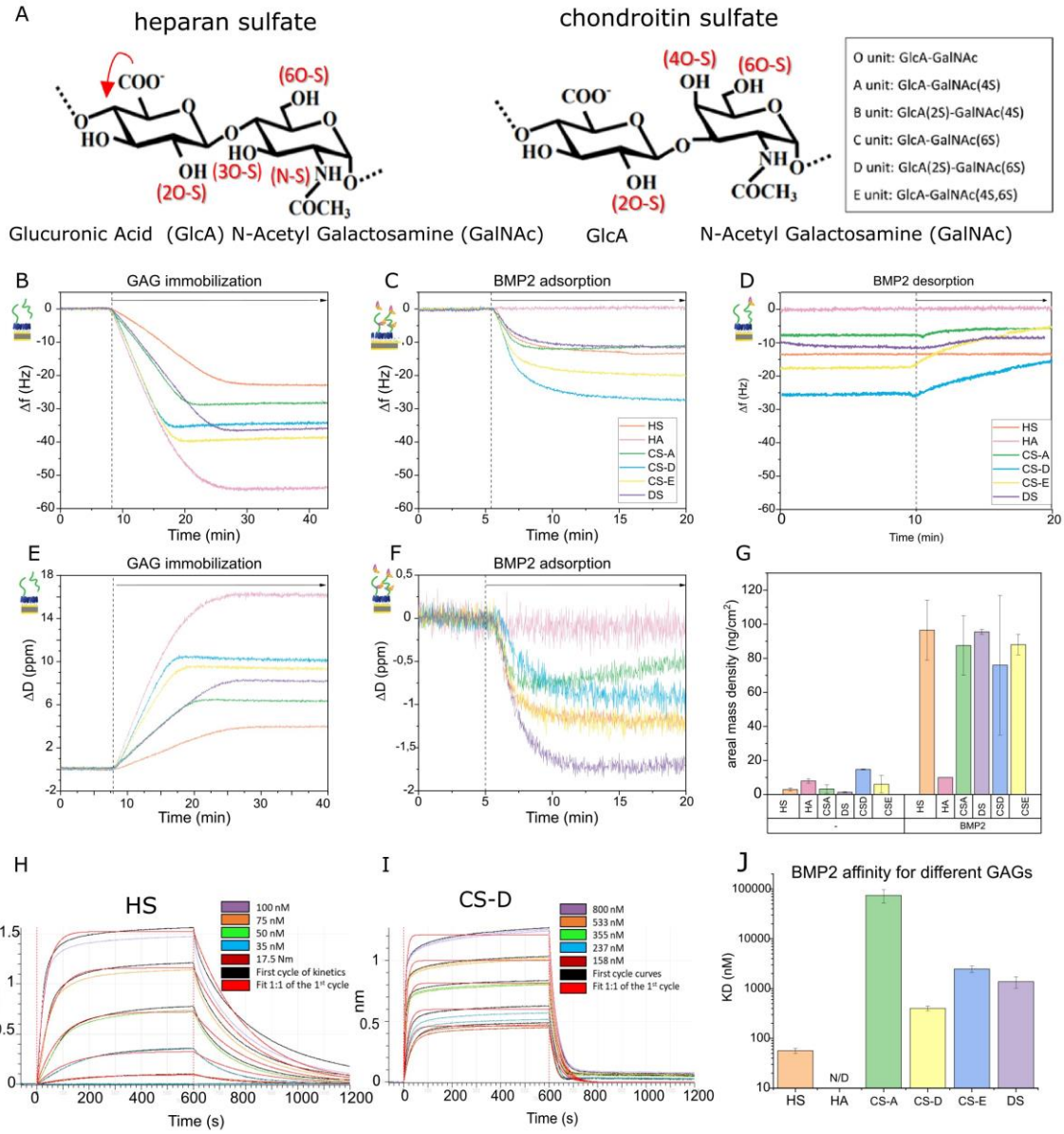

Figure 16: BMP2 binds to CS but with a lower affinity with respect to HS. *a) Heparan Sulfate and Chondroitin Sulfate- disaccharide unit structure. HS is composed by Glucuronic acid (GlcA) and N-acetyl glucosamine (GlcNac). In red the different sulfation positions are represented: N-sulfation, 6-O sulfation and 3-O sulfation of the GlcNAc, epimerization of the GlcA to iduronic acid (IdoA) and 2-O sulfation of the IdoA. In parenthesis,the carbon number on the hexose, the linkage atom and S corresponding to the sulfation group SO^{3-} are reported in order. In the scheme, the different units of CS sulfation are described on the right and sulfation positions are indicated in red on the scheme. b-f) representative QCM-D measurements of the immobilization of different GAGs (HS, HA, CS-A, D and E and DS) to SAv monolayer (b,e) and of BMP2 on each GAG (c,d,f). Frequency shifts (b,c,d) and dissipation shifts (e,f) are reported. The injection is indicated with an arrow the rest of the time Hepes buffer 150 mM NaCl is injected. BMP2 bound more to CS-D and E and did not bind to the unsulfated HA. g) Plot of SE measurements of GAG biding to SAv and of BMP2 binding to GAG (n=3). h,i) BLI kinetic sensograms of BMP2 injected at different concentrations on HS and CS-A films for 200 s. The curves were fitted with a 1:1 Langmuir binding model on the full association and 40 s of the dissociation (red curves) to obtain the kinetic parameters of the interactions. j) The biding affinities of BMP2 (Kd value in nM) to all the GAGs n=3.*

4.1.2. Role of extracellular and cell surface GAGs in early BMP2 signaling

After characterizing the binding of BMP2 to the different GAGs, we investigated the

cellular signaling upon BMP2 presentation *via* the different GAGs immobilized on SAv monolayers as a mimic of the ECM. For this purpose, we used gold surfaces glued on bottom-less 96-well plates and functionalized by the liquid handling robot as described previously (Sefkow-Werner, Le Pennec et al. 2022)**A.1**. Before performing functional studies, we had to readapt the co-functionalization protocol used in the team because few cells adhered to CS and HA platforms. In fact, the CS and HA chains are longer than the HS chains and therefore hid the cRGD peptides needed for cell adhesion (data not shown). By QCM-D, we defined a new protocol for the functionalization of the platforms by increasing the injection time of the cRGD peptide, thus reducing the amount of GAGs on the surface to increase the space between them. This allowed the access of integrins to the cRGD peptides, in order to obtain comparable cellular adhesion between the different platforms. In addition, we noticed that BMP2 binds unexpectedly to some component of the biomimetic platforms or non-specifically to the support material. This binding was not detectable with QCM-D as previously reported (Migliorini, Horn et al. 2017, Sefkow-Werner J., Le Pennec J. et al. 2022)**A.12, A.8** but it generated a strong phosphorylation of SMAD 1/5/9, as strong as the BMP2 presented by HS (**Figure 17a**). It was therefore impossible to distinguish an effect of GAGs on BMP2 presentation and signaling (**Figure 17b**). After a considerable work, we determined the better conditions to significantly reduce the non-specific binding of BMP2 by adding an extended passivation protocol to the surface with BSA and trehalose (**Figure 17c** and **d**). By immunofluorescence we detected the binding of BMP2 with an anti-BMP2 antibody. By passivating the platforms after SAv binding with a mixture of BSA and trehalose we observed a significant decrease of non-specific binding of BMP2, which was further reduced by incubating BSA/trehalose BMP2 solution – the latter experimental condition however was reducing the binding of BMP2 to HS (**Figure 17c**). Cellular data validated the new passivation protocol, as we observed that p-SMAD 1/5/9 levels were higher on HS compared to the cRGD condition with non-specifically bound BMP2 only when the platform was previously passivated with BSA-trehalose (**Figure 17d**). In addition, gold-based platforms performed better than glass-based platforms, suggesting that non-specific binding may be more pronounced on glass than on gold.

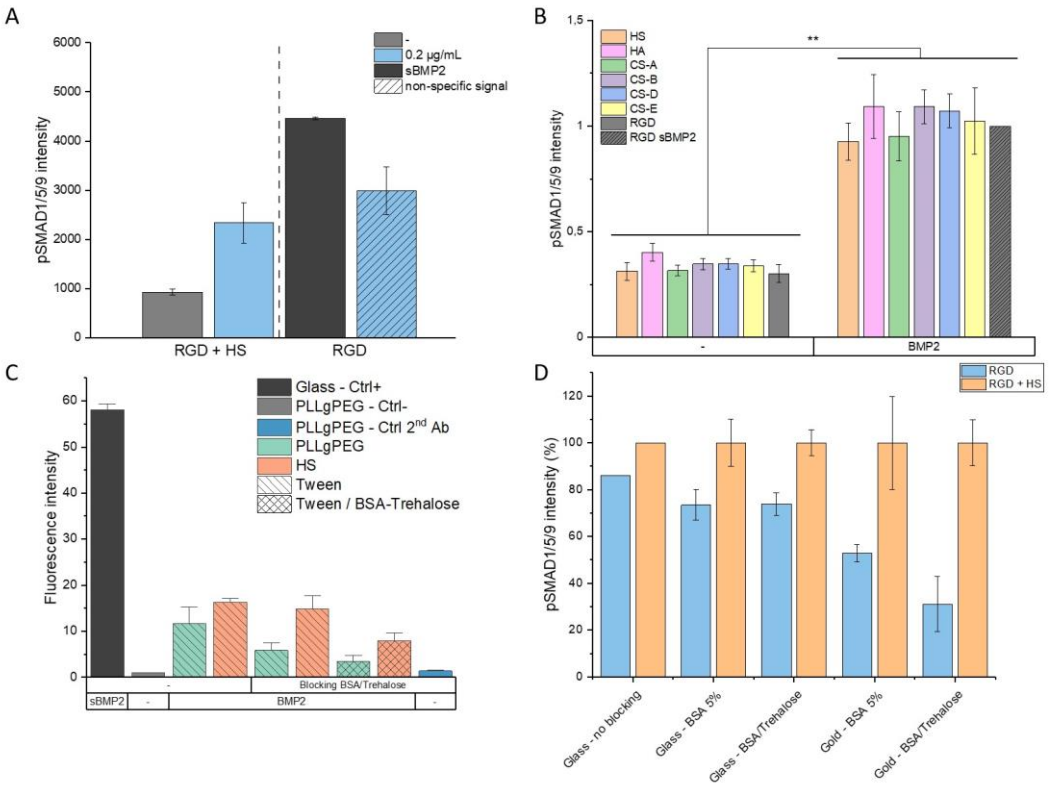

Figure 17: BMP2 binds non specifically to the biomimetic platforms and an extended passivation protocol is needed to prevent this non-specific binding. *a) Plot of the p-SMAD 1/5/9 mean nuclear intensity on gold-based platforms. The signaling induced by the non-specific binding of BMP2 to the platforms is labeled with stripes. b) Plot of the p-SMAD 1/5/9 mean nuclear intensity on gold-based platforms decorated with different GAGs and with or without BMP2. The difference to the negative control is significant but there is no differences between the GAGs, probably due to the non-specific binding of BMP2 to the platform. c) Plot of the fluorescence intensity of anti-BMP2 antibody on glass platforms which has been (or not) passivated with the mixture BSA/trehalose before and during BMP2 incubation. d) Histogram showing the nuclear intensity of p-SMAD1/5/9 of CHO cells plated to glass and gold based platforms with different type of passivation (BSA alone and BSA/trehalose) before BMP2 injection.*

Having demonstrated that the extended passivation procedure reduced the non-specific binding of BMP2 to the biomimetic platforms, we investigated the role of the type of GAG and its localization (cell surface or ECM) on BMP2-mediated SMAD1/5/9 phosphorylation. For this purpose, Chinese hamster ovary wild-type cells (CHO WT), were plated 1.5 h on biomimetic platforms presenting different GAGs with bound BMP2 and the SMAD1/5/9 phosphorylation was tested by immunofluorescence. We observed that the **p-SMAD1/5/9 levels were significantly higher on iHS presenting platforms** with respect to the other GAGs with a slightly but not significant increase of the SMAD1/5/9 phosphorylation on CS-D with respect to the other GAGs (**Figure 18a, b**). In line with the affinity studies presented previously, we can imagine that in the ECM BMP2 binds mainly to HS with respect to the other GAGs. However, it is not clear what happens to BMP2 between its interaction with ECM HS and p-SMAD1/5/9 phosphorylation, and in particular **what is the role of cell surface GAGs in BMP2 signaling**. Our collaborators in the University of Essen have shown an inhibition of SMAD1/5/9 phosphorylation when chondrocytes where treated with chondroitinase (Bachvarova, Dierker et al. 2020). We addressed this subject by treating mutant CHO

cells with sBMP2. We used either mutant CHO pgsD-677 (here called CHO HS KO, lacking the EXT1 enzyme responsible for HS chain elongation) and the pgsA-745 cell line (here called HS/CS KO, lacking the xylotransferase responsible for catalyzing the first sugar transfer in GAG synthesis), as previously characterized by Lidholt et al.(Lidholt, Weinke et al. 1992). In the same study it has also been shown that CHO HS KO presented 3 to 4 times more CS than the CHO WT, probably due to a compensation mechanism. We also measured an up to 6 fold increase of csCS on CHO HS KO compared to CHO WT. We observed that CHO HS KO cells presented a higher p-SMAD1/5/9 level with respect to CHO WT while on CHO HS/CS KO SMAD1/5/9 phosphorylation was at the level of the CHO WT. This result could only be explained by a **positive effect of csCS, which promotes BMP2 signaling, and perhaps also by a possible negative role of csHS, which may inhibit BMP2 bioactivity**. The affinity data may explain this mechanism; indeed, CS with lower affinity for BMP2 may bind transiently BMP2 and transfer it to the BMP receptors (BMPRs), whereas HS with higher affinity may sequester BMP2 and inhibit its interaction with the BMPRs.

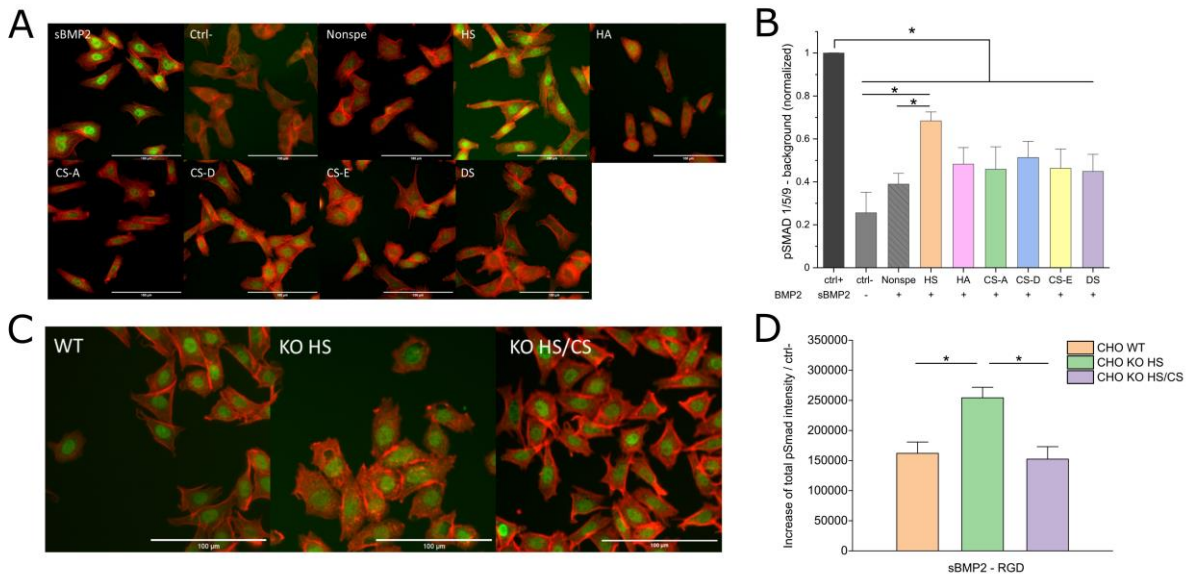

Figure 18: GAGs have different regulatory roles on BMP2 signaling based on their localization. Cell surface CS improves BMP2 signaling. *A. Representative IF images of CHO WT cells after a 90 minute culture on the biomimetic platforms functionalized with different GAGs (extracellular) and BMP2, and stained for actin (red) and p-SMAD1/5/9 (green). Scale bar is 100 µm. Positive control corresponds to cRGD functionalized platforms (without GAGs) exposed to soluble BMP2 at 0.1 µg/mL (sBMP2) and the negative control to the cRGD platforms without BMP2 (ctrl-). The platforms harboring GAGs were incubated with 0.02 µg/mL of BMP2, which was rinsed before cell seeding. cRGD platforms without GAGs followed the same procedure, as a control of BMP2 non-specific binding (Nonspe). B. Corresponding mean fluorescence intensity of nuclear p-SMAD1/5/9 in wild type CHO cells. Values were normalized by the positive sBMP2 positive control (n=4). C. Representative IF images of CHO WT, KO HS and KO HS/CS cells cultured for 90 min on cRGD biomimetic platforms with or without sBMP2 at 0.1 µg/mL, and stained for actin (red) and p-SMAD1/5/9 (green). Scale bar is 100 µm. D. Corresponding total fluorescence intensity of nuclear p-SMAD1/5/9 in CHO WT, KO HS and KO HS/CS cells. For each cell type, the intensity value was plotted after subtraction of the negative control without BMP2 (n=4). Statistical significance between two conditions was tested with Mann-Whitney test and is represented with * for p ≤ 0.05.*

4.1.3. Role of HS localization on cell adhesion

In the literature, some studies suggested that csHS and extracellular HS have opposite roles in cellular adhesion: where extracellular HS was responsible for reduced adhesion (Lundmark *et al.*, 2001) but only cells with csHS were able to adhere to surfaces containing only the heparin binding site (LeBaron *et al.*, 1988). For this purpose, CHO WT and HS KO cells, were plated on biomimetic platforms presenting cRGD with or without HS.

CHO WT and HS KO cells adhered after 75 min with a comparable cell number (**Figure 19a,b**). We observed that CHO HS KO cells were bigger than the CHO WT cells (**Figure 19c**). CHO WT cells were slightly more elongated than the CHO KO (**Figure 19e**) while no differences of compactness were measured. (**Figure 5f**). **CHO KO cells were systematically larger than CHO WT cells on cRGD platforms and less able to polarize**. Thus, we conclude that **csHS is important for proper adhesion and polarization**. To reveal the role of iHS on cellular adhesion we co-presented iHS with cRGD. CHO KO cells adhered much better compared to cRGD platforms (**Figure 19b** stripes). Quantification of cell area and ellipticity revealed a slightly reduced cellular area of CHO WT cells on iHS with respect to cRGD platforms. A less elongated phenotype (**Figure 19c, e**) and a decreased compactness indicated a more circular appearance on iHS platforms with respect to cRGD platforms (**Figure 19f**). We conclude that **iHS is not able to compensate the absence of csHS.** Indeed, there were no changes on cell area and ellipticity on cRGD + HS platforms. On the other way iHS seemed to have a negative effect on cell elongation and area for the CHO WT cells indicating that **csHS plays a cell autonomous role in cellular adhesion while an excess of extracellular HS may interfere with this process**.

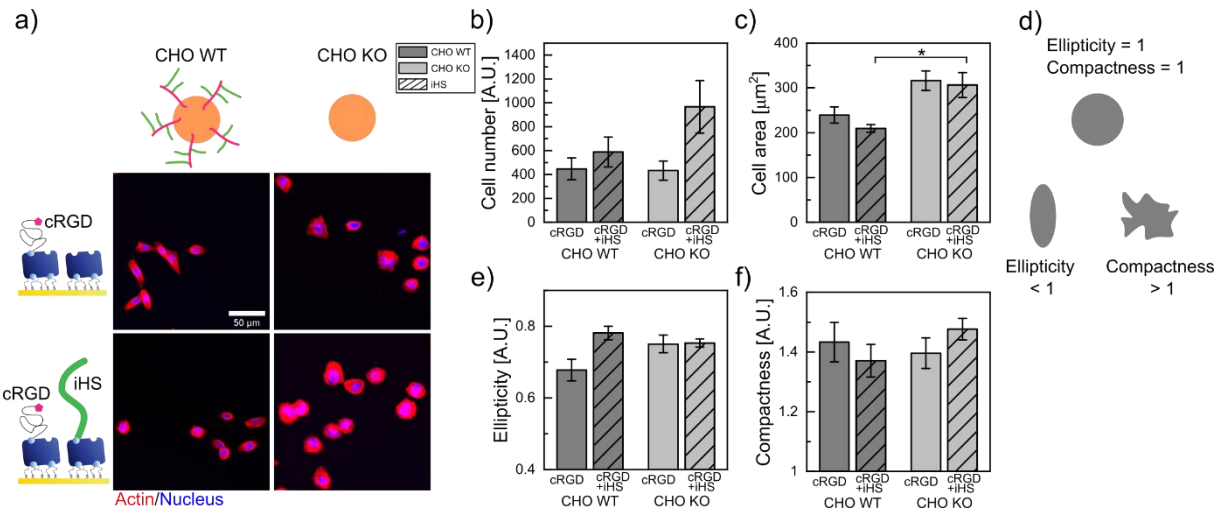

Figure 19: csHS promotes cell elongation on cRGD platforms and iHS negatively influences cell elongation and area in CHO WT cells. *a) Representative images of CHO WT and CHO KO cells plated on cRGD and cRGD + iHS platforms and fixed after 75 min. b) Absolute cell number quantification after rinsing 3 times with PBS and based on 20 20x images with an area of 0.44 cm² per image. c) Cell area quantification. d) Schematic of cell morphology parameters: Ellipticity measures the ratio between the short and the long axis of a fitted cell with 1*

being a perfectly circular cell and 0 being a line. Compactness measures the mean square distance of all pixels to the centroid with the value 1 representing a perfectly round cell and higher values irregularities at the perimeter. e) Ellipticity quantification f) Compactness quantification. SB = 50µm, Values in graphs are mean ± SEM of n ≥ 4 experiments with 2 independent replicates per experiment. Significance was tested with non-parametric Mann-Whitney test and p < 0.05 was considered significant (*).

4.1.4. Role of HS length and sulfation pattern on HS-BMP2

Several lines of evidence demonstrate that specific HS-sulfation motifs (the number and distribution of *N*- or *O*-sulfate groups along the HS chain) work as molecular recognition elements for distinct GFs (Grobe, Ledin et al. 2002, Zhang, Wang et al. 2016) and that the interaction determines the bioactivity of the GF. However, in the absence of a systematic HS sequencing methodology, **the precise HS structure that mediates these interactions has remained largely unknown**. Furthermore, the impact of alterations in the HS structure and the overall level of HS sulfation on the HS–GF interaction have not been systematically investigated nor have such interactions been related to the bioactivity of the GFs. The molecular basis of the interaction of these GFs with HS is still unknown and requires a **systematic investigation of how the HS structure determines the interaction and, subsequently, their bioactivity.**

To find the HS structure able to control the BMP2 bioactivity we first needed to find the minimal length of HS-derived oligosaccharides with a degree of polymerization (called HS-dps) able to bind BMP2. Shorter sequences will permit an easier characterization of the sulfation pattern *via* ion-exchange HPLC. HS-dps were generated in R. Vivès group at IBS by extensive digestion of the polysaccharide chains with heparinase III, an enzyme that specifically cleaves non-sulfated regions of HS, thereby releasing intact sulfated domains. HS can indeed be sulfates at the 3 or 6-O position (GlcNAc(3S) and GlcNAc(6S) respectively) and at the N- position of the GlcNAc (GlcNS) and at the 2-O position of the IdoA (IdoA(2S)) (**Figure 16**a). The resulting mixture of HS fragments was first resolved by size-exclusion chromatography, leading to size-uniform oligosaccharide fractions from dp2 to dp18. We first proved by QCM-D (Error! Reference source not found. **20a**) that **BMP2 binds to HS-dps as short as HS-dp4**. Furthermore, the phosphorylation of SMAD 1/5/9 was up-regulated in cells cultured on BMP2 presenting platforms (**Figure 20b,c**) indicating that BMP2 is bioactive on short tetrasaccharides. Smith et al., 2018 (Smith, Murali et al. 2018) performed a indirect competition assay to identify the minimal length of HS needed for BMP2 binding, but did not detect binding to HS-dp4. We have preliminary evidence that our direct assay is more sensitive to detect GF binding compared to other state of the art methods.

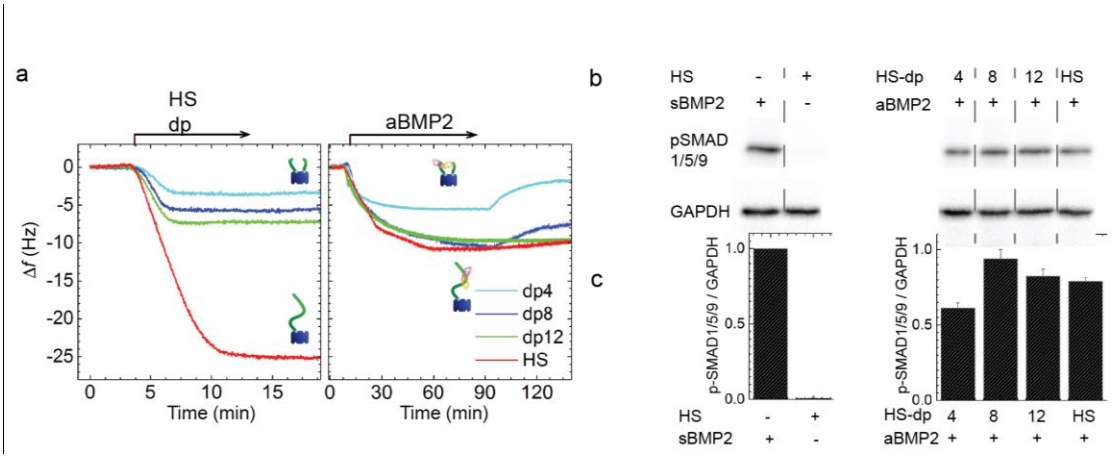

Figure 20: BMP2 can bind to short HS oligosaccharides as short as HS-dp4 and induce p-SMAD1/5/9 signaling *a) QCM-D characterization of the binding BMP2 to of full chain HS and HS-dp of different length (dp4, 8 and 12). Frequency shifts are plotted over the time. Starting and duration of incubation steps are indicated by arrows; during the other times, surfaces were exposed to working buffer. b, c) C2C12 were plated on platforms characterized with QCM-D and lysed after 60 minutes. The expression of phosphorylated SMAD 1/5/9 has been analyzed by western blot and quantified relative to GAPDH expression (loading control) in panel c (n=3).*

The HS-dp4 and dp6 oligosaccharides were then further fractionated by Jean Le Pennec under the supervision of R. Vivès, according to charge using strong anion exchange HPLC (**Figure 21a**). This yielded 39 fractions of dp4 and 28 fractions of dp6 with distinct sulfation patterns. Some of these fractions (corresponding to the most abundant and well-defined peaks) have been biotinylated to measure their interaction with BMP2 by BLI (**Figure 21b**). Disaccharide analysis was also performed with NaBH4 oligosaccharide reduction to identify the disaccharide reducing end (blocked by the reduction), thereby allowing to determine their sequences with high confidence (**Figure 21c)**. By BLI we proved that BMP2 bound with higher affinity to dp6 with respect to dp4 but the affinity was depending on the sulfation patterns (**Figure 21b**). Some specific fractions such as J, L, P, Q, Z and AC presented a KD similar to the full chain HS. The analysis of these fractions showed that the majority of those (J, P, Z and AC) present a **central tri-sulfated disaccharide IdoA(2S)-GlcNS(6S)** that may play a role in high-affinity binding of BMP2. However high affinities have been shown also for other sequences, which did not present this specific pattern. As for example in the dp6-L featuring five consecutive sulfate groups also presented a good affinity for BMP2.

Overall, **BMP2** seems to show a **certain binding plasticity regarding the sulfation types and sequences**, with no striking binding differences between various HS oligosaccharides. The use of molecular modelling is needed to better understand the molecular dynamics of BMP2 binding to these oligosaccharides.

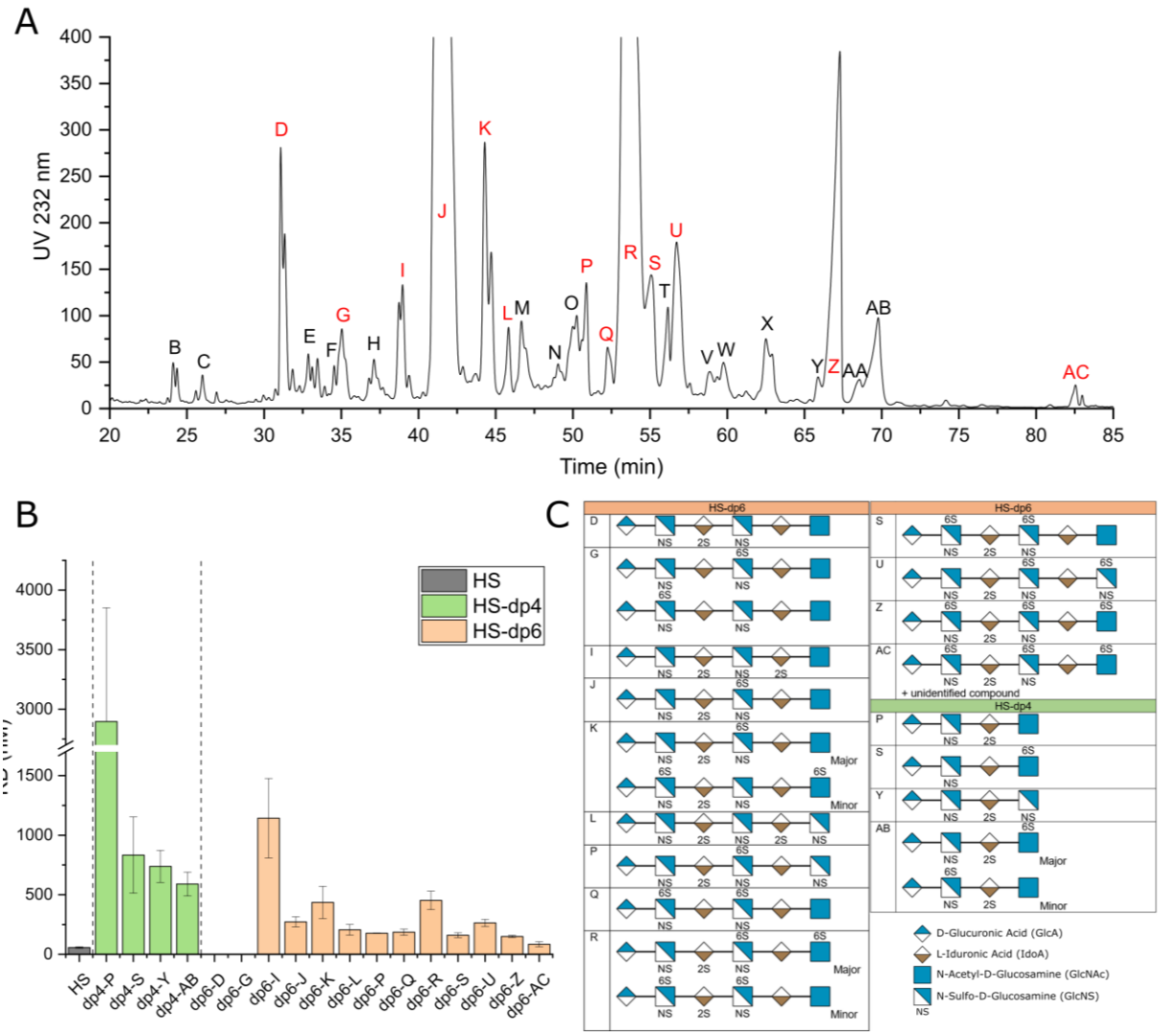

Figure 21: Library of HS-derived oligosaccharides with known sulfation pattern and affinity to BMP2. *a) Separation of HS tetrasaccharides by their charge by SAX- HPLC, b) Plot of the binding affinities between different HS-dp4 and dp6 oligosaccharides and BMP2 measured by BLI. c) composition of the different analyzed HS- shown according to the Symbol Nomenclature for Glycans (SNFG, Version 1.5). Legend for symbols is represented on the bottom right. Few compounds correspond to a mixture of co-eluting species the major and minor components are depicted. For dp6-G, two alternative structures are possible, while there was an unidentified compound in dp6-AC (potentially 3-O sulfated).*

4.2. Conclusions

Over the last four years, we have filled several gaps in our knowledge of the role of GAGs in BMP2 binding and signaling. Firstly, we determined the binding affinity constants between CS, DS, HA and HS within the same study - thus resolving the contradictory binding affinity values found in the literature. Secondly, we demonstrated that cell surface and extracellular GAGs do not play the same role, at least in the signaling of BMP2. In particular, extracellular CS does not improve BMP2 signallingsignaling, probably due to its low capacity to retain the GF, whereas cell surface CS enhances SMAD1/5/9 phosphorylation. On the contrary, extracellular HS seems to allow BMP2 signaling, whereas cell surface HS seems to inhibit it. Finally, we better understood the way in which HS interacts with BMP2 at the molecular level.

Indeed, we proved that there is not a precise sulfation pattern responsible for the binding of BMP2 to HS but there are some central sequences like the tri-sulfated disaccharide IdoA(2S)-GlcNS(6S) or the presence of sulfated groups along the entire oligosaccharide that guarantee a strong binding affinity. Our findings will help the understanding of pathologies such as the multiple osteochondromas where the increased BMP signaling has recently been identified as an early event in tumor formation and Palovarotene- an inhibitor of BMP signaling which reduces osteochondroma formation in mice (Inubushi, Lemire et al. 2018)**.** How loss of HS increases BMP signaling remained unrecognized. **Now we hypothesize that the loss of HS may enhance the csCS which, having a small affinity for BMP2, can facilitate the transport of BMP2 to its receptor**. Our findings are also important for the design of GAG-based biomaterials to be able to more closely mimic the specific properties of the ECM for medical applications, for example, to control multiple osteochondroma development or for regenerative medicine applications, to improve osteogenic and chondrogenic differentiation in cases of bone fractures.

4.3. Perspective for the coming years

These results open several questions that I plan to answer in the future:

- **What is the role of the surface density of GAGs on GFs signaling?**

In animal tissues, the density of GAGs changes depending on the tissue type and throughout lifetime (McKee, Perlman et al. 2019). Information on the GAGs densities on the tissues are rare and often difficult to translate in mass concentration for biomaterial design (Le Pennec, Picart et al. 2023) **S.01**. It is therefore important to consider this aspect when studying the effect of GAGs on GFs signaling. Few examples in literature studied the role of GAGs surface concentration on cellular responses (Tierney, Jaasma et al. 2009, Wang and Yang 2017) and none of them has systematically changed one parameter at the time, namely the GAG density and the surface concentration of the GFs. For that, we aim to tune the biotinylated GAGs surface density on SAv platforms as we have previously done with cRGD molecules (Sefkow-Werner, Machillot et al. 2020) **A.8** and to control the mass adsorption of GAGs and of GFs bound to GAGs by surface sensitive techniques. Thanks to the automatization of surface functionalization, it will be possible to test several types of GAGs and several surface concentrations in the same study. Cellular responses to GFs such as BMPs and TGFβ at short (1 hour) and long (7 days) time points will be analyzed.

- **How the GAGs localization plays a role on cellular adhesion and GFs signaling?**

As reported in **Figure 19**, cell surface and extracellular HS have a role on cellular adhesion since cell morphology changed on CHO HS KO. The mechanism behind this observation is however not clear. In particular, **how HS is involved in the integrins signaling pathway**? Is it a direct influence of HS on integrin-mediated cell adhesion

or is there an indirect effect of HS on GFs - integrins crosstalk ? To answer to these questions specific platforms with different GAGs will be engineered and mutant cells for the synthesis of GAGs will be plated. CHO WT and lacking HS and CS chains (CHO pgsD-677 and CHO IdilD) and limb mesenchymal cells of Ext-1fl/fl. mice (induced by retrovirally delivered Cre, established in the group of A. Vortkamp) will be plated on biomimetic platforms presenting (or not) immobilized HS (iHS) or immobilized CS (iCS). Cellular area and spreading will be quantified together with an analysis of the focal adhesions and on the stress fibers in collaboration with Corinne Albigez-Rizo.

- **How BMP2 binds HS? Is there a conformational change upon BMP2 interaction with HS?**

It has been previously proposed that BMP2 has two heparin binding sites with different affinities for HS. Indeed the N-terminus and basic amino acids gave two electropositive surfaces to the BMP2 dimer, therefore two potential heparin binding sites : one includes residues Lys73, Lys76, His44 and His17, while the second surface is primarily formed by Arg114 (Gandhi and Mancera 2012). We have previously published that BMP2 crosslinks the HS chains (Migliorini, Horn et al. 2017)**A.12** and this can be explain by the presence of multiple heparin binding sites. We expect to express recombinant BMP2 in eukaryotic cells in collaboration with the group of R. Vivés at IBS. By mutating the Arg114 of the BMP2 dimer, we expect to reduce the affinity and the ability of the protein to crosslink HS.

Since the mechanism behind the role of HS on BMP2 signaling is not clear, we hypothesize that HS may modify the conformation of BMP2. In the literature, there is to date no structure of BMP2 in complex with HS, heparin or oligomers. Since in the frame of the ANR GlyCON project we produced homogenous HS-dps with a precise sulfation pattern, we aim to engage towards the crystallization of a BMP2/HS-dps complex and to determine its **crystallographic structure** at high resolution. Crystallogenesis trials will be conducted at the HTX lab high-throughput crystallization platform from the Partnership for Structural Biology (PSB). Promising conditions will be used to produce crystals in manual vapor diffusion experiments and diffraction data will be collected at the MASSIF ESRF beam line. While the crystal structure of BMP2 has already been solved, obtaining high quality diffracting crystals of a BMP2/HS complex could be challenging. If the crystallization trials failed to provide exploitable crystals, alternative will be envisaged, such as crystal soaking approaches

In order to respond to all three aspects, I intend to apply for various local and national grants such as the EUR-CBS grant in collaboration with R. Vivés and the ANR-DFG in collaboration with Andrea Vortkamp in Essen and Corinne Albiges-Rizo at IAB, Grenoble.

Newly started projects

5. Development of biomimetic materials to study neuroblastoma

PEOPLE INVOLVED: Mr. João Lopes (PhD), Mr. Nathan Thibieroz (M2), Dr. E. Migliorini (CRCN) and Prof. C. Picart (team leader)

COLLABORATORS: Dr. Fabrice Cordelieres (Bordeaux imaging center)

FUNDING: FRM maladie rares (Phd fellowship of JL), IDEX-IRGA (P.I E. Migliorini), Ligue contre le cancer region Rhone Alpes (P.I: C. Picart)

BMPs are now well known not only for their role in bone homeostasis, but also for their involvement in the physiological and pathological development of multiple organs (Hiepen, Yadin et al. 2016). The complex nervous system and all its associated pathologies were at the center of my PhD research where I studied the neuronal differentiation of stem cells by adapting surface stiffness and topography (Migliorini, Grenci et al. 2011, Migliorini, Ban et al. 2013)**A.24, A.25**. However, surface chemistry has not been well-controlled. One of the main challenges I would like to achieve is the independent control of substrate stiffness, geometry and chemistry to better study the nervous system. Indeed, neurons are particularly soft and designing adapted biomaterials with controlled chemical and physical properties is still a challenge.

During Joao Lopes' PhD we became interested in neuroblastoma (NB) which is a pediatric cancer of the peripheral nervous system. It has been shown that BMP2 and 4 are inhibit of the cellular proliferation and differentiation of neuroblastoma cell (Du and Yip 2010, Ferlemann, Menon et al. 2017, Szemes, Melegh et al. 2020). Moreover, the composition of the ECM appears also to play a role in the NB development. In particular, the presence of a specific proteoglycan Neurocan (chondroitin sulfate proteoglycan) increases the malignant phenotype of NB cells (Su, Kishida et al. 2017) while the treatment of NB cells with heparan sulfate proteoglycans reduces NB proliferation (Knelson, Gaviglio et al. 2014, Knelson, Nee et al. 2014). Finally, also matrix elasticity has an effect on the proliferation and the differentiation of the NB cells (Lam, Cao et al. 2010, Labat, Buchbinder et al. 2021, Mundhara, Yadav et al. 2021)

For all these reasons, we aim to **create a tumor microenvironment closer to the *in vivo* one** by tuning chemical and mechanical properties of the biomaterial. In this way, we will **improve the reliability of cellular responses to anticancer drugs.** We also aim to understand the role of BMPs (BMP2, 4, 7 and 9) and TGFβ on neuroblastoma progression when presented by biomaterials with controlled chemical and physical properties.

5.1. Major scientific achievements

This project was the PhD subject of João Lopes who passed away during his third year of PhD in August 2023. We obtained a PhD fellowship by Pfizer to continue this project

with Nathan Thibieroz, a former M2 student in my group who started his PhD in October 2023. Some of the data collected during João's PhD on neurites analysis (not shown here) will be included in a first methodological publication, set to appear.

5.1.1. Study the effect of matrix-bound BMPs and TGFβ on neuroblastoma cell proliferation

To study the effect of substrate stiffness and the role of bioactive molecules incorporated into the film, João Lopes first adopted a layer-by-layer film of poly-L-lysine and hyaluronic acid with tunable stiffness. This approach has been well characterized by the BRM team for the controlled binding and release of BMPs and TGFβ (Crouzier, Ren et al. 2009, Machillot, Quintal et al. 2018, Sales, Khodr et al. 2022) **A.3**.

Soft (~200 kPa) and stiff (~400 kPa) films have been prepared by a liquid handling robot inside 96-well plates (Machillot, Quintal et al. 2018) and have been loaded with BMP2, 4, 9 and TGFβ. As control, we used retinoic acid since it has been proven *in vitro* and *in vivo* that retinoic acid reduces cellular proliferation by improving neuronal differentiation (Amatruda, Sidell et al. 1985). Human SH SY5Y and murine Neuro2a (N2A) neuroblastoma cell lines were plated on the films and on plastic Petri dishes (TCPS) and their proliferation was observed using Incucyte live cell microscopy. We first observed that substrate stiffness has a strong influence on cell adhesion and proliferation. In fact, cells proliferated less on the stiff LbL films than on the glass supports, while they formed aggregates on the soft films **Figure 22**). These aggregates were growing during the three days' time lapse and their growth has been quantified (data not shown). On human SH-SY5Y cells we observed that **BMP9 and TGFβ reduced cellular proliferation on stiff films while they presented no effects on TCPS**. This result proved that biomimetic films are able to reveal cellular mechanism otherwise hidden by the rigidity of the plastic petri dishes. We now expect to look at the neurite length and at the expression of differentiation markers on these biomimetic conditions to prove the role of BMP9 and TGFβ on NB cells differentiation.

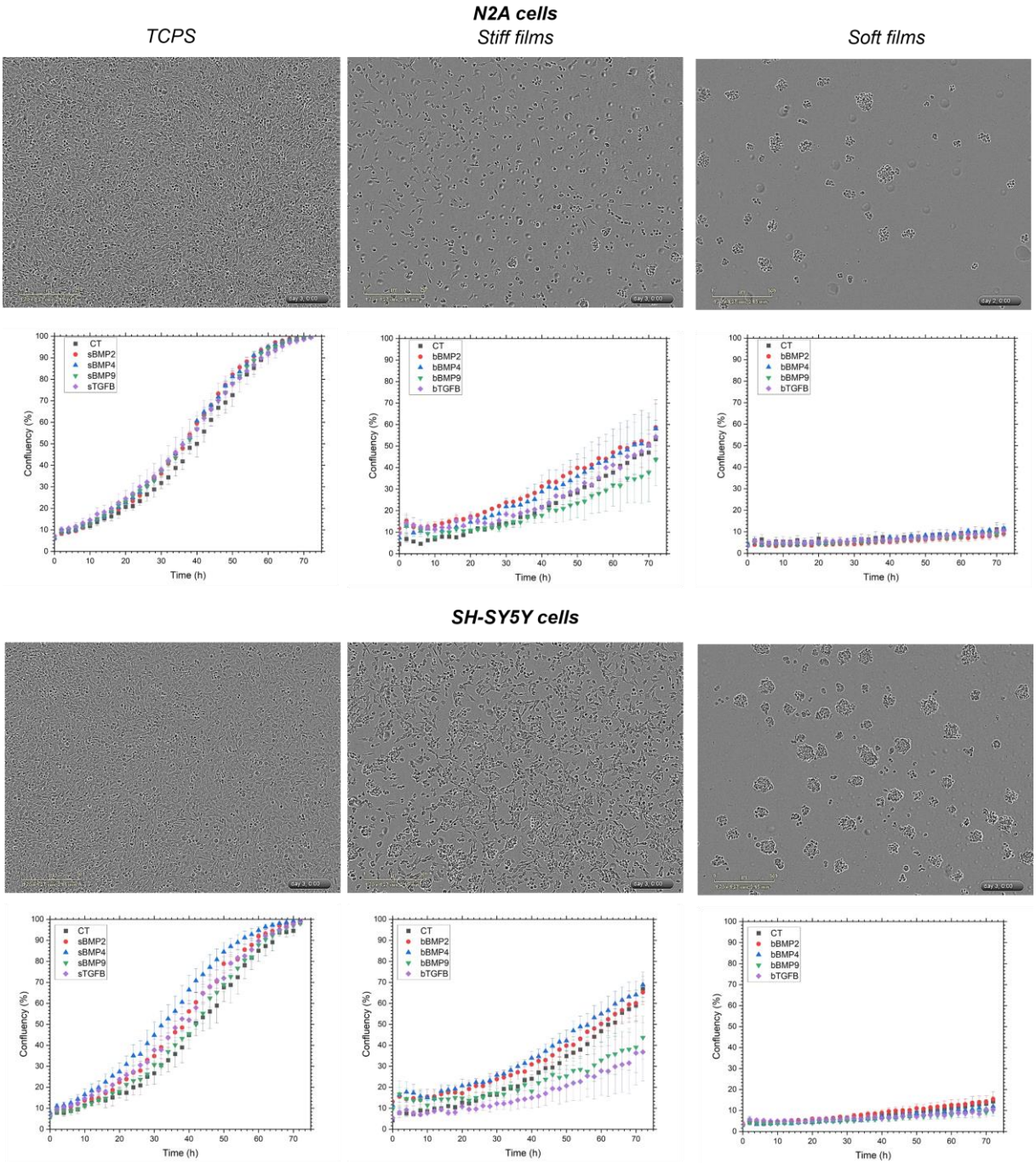

Figure 22: Substrate stiffness combined with BMPs affect NB cells proliferation. *N2A and SH-SY5Y cells were plated on plastic petri dishes and on stiff (~400 kPa) and soft (~200 kPa) LbL films. Bright field images have been acquired by Incucyte video microscopy for three days every 2 hours and the last picture for each control condition has been shown here. The confluence curve is a measure of cell proliferation automatically provided by Incucyte software. This measurement has no meaning for the soft films where the cells formed aggregates.*

5.1.2. Influence of mechanical properties on neurites length

One strategy to study the role of specific ECM components such as adhesion ligands and the presence of specific GAGs on cell proliferation and differentiation is to build the biomimetic streptavidin-based platforms on soft supports such as polydimethylsiloxane (PDMS). PDMS is a widely used elastomer with a backbone of -

O-Si(CH_3)$_2$- units. The network of PDMS polymer is formed by cross-linking these polymer chains. It is possible to use different percentage of crosslinking reagent (from 10 to 2% (w)) to modify the substrate stiffness from ~400 to ~40 kPa (Migliorini, Ban et al. 2013)**A.20**. The study by Zhang et al. (Zhang, Tan et al. 2020) also investigated the effect of substrate stiffness on various N2A cell parameters, using hardener or PDMS ratios to vary stiffness. In this study, PDMS did not appear to be cytotoxic. We have shown that streptavidin platforms can be built on SiO_2 and glass substrates thanks to the PLL-g-PEG-biotin linker (Sefkow-Werner J., Le Pennec J. et al. 2022)**A.1**. Upon exposure to plasma, PDMS develops silanol groups (-OH) as a result of oxidation of the surface layer (Bhattacharya, Datta et al. 2005) – this surface chemistry being comparable to that of glass after plasma treatment, we expected to reproduce the surface functionalization on PDMS as on glass surfaces.

With N. Thibieroz (during his M2 internship) we have demonstrated by QCM-D and SE that **we can functionalize PDMS support with the biomimetic platform (Figure 23** a-b**)**. Although the frequency shift for the adsorbed molecules is generally lower on PDMS than on glass, we showed that PLL-g-PEGbiotin(50%) can bind to PDMS and the other molecules such as SAv, cRGD, HS and BMP2 can be subsequently grafted

To investigate the role of substrate stiffness on neuroblastoma cell growth and differentiation we plated SH-SY5Y and N2A cells on PDMS platforms presenting only cRGD as an adhesion motif but variable stiffness. To tune the stiffness we used different ratios of PDMS/curing agent (10:1; 60:1 and 100:1) of PDMS Sylgard 184 and we also employed a different PDMS (Sylgard 527) known to generate soft films in the range of 45 KPa (Rathod, Ahn et al. 2018). One of the readouts of cell differentiation is the length of neurites, were longer neurites are a marker of neuronal differentiation. The analysis of neurite growth remained challenging and most computational macros involved an almost manual analysis of neurite lengths. This was incompatible with our high-throughput analysis in 96-well plates. A specific macro in ImageJ to analyze the length of neurites of single cells was developed in collaboration with F. Cordelieres at BIC. A methodological paper on the use of this macro, which is important for neurobiologists, is in preparation.

We observed that **N2A neurites were longer on softer than on stiff PDMS** (**Figure 23**f). We also observed that SH-SY5Y cells formed aggregates on all substrates, which may have been triggered by the chemical functionalization of the substrates. On **soft substrates, we measured a significant increase in the size of the aggregates**. We can speculate that SH-SY5Y cells prefer to form 3D clusters, similar because they interact more with each other than with the substrate.

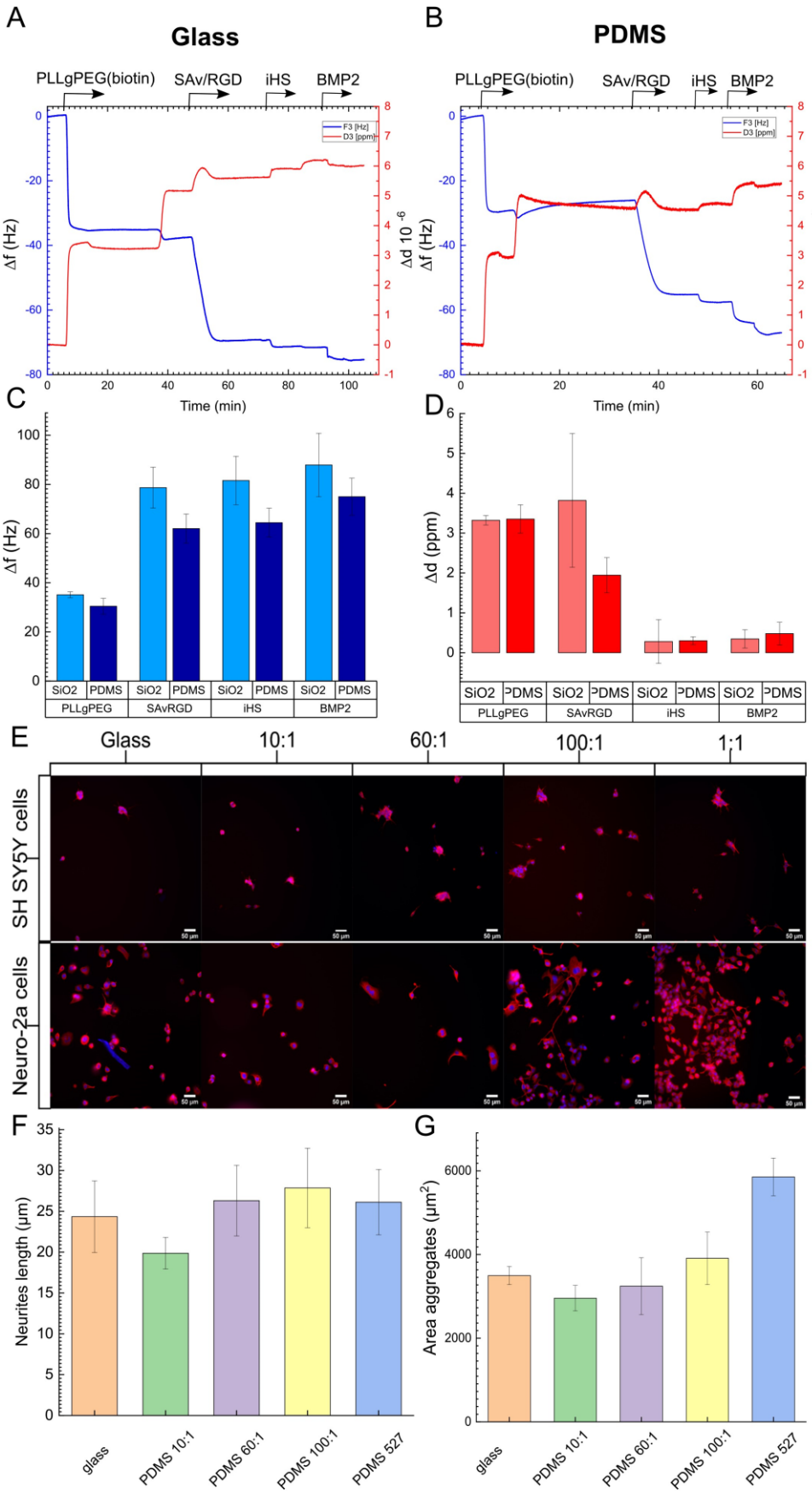
A
Glass
PLLgPEG(biotin)
SAv/RGD
iHS
BMP2
F3 [Hz]
D3 [ppm]
Δf (Hz)
Δd 10 -6
Time (min)
B
PDMS
PLLgPEG(biotin)
SAv/RGD
iHS
BMP2
F3 [Hz]
D3 [ppm]
Δf (Hz)
Δd 10 -6
Time (min)
C
Δf (Hz)
SiO2
PDMS
PLLgPEG
SAvRGD
iHS
BMP2
D
Δd (ppm)
SiO2
PDMS
PLLgPEG
SAvRGD
iHS
BMP2
E
Glass
10:1
60:1
100:1
1:1
SH SY5Y cells
Neuro-2a cells
F
Neurites length (µm)
glass
PDMS 10:1
PDMS 60:1
PDMS 100:1
PDMS 527
G
Area aggregates (µm2)
glass
PDMS 10:1
PDMS 60:1
PDMS 100:1
PDMS 527

***Figure 23: Tuning the stiffness of SAv platforms. a**,b) QCM-D representative graphs of SAv platforms molecular assembling on glass (a) and on PDMS (b) supports. The injections are labeled with an arrow, during the rest of the time different running buffers were injected (10 Mm Hepes before and after PLLgPEGbiotin(50%); 10 Mm Hepes 150 mM NaCl for SAv/RGD and iHS and 10Mm Hepes 150 mM NaCl 0.02% Tween20 before and after BMP2 injection) c) Frequency and d) Dissipation plot of the average shifts upon the injection of each molecule (n=3). The error bars correspond to the standard deviation from the mean. e) Representative images of SH-SY5Y and N2A cells cultured for 3 days on the glass and on different PDMS with different stiffness (from the stiffer at the left to the softer at the right). The ratio of base/cross linker of PDMS Sylgard 184 that were compared are 10:1, 60:1 and 100:1. PDMS Sylgard 527 was also used since it is known to be softer than the PDMS Sylgard 184. f) Plot of the neurites lengths based on the different substrates stiffness. The mean value and the standard deviation are represented (n=4). g) Variation of the mean area of SH-SY5Y cells aggregates induced by the substrate stiffness. The mean value and the standard deviation are represented (n=3).*

5.2. Conclusions

This recently started project has shown encouraging results on the role of stiffness on neuroblastoma cell proliferation and differentiation. In particular, we show that cell **proliferation was reduced on LbL films compared to TCPS supports** and that the effect of GFs on cell proliferation was revealed on biomimetic materials. We have also shown that a possible way to tune the stiffness and chemical properties of the substrate (to better mimic the ECM) is to functionalize PDMS with the SAv platforms. Unfortunately, PDMS may not be the easiest solution to tune substrate stiffness due to the low throughput and high variability between the surfaces. Nathan Thibieroz will continue this project initially aiming at developing a 3D biomimetic material, which maintains cell behavior as *in vivo* to then study the role of BMPs and TGFβ as potential drugs to reduce NB progression.

5.3. Perspective for the coming years

Since testing the sensitivity of a patient's cells to a specific drug *in vitro* before treating the patient could be a major step towards personalized therapy, we aim to create a tumor environment that more closely mimics *in vivo* conditions. To this end, we will develop new biomaterials that better mimic the ECM of the neuroblastoma, as described in the literature, and in a design compatible with high-throughput studies. These biomaterials will combine the properties of the LbL and SAv platforms, in particular the control of stiffness and chemical properties respectively. For this purpose, we expect to develop an LbL film made of PLL - poly(L-glutamic acid) (PGA) with different stiffness levels. (Gribova, Gauthier-Rouvière et al. 2013) on which we will adsorb a last layer of PLLgPEG biotin to build the SAv platforms presenting different biotinylated adhesion peptides and biotinylated GAGs such as HS and/or chondroitin sulfate where BMP2, 4, 6 and 7 and TGFβ can bind (Sefkow-Werner, Le Pennec et al. 2022) **A.1**.

As a first step, we will identify the best in vitro conditions to mimic the NB microenvironment, i.e. where NB will progress as *in vivo*. On these biomaterials, we expect the cells to respond to NB treatments in a similar way to *in vivo*. In a second step, thanks to the collaboration with Dr. Denis Barbier at 3DMicrolight, we aim at reproducing the same coatings on a 3D scaffold. (La Tronche). The team has

previously functionalized 3D scaffolds with LbL films (Rengaraj, Bosc et al. 2022) however cells were not attracted by the LbL film since no adhesion ligand was present.

NB cells will then be exposed to BMPs as potential drugs to reduce cancer progression. The long-term goal is to develop a **biomimetic material that can be used by doctors to test the response of patient cells to BMPs or other drugs before treatment**.

6. Engineering a bone on chip as metastasis trap

PEOPLE INVOLVED: Dr. Elisa Lambert (PostDoc), Ms. Laura Clauzier (engineer). Collaborators: Dr. O. Filhol-Cochet (IMAC, Biosanté, CEA), Dr. F. Navarro (LSMB, Leti, CEA) and Dr. S. Morales (LSIV, Leti, CEA)

FUNDING: Focus Organ on Chip (CEA)

Bone represents a critical site for the development of primary and secondary tumors. Solid tumors for example at breast, prostate, lung and kidney primarily metastasize to the bone and then the bone microenvironment facilitates cancer cells to further metastasize and establish multi-organ secondary metastases (Zhang et al. 2021). Our knowledge of the premetastatic niche that leads to this phenotype is limited and, in particular, *in vitro* models allowing the optimization of appropriate treatments are lacking (Ganesh 2021). As animal tests have to be dramatically reduced due to European laws, alternative mimetic “on chip” models have to be developed**. Organ-on-chip (Ooc) is a powerful strategy in the direction of personalized therapies to create a biomimetic tissue recapitulating the main features of tumoral niche**, to then test the effect of anti-metastatic drugs on a chip before patient treatment. Surprisingly, only few Ooc models focus on the study of tumor metastases to bone (Arrigoni et al. 2017) except few example of bone metastasis on breast cancer (Bersini, Jeon et al. 2014, Conceição, Sousa et al. 2022) based on co-culture experiments where the migration of metastatic cells towards the bone niche has not been addressed.

For that, in this project we aim at **recreating a bone niche** (i.e: *in vitro* differentiated stem cells on an ECM that mimic the bone tissue) inside a microfluidic device to then **study the invasion of the bone by metastatic cells** and in the future to test patient cells sensitivity to anti-metastatic drugs. As proof-of-concept we employ spheroids from kidney cancer, obtained thanks to the collaboration with Odile Filhol-Cochet at IMAC team, Biosanté, CEA, specialist of kidney cancer (Roelants, Pillet et al. 2020, Giacosa, Pillet et al. 2021).

The bone niche will be engineered in a biomimetic microenvironment recapitulating some features of the *in vivo* bone extracellular matrix (ECM). In a first step, we aim to **design biomimetic streptavidin platforms inside a microfluidic device to promote osteogenic stem cell differentiation**. In a second step, we aim at fabricating a 3D scaffold and to functionalize it with osteo-inductive biomaterials (see perspective for the coming years). After that, we will differentiate human periosteum derived stem cells

(hPDSCs) towards bone in the microfluidic device (**Figure 24**). We aim at visualizing how kidney cancer cells generate metastases on/at the bone with standard microscopy but also with lens-free microscopy in collaboration with Dr. Sophie Morales (LSIV, CEA-Leti, Grenoble). Holographic video microscopy is a label-free innovative approach developed at CEA (Allier, Vincent et al. 2018) that will be of great help to analyze tumor cell migration towards bone niche since it permits the observation of a large field of view (30 mm^2). Thanks to this technique and the collaboration with LSIV laboratory at LETI, we will be able to **distinguish single cell features that characterize a metastatic cell** (such as the dry mass, the size and the migration speed) for a future screening of metastatic *vs* non metastatic cells.

6.1. Major scientific achievements

Thanks to the new collaborations with Odile Filhol-Cochet and LETI I have obtained a funding in 2022 to enroll a postdoc, expert in microfluidics. The following results are from Elisa Lambert's first year as a postdoc working under my supervision and in collaboration with the IMAC group.

6.1.1. Set-up the microfluidic experiment

We recently started to develop a **bone-on-chip**. The initial prototype of the microfluidic device is available in PDMS (**Figure 24b,c**) thanks to the collaboration with F. Maloggi (CEA Saclay) and F. Navarro (CEA-Leti, Grenoble)**.** Two microfluidic chambers (one hosting the kidney cancer tumoroid and the other one the bone niche) are connected with a channel of 500 µm having several pillars of 100µm diameter to filter tumor cell migration and to select potential metastatic cells. A third entry is used for the functionalization of the bone chamber and for the injection of anti-metastatic drugs (**Figure 24a**). The unit is connected to external flow controllers and flow sensors. Recently, a new design has been developed with the inlet from the top of the chambers to allow the renewal of all the liquid inside the chamber and to favor the exit of possible air bubbles (**Figure 24b).** The choice of the pillar size and number has been dictated by preliminary data: (i) the functionalization of the bone chamber on a device with a channel without pillars was complicated since molecules invaded the secondary renal cancer chamber; (ii) higher pillar density was blocking tumor cell migration.

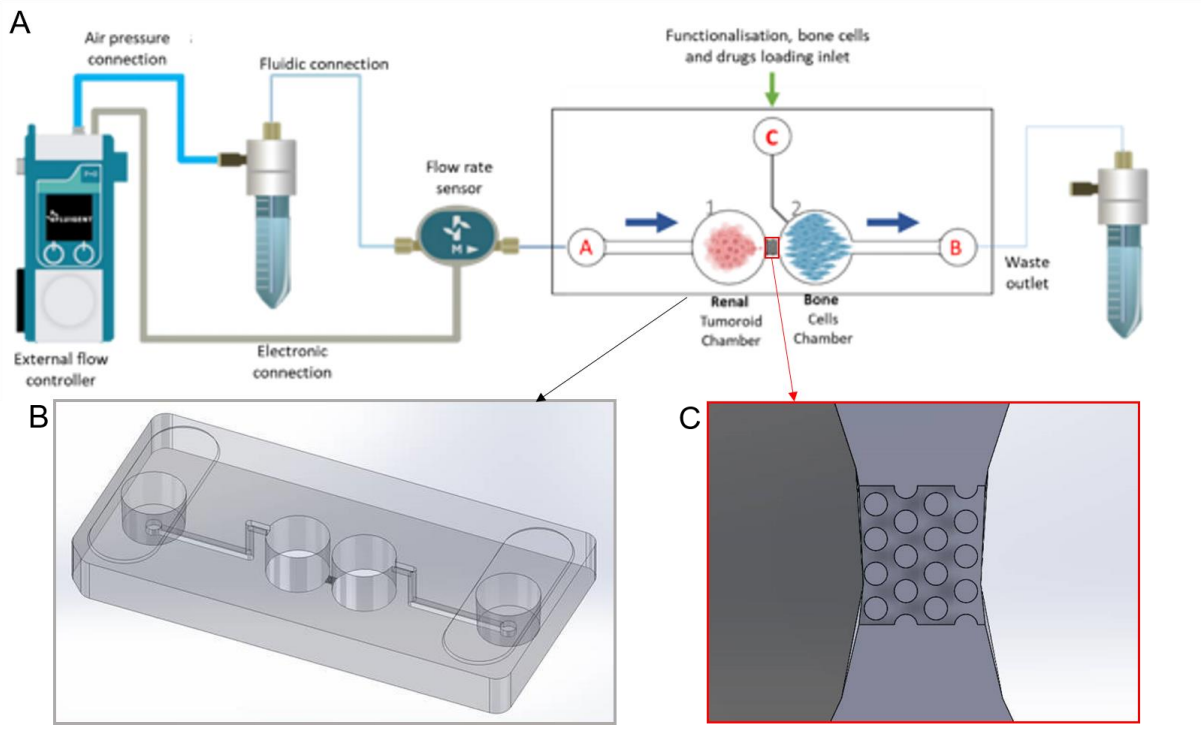

Figure 24: Development of a microfluidic setup to study kidney cancer metastasis to bone niche. *a) schematic representation of the microfluidic setup installed with flow controllers and flow rate sensors (taken from www.fluigent.com and created by BioRender). b) final design of the microfluidic chip that is under construction with the entries from the top of the chamber. c) detail of the pillars number and distribution inside the channel.*

6.1.2. Functionalization of the bone chamber

The locally-specific functionalization of the bone chamber is a critical step of the project. Indeed, it is important that renal cancer cell do not come in contact with BMP2 since BMP2 induces renal cells profibrotic phenotype (Simone, Cosola et al. 2012). We demonstrated that the bone chamber can be locally-specific functionalized with the biomimetic platforms and that no BMP2 enters the renal chamber. For this, we developed a protocol that avoids the contamination of the renal chamber with the molecules used to build the biomimetic platforms thanks to a counter pressure at the entry A and a constant flow between the entries C and B (**Figure 24a**). We proved a homogenous coating of the bone chamber with SAv-Alexa565 (**Figure 25a left**) and we followed the functionalization with cRGD, iHS and we revealed BMP2-fluorescein bound to iHS (**Figure 25a right**)

6.1.3. Renal cancer cells have a tropism to bone cells

We demonstrated on a preliminary co-culture experiment that tumor cells (786-O spheroids) strongly interact with differentiated bone cells by forming a complex network, while on undifferentiated cells the spheroids remain compact (**Figure 25b**). This result is fundamental to prove the existence of a tropism between the two types of cells. This result has to be confirmed in the following weeks. Until now we encountered several complications: hPDSCs sometimes detached from the biomimetic

platforms since they formed nodules and 3D structures with low cell-biomaterial adhesion; inhomogeneous distribution of the cells on the well and therefore a difficult positioning of the spheroid on the top of the cell; contaminations due to the long cell culture (>14 days).

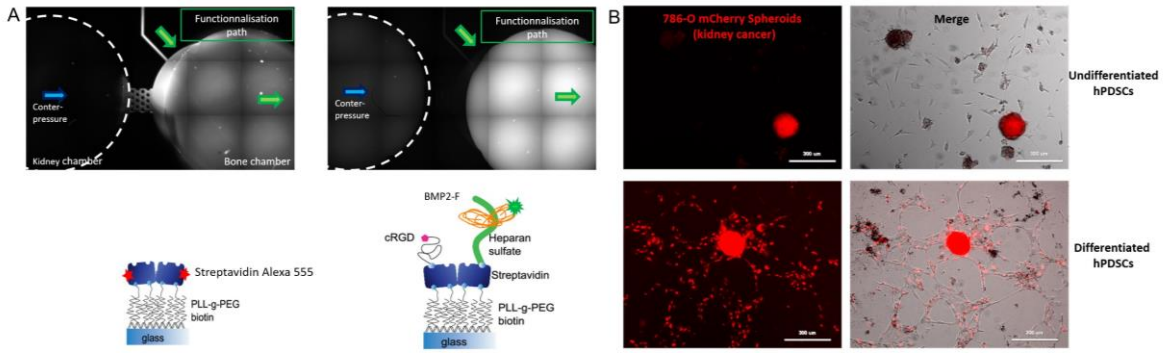

Figure 25: preliminary results on the project. *a: the bone chamber of the microfluidic device was locally-specific functionalized with Streptavidin Alexa555 (left image) here represented in shades of grey. Then the rest of the functionalization was carried out with cRGD, iHS and BMP2-fluoresceine that homogenously bound to iHS specifically inside the bone chamber (right image). BMP2-fluoresceine is also represented in shades of grey. This protocol prevented contaminations of the channel and of the renal chamber. b: 786-O kidney cancer spheroids (mCharry labeled in red) – done by IMAC team – co-cultured with differentiated and non-differentiated hPDSCs (not labeled). The spheroids remained compact on the non-differentiated cells while it follows the hPDSCs network of differentiated hPDSCs.*

Cell detachment from the biomimetic platforms often arose on long term cell culture. The traction forces exerted by adhering cells may indeed disrupt the electrostatic interactions of PLLgPEGbiotin with the surface or/and the biotin-SAv binding which is the strongest noncovalent interaction in nature (10^{-14} M) (Jurchenko, Chang et al. 2014).

To solve that issue, we are considering either modifying the functionalization of the platforms with new passivating ligands, which bind covalently to glass or using a new biomaterial (see “development of polymer-brush biomaterial carrying BMPs”).

6.2. Conclusions

The microfluidic device to study the metastatic invasion of renal cancer cells into the bone niche is now available with PDMS material. A protocol to specifically functionalize the bone chamber is now available and we will soon plate hPDSCs on the bone chamber inside the microfluidic device to test their osteogenic differentiation after 7 days using alkaline phosphatase staining.

Preliminary co-culture tests have shown encouraging results on the attraction between hPDSCs and renal cancer cell lines.

A critical aspect of the project is the lack of an endothelial barrier, which is fundamental to the process of tumor cell intravasation into the bloodstream and extravasation from the bloodstream into the metastatic niche. One possible solution is to work with the

MIVO® technology from React4Life, a company that sells a microfluidic device similar to our prototype but with an endothelial barrier. Functionalization of these devices will be done prior to seeding with endothelial HUVEC cells. To further develop this project, we are applying to the INCA PLBIO call (2023-2024) together with Odile Filhol.

6.3. Perspective for the coming years

This ambitious project will certainly evolve in the next 5 years in 4 main aspects: (i) the microfluidic device should be parallelized, (ii) the bone niche should be more representative of the *in vivo* tissue, (iii) we expect to perform a proof of concept of the efficacy of metastatic drugs, (iv) the detection of metastatic invasion should be integrated in the microfluidic device.

Parallelization: In line with the need to compare different conditions within the same experiment, it is necessary to parallelize our approach and run multiple experiments simultaneously. The commercially available AKITA® device from FinnAdvance will be a good step towards miniaturization and parallelization.

Improvements of the bone niche: Despite their great contribution to advancing basic knowledge of bone biology, there is growing evidence that 2D models cannot mimic the complex conditions *in vivo*. 3D models allow cells to maintain the original shape of osteoblasts, have higher stability and longer lifespan, have a less altered genotype, and thus provide a good approximation to the real *in vivo* microenvironment (Knight and Przyborski 2015). Today, several 3D scaffolds have been developed for regenerative medicine applications. It has been shown that the chemical, mechanical and geometrical properties of the scaffolds are important for osteogenic differentiation (Yuste, Luciano et al. 2021). However, the **design of scaffolds with simultaneous control of geometric and chemical properties** is still a challenge**.** In addition, the concept of bone niche to **study the potential effect of drugs on bone metastasis, has only recently emerged** and is not fully explored (Kim, Paek et al. 2023). To this end, we aim to fabricate 3D scaffolds inside the microfluidic device thanks to the two-photon polymerization technique in collaboration with Microlight3D (La Tronche, France). The scaffolds will be functionalized with biomimetic streptavidin platforms as previously done in the team with polyelectrolyte layer-by-layer films (Rengaraj, Bosc et al. 2022). This 3D scaffold can also be fabricated on a glass slide and then manually deposited into commercially available microfluidic devices (such as MIVO® or AKITA® technology). On this specific aspect, in October 2023, I applied for CNRS funding (emergences INC) for 2 years postdoc with consumables.

Drug testing: For proof of concept, we expect to test known drugs for the treatment of renal cancer metastases. In particular, we will initially test FDA-approved kinase inhibitors for RCC (Drugs Approved for Kidney Cancer-NCI, 2022). Immunotherapy will also be a possibility thanks to O. Filhol's collaborators. Finally, we expect to develop new anti-metastatic drugs based on nanobodies in collaboration with Patrick Charmes CRCM Marseille.

Integration of the detection mode: for clinical use of the final parallelized device, we need to develop a novel method to detect metastatic cells that escape from the patient's tumor, invade the bone niche and proliferate there. We are currently looking for collaborators who can help us achieve this ambitious goal.

7. Development of polymer-brush biomaterial carrying BMPs

PEOPLE INVOLVED: Dr. Elisa Lambert (PostDoc), Bojana Bogdanovic (M2 student)

Collaborators: Dr. Julien Gautrot, Queen Mary University of London

FUNDING: CNRS-IEA 2021-2023

As previously stated, a novel biomaterial to encompass the issues of the non-specific binding of proteins to the platforms and to prevent cellular detachment to the glass biomimetic platforms may be needed. In addition, using SAv platforms to present BMPs bound to HS for *in vivo* applications is complicated since HS encounters short lifetime if placed in an injured site due to its degradation by heparinases which are released by cells involved in the immunity response (Eming, Krieg, and Davidson 2007). Moreover, HS is a chemically complex molecule and highly heterogeneous.

Polymer brushes are an attractive approach for tissue engineering thanks to their simple fabrication, ECM-like structure and *in vivo* stability (Kim and Jung 2016). Depending on their charges, surface density and length, polymeric brushes can be used to immobilize proteins and therefore GFs (Krishnamoorthy et al. 2014).

The group of J. Gautrot has developed an international track record in the synthesis, characterization and chemical functionalization of polymeric brushes. His group is focusing on the characterization of their morphology in different buffers and interaction with proteins and cells, as well as their application in regenerative medicine. Polymer brushes interaction and presentation of GFs for regenerative medicine applications has received relatively little attention. Few studies took the challenge to combine chemically functionalized brushes with cell adhesion motifs and GFs delivery to regulate cell phenotype. (Psarra et al. 2015; Ren et al. 2011). We therefore started to collaborate with the group of J. Gautrot to develop polymeric brushes and to study their interaction with BMPs. We hypothesize that polymer brushes presenting negatively charged sulfonate groups might interact with the positively charged heparin binding sites of BMPs and that these coatings could constitute a novel generation of interfaces able to mimic the physico-chemical properties of HS, for *in vitro* and *in vivo* studies.

7.1. Major scientific achievements

The postdoc Elisa Lambert and the master student Bojana Bogdanovic performed some preliminary experiments that are briefly summarized below. Data analysis and treatment are in progress.

7.1.1. Synthesis of the polymeric brushed in Grenoble

E. Lambert and B. Bogdanovic spent some weeks in J. Gautrot's lab in QMUL to learn how to grow polymeric brushes and to transfer the protocol at BRM team in CEA, Grenoble. One of the most versatile synthesis methods for the polymeric brushes is atom transfer radical polymerization (ATRP) which needs copper to form an alkyl radicals (Krishnamoorthy, Hakobyan et al. 2014). In Gautrot's group they have adopted a variation of this protocol, called "activators regenerated by electron transfer" (ARGET) to avoid oxygen sensitivity and the presence of biologically toxic residual traces (Matyjaszewski, Dong et al. 2007), making polymer brushes biologically friendly. This technique was employed to synthetize poly(3-Sulfopropyl methacrylate) (PSPMA) brush on silica wafers, SiO2 covered quartz crystals and glass slides. These brushes present sulfonate groups negatively charged that can potentially bind to the positively charged residues of BMPs *via* electrostatic interactions. The reproducibility of the protocol in the two laboratories have been proven by following the kinetic of growth of PSPMA brushes on silica wafers. To this end, the thickness of the brushes was measured by spectroscopic ellipsometry (data not shown). We have demonstrated that the protocol is reliably transferable and reproducible in our laboratory.

7.1.2. Polymer brushes can immobilize BMP2 and BMP4

To study how PSPMA brushes with different densities and length are able to bind BMP2 and BMP4 we are performing a comparative study in QCM-D (**Figure 26**). To this end, silica-coated quartz crystals are functionalized with PSPMA brushes with different thickness (thin corresponds to 1 and thick to 20 nm thickness) and with different density (high corresponds to 100% and low to 5% of initiator on the surface). Our preliminary data show that BMP2 binds more than BMP4 to the PSPMA brushes (**Figure 26**). Mass analysis with the viscoelastic modulus (not shown) reported a higher mass adsorption of BMP2 to the thick and high density brushes. The results obtained by QCM-D are in line with their SPR measurements done in J. Gautrot. We will write a paper on the characterization of the PSPMA brushes obtained by the ARGET protocol once all the experiments have been completed.

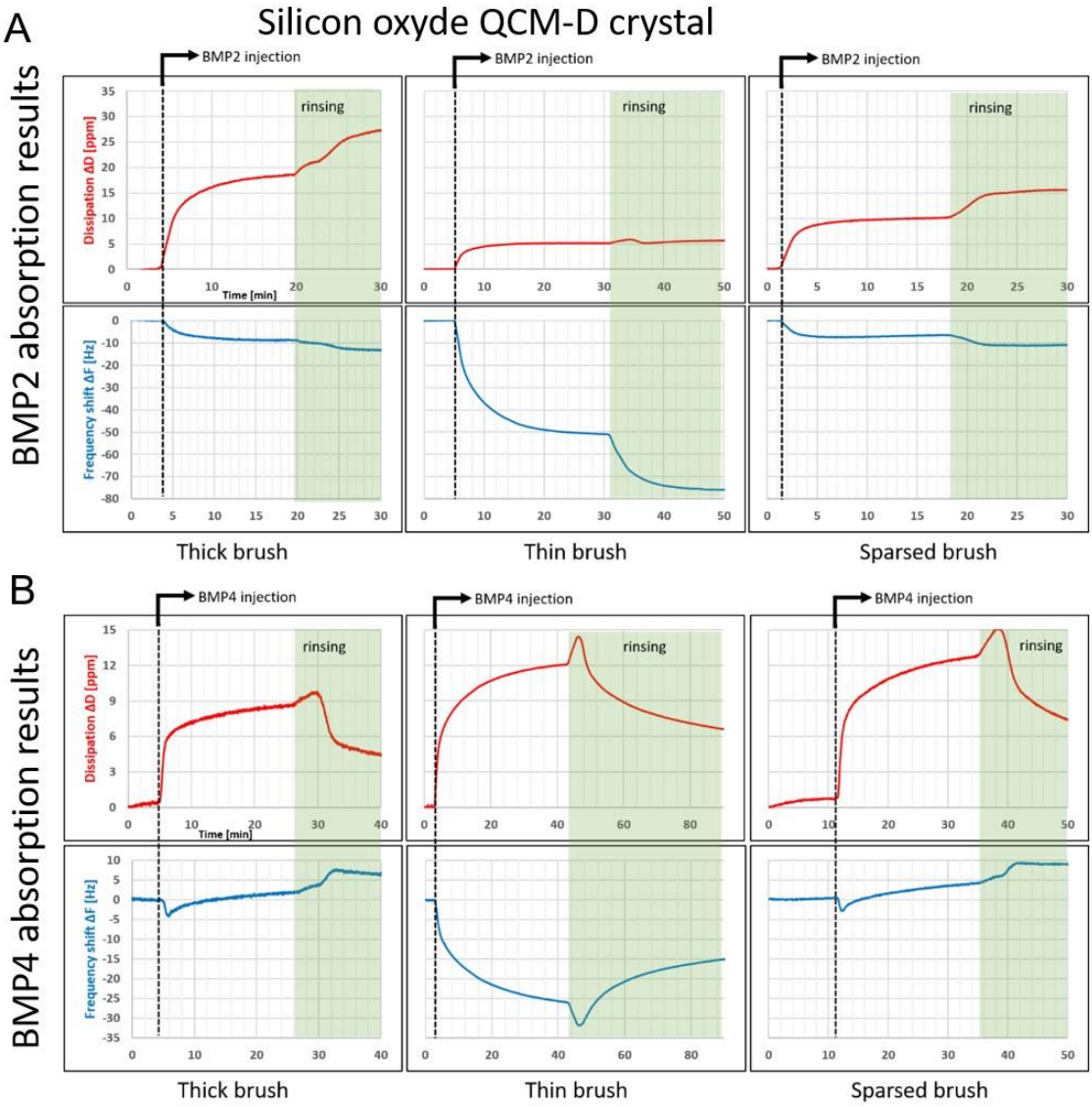

***Figure 26**: BMP2 binds more than BMP4 on polymeric PSPMA brushes. QCMD study of BMP2 (A) and BMP4 (B) binding on PSPMA brushes thick, thin or sparse grown on SiO2 QCM-D crystals. Blue curves represent the frequency and red curves the dissipation shifts for all conditions. Here representative curves have been chosen (n=3)*

7.1.3. Cell repellent effect of polymeric brushes

To study cellular responses to the PSPMA brushes we plated C2C12 cells to PSPMA brushes presenting BMPs. Unfortunately, no cells adhered to these brushes since they are probably cell-repellent. To solve this problem, we expect to covalently bind a cRGD-alkyne peptide presenting azyde groups to PSPMA brushes presenting azyde groups, synthetized in collaboration with Didier Boturyn (DCM).

7.2. Perspective for the coming years

An important aspect to allow the use of the polymer brushes for *in vitro* studies is the

promotion of cellular adhesion and BMPs signaling. If we succeed in this important aspect, we can use these new biomaterials to induce osteogenic differentiation and promote the formation of a 3D bone niche as described previously.

To this end, we aim to synthesize these brushes in 96-well plates and on the microfluidic device to test their performance in long-term cellular studies. If successful, their synthesis will be transferred to 3D scaffolds. We expect to apply to international funding to continue this interesting collaboration. Marie Sklodowska-Curie Individual fellowship is one option.

BIBLIOGRAPHY

Abdiche, Y., D. Malashock, A. Pinkerton and J. Pons (2008). "Determining kinetics and affinities of protein interactions using a parallel real-time label-free biosensor, the Octet." Anal Biochem **377**(2): 209-217.

Allier, C., R. Vincent, F. Navarro, M. Menneteau, L. Ghenim, X. Gidrol, T. Bordy, L. Hervé, O. Cioni, S. Bardin, M. Bornens, Y. Usson and S. Morales (2018). "Lens-free Video Microscopy for the Dynamic and Quantitative Analysis of Adherent Cell Culture." J Vis Exp(132).

Amatruda, T. T., N. Sidell, J. Ranyard and H. P. Koeffler (1985). "Retinoic acid treatment of human neuroblastoma cells is associated with decreased N-myc expression." Biochemical and Biophysical Research Communications **126**(3): 1189-1195.

Arnold, M., E. A. Cavalcanti-Adam, R. Glass, J. Blummel, W. Eck, M. Kantlehner, H. Kessler and J. P. Spatz (2004). "Activation of integrin function by nanopatterned adhesive interfaces." Chemphyschem **5**(3): 383-388.

Bachvarova, V., T. Dierker, J. Esko, D. Hoffmann, L. Kjellen and A. Vortkamp (2020). "Chondrocytes respond to an altered heparan sulfate composition with distinct changes of heparan sulfate structure and increased levels of chondroitin sulfate." Matrix Biol.

Barczyk, M., S. Carracedo and D. Gullberg (2009). "Integrins." Cell and Tissue Research **339**(1): 269-280.

Bersini, S., J. S. Jeon, G. Dubini, C. Arrigoni, S. Chung, J. L. Charest, M. Moretti and R. D. Kamm (2014). "A microfluidic 3D in vitro model for specificity of breast cancer metastasis to bone." Biomaterials **35**(8): 2454-2461.

Bhattacharya, S., A. Datta, J. M. Berg and S. Gangopadhyay (2005). "Studies on surface wettability of poly(dimethyl) siloxane (PDMS) and glass under oxygen-plasma treatment and correlation with bond strength." Journal of Microelectromechanical Systems **14**(3): 590-597.

Billings, P. C., E. Yang, C. Mundy and M. Pacifici (2018). "Domains with highest heparan sulfate-binding affinity reside at opposite ends in BMP2/4 versus BMP5/6/7: Implications for function." J Biol Chem **293**(37): 14371-14383.

Bovee, J. V., A. M. Cleton-Jansen, W. Wuyts, G. Caethoven, A. H. Taminiau, E. Bakker, W. Van Hul, C. J. Cornelisse and P. C. Hogendoorn (1999). "EXT-mutation analysis and loss of heterozygosity in sporadic and hereditary osteochondromas and secondary chondrosarcomas." Am J Hum Genet **65**(3): 689-698.

Carragee, E. J., E. L. Hurwitz and B. K. Weiner (2011). "A critical review of recombinant human bone morphogenetic protein-2 trials in spinal surgery: emerging safety concerns and lessons learned." Spine J **11**(6): 471-491.

Chouchane, K., T. Frachon, L. Marichal, L. Nault, C. Vendrely, A. Maze, F. Bruckert and M. Weidenhaupt (2022). "Insulin aggregation starts at dynamic triple interfaces, originating from solution agitation." Colloids Surf B Biointerfaces **214**: 112451.

Conceição, F., D. M. Sousa, J. Loessberg-Zahl, A. R. Vollertsen, E. Neto, K. Søe, J. Paredes, A. Leferink and M. Lamghari (2022). "A metastasis-on-a-chip approach to explore the sympathetic modulation of breast cancer bone metastasis." Mater Today Bio **13**: 100219.

Costas, C., V. López-Puente, G. Bodelón, C. González-Bello, J. Pérez-Juste, I. Pastoriza-Santos and L. M. Liz-Marzán (2015). "Using Surface Enhanced Raman Scattering to Analyze the Interactions of Protein Receptors with Bacterial Quorum Sensing Modulators." ACS Nano **9**(5): 5567-5576.

Crouzier, T., K. Ren, C. Nicolas, C. Roy and C. Picart (2009). "Layer-by-layer films as a biomimetic reservoir for rhBMP-2 delivery: controlled differentiation of myoblasts to osteoblasts." Small **5**(5): 598-608.

Dixon, M. C. (2008). "Quartz Crystal Microbalance with Dissipation Monitoring: Enabling Real-Time Characterization of Biological Materials and Their Interactions." J Biomol Tech **19**(3): 151-158.

Do, T., F. Ho, B. Heidecker, K. Witte, L. Chang and L. Lerner (2008). "A rapid method for determining dynamic binding capacity of resins for the purification of proteins." Protein Expr Purif **60**(2): 147-150.

Domack, A., O. Prucker, J. Rühe and D. Johannsmann (1997). "Swelling of a polymer brush probed with a quartz crystal resonator." Phys. Rev. E **56**: 680.

Du, Y. and H. K.-F. Yip (2010). "Effects of bone morphogenetic protein 2 on Id expression and neuroblastoma

cell differentiation." Differentiation; research in biological diversity **79 2**: 84-92.

Faye, C., C. Moreau, E. Chautard, R. Jetne, N. Fukai, F. Ruggiero, M. J. Humphries, B. R. Olsen and S. Ricard-Blum (2009). "Molecular interplay between endostatin, integrins, and heparan sulfate." J Biol Chem **284**(33): 22029-22040.

Ferlemann, F. C., V. Menon, A. L. Condurat, J. Rössler and J. Pruszak (2017). "Surface marker profiling of SH-SY5Y cells enables small molecule screens identifying BMP4 as a modulator of neuroblastoma differentiation." Scientific Reports **7**.

Fitzpatrick, V., L. Fourel, O. Destaing, F. Gilde, C. Albiges-Rizo, C. Picart and T. Boudou (2017). "Signal mingle: Micropatterns of BMP-2 and fibronectin on soft biopolymeric films regulate myoblast shape and SMAD signaling." Sci Rep **7**: 41479.

Fourel, L., A. Valat, E. Faurobert, R. Guillot, I. Bourrin-Reynard, K. Ren, L. Lafanechere, E. Planus, C. Picart and C. Albiges-Rizo (2016). "beta3 integrin-mediated spreading induced by matrix-bound BMP-2 controls Smad signaling in a stiffness-independent manner." J Cell Biol **212**(6): 693-706.

Frith, J. E., R. J. Mills and J. J. Cooper-White (2012). "Lateral spacing of adhesion peptides influences human mesenchymal stem cell behaviour." J Cell Sci **125**(Pt 2): 317-327.

Fu, R., S. Selph, M. McDonagh, K. Peterson, A. Tiwari, R. Chou and M. Helfand (2013). "Effectiveness and harms of recombinant human bone morphogenetic protein-2 in spine fusion: a systematic review and meta-analysis." Ann Intern Med **158**(12): 890-902.

Fujiwara H. (2007). Spectroscopic ellipsometry; principles and applications.

Gandhi, N. S. and R. L. Mancera (2012). "Prediction of heparin binding sites in bone morphogenetic proteins (BMPs)." Biochim Biophys Acta **1824**(12): 1374-1381.

Garcia, J. R., A. Y. Clark and A. J. Garcia (2016). "Integrin-specific hydrogels functionalized with VEGF for vascularization and bone regeneration of critical-size bone defects." J Biomed Mater Res A **104**(4): 889-900.

Giacosa, S., C. Pillet, I. Séraudie, L. Guyon, Y. Wallez, C. Roelants, C. Battail, B. Evrard, F. Chalmel, C. Barette, E. Soleilhac, M.-O. Fauvarque, Q. Franquet, C. Sarrazin, N. Peilleron, G. Fiard, J.-A. Long, J.-L. Descotes, C. Cochet and O. Filhol (2021). "Cooperative Blockade of CK2 and ATM Kinases Drives Apoptosis in VHL-Deficient Renal Carcinoma Cells through ROS Overproduction." Cancers **13**(3): 576.

Gribova, V., C. Gauthier-Rouvière, C. Albigès-Rizo, R. Auzely-Velty and C. Picart (2013). "Effect of RGD functionalization and stiffness modulation of polyelectrolyte multilayer films on muscle cell differentiation." Acta Biomater **9**(5): 6468-6480.

Grobe, K., J. Ledin, M. Ringvall, K. Holmborn, E. Forsberg, J. D. Esko and L. Kjellen (2002). "Heparan sulfate and development: differential roles of the N-acetylglucosamine N-deacetylase/N-sulfotransferase isozymes." Biochim Biophys Acta **1573**(3): 209-215.

Hall, C. R., W. G. Cole, R. Haynes and J. T. Hecht (2002). "Reevaluation of a genetic model for the development of exostosis in hereditary multiple exostosis." Am J Med Genet **112**(1): 1-5.

Hammers, D. W., M. Merscham-Banda, J. Y. Hsiao, S. Engst, J. J. Hartman and H. L. Sweeney (2017). "Supraphysiological levels of <scp>GDF</scp> 11 induce striated muscle atrophy." EMBO Molecular Medicine **9**(4): 531-544.

Hiepen, C., D. Yadin, P. Rikeit, G. Dorpholz and P. Knaus (2016). "Actions from head to toe: An update on Bone/Body Morphogenetic Proteins in health and disease." Cytokine Growth Factor Rev **27**: 1-11.

Hintze, V., S. A. Samsonov, M. Anselmi, S. Moeller, J. Becher, M. Schnabelrauch, D. Scharnweber and M. T. Pisabarro (2014). "Sulfated glycosaminoglycans exploit the conformational plasticity of bone morphogenetic protein-2 (BMP-2) and alter the interaction profile with its receptor." Biomacromolecules **15**(8): 3083-3092.

Hogg, N., M. Laschinger, K. Giles and A. McDowall (2003). "T-cell integrins: More than just sticking points." Journal of Cell Science **116**(23): 4695-4705.

Huang, N.-P., J. Vörös, S. M. De Paul, M. Textor and N. D. Spencer (2002). "Biotin-Derivatized Poly(l-lysine)-g-poly(ethylene glycol): A Novel Polymeric Interface for Bioaffinity Sensing." Langmuir **18**(1): 220-230.

Huegel, J., M. Enomoto-Iwamoto, F. Sgariglia, E. Koyama and M. Pacifici (2015). "Heparanase stimulates chondrogenesis and is up-regulated in human ectopic cartilage: a mechanism possibly involved in hereditary multiple exostoses." Am J Pathol **185**(6): 1676-1685.

Inubushi, T., I. Lemire, F. Irie and Y. Yamaguchi (2018). "Palovarotene Inhibits Osteochondroma Formation in a Mouse Model of Multiple Hereditary Exostoses." J Bone Miner Res **33**(4): 658-666.

Iozzo, R. V. and L. Schaefer (2015). "Proteoglycan form and function: A comprehensive nomenclature of proteoglycans." Matrix Biol **42**: 11-55.

Ivaska, J. and J. Heino (2011). "Cooperation between integrins and growth factor receptors in signaling and endocytosis." Annu Rev Cell Dev Biol **27**: 291-320.

Jurchenko, C., Y. Chang, Y. Narui, Y. Zhang and K. S. Salaita (2014). "Integrin-generated forces lead to streptavidin-biotin unbinding in cellular adhesions." Biophys J **106**(7): 1436-1446.

Kamat, V. and A. Rafique (2017). "Designing binding kinetic assay on the bio-layer interferometry (BLI) biosensor to characterize antibody-antigen interactions." Anal Biochem **536**: 16-31.

Katagiri, T., S. Akiyama, M. Namiki, M. Komaki, A. Yamaguchi, V. Rosen, J. M. Wozney, A. Fujisawa-Sehara and T. Suda (1997). "Bone morphogenetic protein-2 inhibits terminal differentiation of myogenic cells by suppressing the transcriptional activity of MyoD and myogenin." Exp Cell Res **230**(2): 342-351.

Kim, H. D. and R. F. Valentini (2002). "Retention and activity of BMP-2 in hyaluronic acid-based scaffolds in vitro." J Biomed Mater Res **59**(3): 573-584.

Kim, M. K., K. Paek, S. M. Woo and J. A. Kim (2023). "Bone-on-a-Chip: Biomimetic Models Based on Microfluidic Technologies for Biomedical Applications." ACS Biomater Sci Eng **9**(6): 3058-3073.

Kisiel, M., A. S. Klar, M. Ventura, J. Buijs, M. K. Mafina, S. M. Cool and J. Hilborn (2013). "Complexation and sequestration of BMP-2 from an ECM mimetic hyaluronan gel for improved bone formation." PLoS One **8**(10): e78551.

Knelson, E. H., A. L. Gaviglio, J. C. Nee, M. D. Starr, A. B. Nixon, S. G. Marcus and G. C. Blobe (2014). "Stromal heparan sulfate differentiates neuroblasts to suppress neuroblastoma growth." J Clin Invest **124**(7): 3016-3031.

Knelson, E. H., J. C. Nee and G. C. Blobe (2014). "Heparan sulfate signaling in cancer." Trends Biochem Sci **39**(6): 277-288.

Knight, E. and S. Przyborski (2015). "Advances in 3D cell culture technologies enabling tissue-like structures to be created in vitro." J Anat **227**(6): 746-756.

Koziel, L., M. Kunath, O. G. Kelly and A. Vortkamp (2004). "Ext1-dependent heparan sulfate regulates the range of Ihh signaling during endochondral ossification." Dev Cell **6**(6): 801-813.

Krishnamoorthy, M., S. Hakobyan, M. Ramstedt and J. E. Gautrot (2014). "Surface-initiated polymer brushes in the biomedical field: applications in membrane science, biosensing, cell culture, regenerative medicine and antibacterial coatings." Chem Rev **114**(21): 10976-11026.

Kuhnle, J. (2007). "Lipid assemblies on nanostructured surfaces."

Labat, B., N. Buchbinder, S. Morin-Grognet, G. Ladam, H. Atmani and J. P. Vannier (2021). "Biomimetic matrix for the study of neuroblastoma cells: A promising combination of stiffness and retinoic acid." Acta Biomater **135**: 383-392.

Laguri, C., R. Sadir, P. Rueda, F. Baleux, P. Gans, F. Arenzana-Seisdedos and H. Lortat-Jacob (2007). "The novel CXCL12gamma isoform encodes an unstructured cationic domain which regulates bioactivity and interaction with both glycosaminoglycans and CXCR4." PLoS One **2**(10): e1110.

Lam, W. A., L. Cao, V. Umesh, A. J. Keung, S. Sen and S. Kumar (2010). "Extracellular matrix rigidity modulates neuroblastoma cell differentiation and N-myc expression." Mol Cancer **9**: 35.

Le Pennec, J., C. Picart, R. R. Vivès and E. Migliorini (2023). "Sweet but challenging: tackling the complexity of GAGs with engineered tailor-made biomaterials." Advanced Materials.

Legeai-Mallet, L., A. Rossi, C. Benoist-Lasselin, R. Piazza, J. F. Mallet, A. L. Delezoide, A. Munnich, J. Bonaventure and L. Zylberberg (2000). "EXT 1 gene mutation induces chondrocyte cytoskeletal abnormalities and defective collagen expression in the exostoses." J Bone Miner Res **15**(8): 1489-1500.

Lidholt, K., J. L. Weinke, C. S. Kiser, F. N. Lugemwa, K. J. Bame, S. Cheifetz, J. Massagué, U. Lindahl and J. D. Esko (1992). "A single mutation affects both N-acetylglucosaminyltransferase and glucuronosyltransferase activities in a Chinese hamster ovary cell mutant defective in heparan sulfate biosynthesis." Proc Natl Acad Sci U S A **89**(6): 2267-2271.

Lin, X., G. Wei, Z. Shi, L. Dryer, J. D. Esko, D. E. Wells and M. M. Matzuk (2000). "Disruption of gastrulation and heparan sulfate biosynthesis in EXT1-deficient mice." Dev Biol **224**(2): 299-311.

Machillot, P., C. Quintal, F. Dalonneau, L. Hermant, P. Monnot, K. Matthews, V. Fitzpatrick, J. Liu, I. Pignot-Paintrand and C. Picart (2018). "Automated Buildup of Biomimetic Films in Cell Culture Microplates for High-Throughput Screening of Cellular Behaviors." Adv Mater **30**(27): e1801097.

Matsumoto, Y., K. Matsumoto, F. Irie, J. Fukushi, W. B. Stallcup and Y. Yamaguchi (2010). "Conditional ablation of the heparan sulfate-synthesizing enzyme Ext1 leads to dysregulation of bone morphogenic protein signaling and severe skeletal defects." J Biol Chem **285**(25): 19227-19234.

Matyjaszewski, K., H. Dong, W. Jakubowski, J. Pietrasik and A. Kusumo (2007). "Grafting from surfaces for "everyone": ARGET ATRP in the presence of air." Langmuir **23**(8): 4528-4531.

McKee, T. J., G. Perlman, M. Morris and S. V. Komarova (2019). "Extracellular matrix composition of connective tissues: a systematic review and meta-analysis." Sci Rep **9**(1): 10542.

Migliorini, E., J. Ban, G. Grenci, L. Andolfi, A. Pozzato, M. Tormen, V. Torre and M. Lazzarino (2013). "Nanomechanics controls neuronal precursors adhesion and differentiation." Biotechnol Bioeng **110**(8): 2301-2310.

Migliorini, E., G. Grenci, J. Ban, A. Pozzato, M. Tormen, M. Lazzarino, V. Torre and M. E. Ruaro (2011). "Acceleration of neuronal precursors differentiation induced by substrate nanotopography." Biotechnol Bioeng **108**(11): 2736-2746.

Migliorini, E., A. Guevara-Garcia, C. Albiges-Rizo and C. Picart (2020). "Learning from BMPs and their biophysical extracellular matrix microenvironment for biomaterial design." Bone **141**: 115540.

Migliorini, E., P. Horn, T. Haraszti, S. Wegner, C. Hiepen, P. Knaus, P. Richter and E. Cavalcanti-Adam (2017). "Enhanced biological activity of BMP-2 bound to surface-grafted heparan sulfate." Advanced Biosystems **1**(4): 1600041.

Migliorini, E., D. Thakar, J. Kuhnle, R. Sadir, D. P. Dyer, Y. Li, C. Sun, B. F. Volkman, T. M. Handel, L. Coche-Guerente, D. G. Fernig, H. Lortat-Jacob and R. P. Richter (2015). "Cytokines and growth factors cross-link heparan sulfate." Open Biol **5**(8).

Migliorini, E., D. Thakar, R. Sadir, T. Pleiner, F. Baleux, H. Lortat-Jacob, L. Coche-Guerente and R. P. Richter (2014). "Well-defined biomimetic surfaces to characterize glycosaminoglycan-mediated interactions on the molecular, supramolecular and cellular levels." Biomaterials **35**(32): 8903-8915.

Migliorini, E., A. Valat, C. Picart and E. A. Cavalcanti-Adam (2016). "Tuning cellular responses to BMP-2 with material surfaces." Cytokine Growth Factor Rev **27**: 43-54.

Migliorini, E., M. Weidenhaupt and C. Picart (2018). "Practical guide to characterize biomolecule adsorption on solid surfaces (Review)." Biointerphases **13**(6): 06d303.

Monteiro, A. I., T. Kollmetz and J. Malmstrom (2018). "Engineered systems to study the synergistic signaling between integrin-mediated mechanotransduction and growth factors (Review)." Biointerphases **13**(6): 06d302.

Mundhara, N., S. Yadav, P. U. Shirke, D. Panda and A. Majumder (2021). "Substrate loss modulus promotes the differentiation of SHSY-5Y neuroblastoma cells." Materialia **15**: 100968.

Murali, S., B. Rai, C. Dombrowski, J. L. Lee, Z. X. Lim, D. S. Bramono, L. Ling, T. Bell, S. Hinkley, S. S. Nathan, J. H. Hui, H. K. Wong, V. Nurcombe and S. M. Cool (2013). "Affinity-selected heparan sulfate for bone repair." Biomaterials **34**(22): 5594-5605.

Perez, V. A., Z. Ali, T. P. Alastalo, F. Ikeno, H. Sawada, Y. J. Lai, T. Kleisli, E. Spiekerkoetter, X. Qu, L. H. Rubinos, E. Ashley, M. Amieva, S. Dedhar and M. Rabinovitch (2011). "BMP promotes motility and represses growth of smooth muscle cells by activation of tandem Wnt pathways." J Cell Biol **192**(1): 171-188.

Petersen, N. O., P. L. Höddelius, P. W. Wiseman, O. Seger and K. E. Magnusson (1993). "Quantitation of membrane receptor distributions by image correlation spectroscopy: concept and application." Biophysical Journal **65**(3): 1135-1146.

Pfaff, M., K. Tangemann, B. Muller, M. Gurrath, G. Muller, H. Kessler, R. Timpl and J. Engel (1994). "Selective recognition of cyclic RGD peptides of NMR defined conformation by alpha IIb beta 3, alpha V beta 3, and alpha 5 beta 1 integrins." J Biol Chem **269**(32): 20233-20238.

Rathod, M. L., J. Ahn, B. Saha, P. Purwar, Y. Lee, N. L. Jeon and J. Lee (2018). "PDMS Sylgard 527-Based Freely

Suspended Ultrathin Membranes Exhibiting Mechanistic Characteristics of Vascular Basement Membranes." ACS Appl Mater Interfaces **10**(47): 40388-40400.

Reijnders, C. M., C. J. Waaijer, A. Hamilton, E. P. Buddingh, S. P. Dijkstra, J. Ham, E. Bakker, K. Szuhai, M. Karperien, P. C. Hogendoorn, S. E. Stringer and J. V. Bovee (2010). "No haploinsufficiency but loss of heterozygosity for EXT in multiple osteochondromas." Am J Pathol **177**(4): 1946-1957.

Rengaraj, A., L. Bosc, P. Machillot, C. McGuckin, C. Milet, N. Forraz, P. Paliard, D. Barbier and C. Picart (2022). "Engineering of a Microscale Niche for Pancreatic Tumor Cells Using Bioactive Film Coatings Combined with 3D-Architectured Scaffolds." ACS Appl Mater Interfaces **14**(11): 13107-13121.

Reviakine, I., D. Johannsmann and R. P. Richter (2011). "Hearing what you cannot see and visualizing what you hear: interpreting quartz crystal microbalance data from solvated interfaces." Anal Chem **83**(23): 8838-8848.

Roelants, C., C. Pillet, Q. Franquet, C. Sarrazin, N. Peilleron, S. Giacosa, L. Guyon, A. Fontanell, G. Fiard, J. A. Long, J. L. Descotes, C. Cochet and O. Filhol (2020). "Ex-Vivo Treatment of Tumor Tissue Slices as a Predictive Preclinical Method to Evaluate Targeted Therapies for Patients with Renal Carcinoma." Cancers (Basel) **12**(1).

Ruppert, R., E. Hoffmann and W. Sebald (1996). "Human bone morphogenetic protein 2 contains a heparin-binding site which modifies its biological activity." Eur J Biochem **237**(1): 295-302.

Ryoo, H. M., M. H. Lee and Y. J. Kim (2006). "Critical molecular switches involved in BMP-2-induced osteogenic differentiation of mesenchymal cells." Gene **366**(1): 51-57.

Sales, A., V. Khodr, P. Machillot, L. Chaar, L. Fourel, A. Guevara-Garcia, E. Migliorini, C. Albigès-Rizo and C. Picart (2022). "Differential bioactivity of four BMP-family members as function of biomaterial stiffness." Biomaterials: 121363.

Sales, A., V. Khodr, P. Machillot, L. Fourel, A. Guevara-Garcia, E. Migliorini, C. Albigès-Rizo and C. Picart (2021). "Differential bioactivity of four BMP-family members as function of biomaterial stiffness." bioRxiv: 2021.2002.2010.430282.

Sawala, A., M. Scarcia, C. Sutcliffe, S. G. Wilcockson and H. L. Ashe (2015). "Peak BMP responses in the drosophila embryo are dependent on the activation of integrin signaling." Cell Rep **12**(10): 1584-1593.

Scheufler, C., W. Sebald and M. Hulsmeyer (1999). "Crystal structure of human bone morphogenetic protein-2 at 2.7 A resolution." J Mol Biol **287**(1): 103-115.

Sefkow-Werner, J., J. Le Pennec, P. Machillot, B. Ndayishimiye, E. Castro-Ramirez, J. Lopes, C. Licitra, I. Wang, A. Delon, C. Picart and E. Migliorini (2022). "Automated Fabrication of Streptavidin-Based Self-assembled Materials for High-Content Analysis of Cellular Response to Growth Factors." ACS Applied Materials & Interfaces.

Sefkow-Werner, J., P. Machillot, A. Sales, E. Castro-Ramirez, M. Degardin, D. Boturyn, E.-A. Cavalcanti-Adam, C. Albiges-Rizo, C. Picart and E. Migliorini (2020). "Heparan sulfate co-immobilized with cRGD ligands and BMP2 on biomimetic platforms promotes BMP2-mediated osteogenic differentiation." Acta Biomaterialia.

Sefkow-Werner, J., P. Machillot, A. Sales, E. Castro-Ramirez, M. Degardin, D. Boturyn, E. A. Cavalcanti-Adam, C. Albiges-Rizo, C. Picart and E. Migliorini (2020). "Heparan sulfate co-immobilized with cRGD ligands and BMP2 on biomimetic platforms promotes BMP2-mediated osteogenic differentiation." Acta biomaterialia **114**: 90-103.

Sefkow-Werner, J., E. Migliorini, C. Picart, D. Wahyuni, I. Wang and A. Delon (2021). "Combining fluorescence fluctuations and photobleaching to quantify surface density." arXiv(physics.bio-ph).

Sefkow-Werner, J., E. Migliorini, C. Picart, D. Wahyuni, I. Wang and A. Delon (2022). "Combining Fluorescence Fluctuations and Photobleaching to Quantify Surface Density." Analytical Chemistry.

Sefkow-Werner J., Le Pennec J., Machillot P., Ndayishimiye B., Castro-Ramirez E., Lopes J., Licitra C., Wang I., Delon A., Picart C. and M. E. (2022). "Automated fabrication of biomimetic streptavidin platforms for high quantity analysis of cellular response to growth factors." ACS Applied materials and Interfaces **submitted**.

Sieber, C., J. Kopf, C. Hiepen and P. Knaus (2009). "Recent advances in BMP receptor signaling." Cytokine Growth Factor Rev **20**(5-6): 343-355.

Simone, S., C. Cosola, A. Loverre, M. Cariello, F. Sallustio, F. Rascio, L. Gesualdo, F. P. Schena, G. Grandaliano and G. Pertosa (2012). "BMP-2 induces a profibrotic phenotype in adult renal progenitor cells through Nox4 activation." Am J Physiol Renal Physiol **303**(1): F23-34.

Smith, R. A. A., S. Murali, B. Rai, X. Lu, Z. X. H. Lim, J. J. L. Lee, V. Nurcombe and S. M. Cool (2018). "Minimum structural requirements for BMP-2-binding of heparin oligosaccharides." Biomaterials **184**: 41-55.

Su, Z., S. Kishida, S. Tsubota, K. Sakamoto, D. Cao, S. Kiyonari, M. Ohira, T. Kamijo, A. Narita, Y. Xu, Y. Takahashi and K. Kadomatsu (2017). "Neurocan, an extracellular chondroitin sulfate proteoglycan, stimulates neuroblastoma cells to promote malignant phenotypes." Oncotarget **8**(63): 106296-106310.

Superti-Furga, A. and S. Unger (1993). CHST3-Related Skeletal Dysplasia. GeneReviews(®). M. P. Adam, G. M. Mirzaa, R. A. Pagon et al. Seattle (WA), University of Washington, Seattle

Szemes, M., Z. Melegh, J. Bellamy, A. Greenhough, M. Kollareddy, D. R. Catchpoole and K. T. A. Malik (2020). "A Wnt-BMP4 Signaling Axis Induces MSX and NOTCH Proteins and Promotes Growth Suppression and Differentiation in Neuroblastoma." Cells **9**.

Tang, Y., X. Zeng and J. Liang (2010). "Surface Plasmon Resonance: An Introduction to a Surface Spectroscopy Technique." Journal of Chemical Education **87**(7): 742-746.

Thakar, D., F. Dalonneau, E. Migliorini, H. Lortat-Jacob, D. Boturyn, C. Albiges-Rizo, L. Coche-Guerente, C. Picart and R. P. Richter (2017). "Binding of the chemokine CXCL12alpha to its natural extracellular matrix ligand heparan sulfate enables myoblast adhesion and facilitates cell motility." Biomaterials **123**: 24-38.

Thakar, D., E. Migliorini, L. Coche-Guerente, R. Sadir, H. Lortat-Jacob, D. Boturyn, O. Renaudet, P. Labbe and R. P. Richter (2014). "A quartz crystal microbalance method to study the terminal functionalization of glycosaminoglycans." Chem Commun (Camb) **50**(96): 15148-15151.

Tierney, C. M., M. J. Jaasma and F. J. O'Brien (2009). "Osteoblast activity on collagen-GAG scaffolds is affected by collagen and GAG concentrations." J Biomed Mater Res A **91**(1): 92-101.

Urist, M. R. (1965). "Bone: formation by autoinduction." Science **150**(3698): 893-899.

Urist, M. R. and B. S. Strates (1971). "Bone morphogenetic protein." J Dent Res **50**(6): 1392-1406.

van der Meulen, S. A., G. V. Dubacheva, M. Dogterom, R. P. Richter and M. E. Leunissen (2014). "Quartz crystal microbalance with dissipation monitoring and spectroscopic ellipsometry measurements of the phospholipid bilayer anchoring stability and kinetics of hydrophobically modified DNA oligonucleotides." Langmuir **30**(22): 6525-6533.

Wang, E. A., V. Rosen, P. Cordes, R. M. Hewick, M. J. Kriz, D. P. Luxenberg, B. S. Sibley and J. M. Wozney (1988). "Purification and characterization of other distinct bone-inducing factors." Proc Natl Acad Sci U S A **85**(24): 9484-9488.

Wang, T. and F. Yang (2017). "A comparative study of chondroitin sulfate and heparan sulfate for directing three-dimensional chondrogenesis of mesenchymal stem cells." Stem Cell Res Ther **8**(1): 284.

Wuyts, W., W. Van Hul, K. De Boulle, J. Hendrickx, E. Bakker, F. Vanhoenacker, F. Mollica, H. J. Ludecke, B. S. Sayli, U. E. Pazzaglia, G. Mortier, B. Hamel, E. U. Conrad, M. Matsushita, W. H. Raskind and P. J. Willems (1998). "Mutations in the EXT1 and EXT2 genes in hereditary multiple exostoses." Am J Hum Genet **62**(2): 346-354.

Yuste, I., F. C. Luciano, E. González-Burgos, A. Lalatsa and D. R. Serrano (2021). "Mimicking bone microenvironment: 2D and 3D in vitro models of human osteoblasts." Pharmacol Res **169**: 105626.

Zhang, C., Y. Tan, J. Feng, C. Huang, B. Liu, Z. Fan, B. Xu and T. Lu (2020). "Exploration of the Effects of Substrate Stiffness on Biological Responses of Neural Cells and Their Mechanisms." ACS Omega **5**(48): 31115-31125.

Zhang, X., F. Wang and J. Sheng (2016). ""Coding" and "Decoding": hypothesis for the regulatory mechanism involved in heparan sulfate biosynthesis." Carbohydr Res **428**: 1-7.

Zhen, G., V. Eggli, J. Vörös, P. Zammaretti, M. Textor, R. Glockshuber and E. Kuennemann (2004). "Immobilization of the Enzyme β-Lactamase on Biotin-Derivatized Poly(<scp>l</scp> -lysine)- g -poly(ethylene glycol)-Coated Sensor Chips: A Study on Oriented Attachment and Surface Activity by Enzyme Kinetics and in Situ Optical Sensing." Langmuir **20**(24): 10464-10473.

Ziarek, J. J., C. T. Veldkamp, F. Zhang, N. J. Murray, G. A. Kartz, X. Liang, J. Su, J. E. Baker, R. J. Linhardt and B. F. Volkman (2013). "Heparin oligosaccharides inhibit chemokine (CXC motif) ligand 12 (CXCL12)

cardioprotection by binding orthogonal to the dimerization interface, promoting oligomerization, and competing with the chemokine (CXC motif) receptor 4 (CXCR4) N terminus." J Biol Chem **288**(1): 737-746.

Zimmerman, L. B., J. M. De Jesús-Escobar and R. M. Harland (1996). "The Spemann organizer signal noggin binds and inactivates bone morphogenetic protein 4." Cell **86**(4): 599-606.

ANNEX I: CHARACTERIZATION TECHNIQUES

Quartz crystal microbalance with dissipation monitoring (QCM-D) technique measures the frequency and the dissipation shifts of a quartz crystal which vibrates at its resonance frequency (Dixon 2008, Reviakine, Johannsmann et al. 2011, Migliorini, Weidenhaupt et al. 2018). The frequency shift measured is linked to the mass of the film adsorbed on the platforms (molecules + solvent) following the Sauerbrey equation

$$\Delta m = -\mathrm{C}\frac{\boldsymbol{n}}{\Delta f}$$

where C is the mass sensitivity constant (17.7 ng.cm-2Hz-1 at 5 MHz) and n is the overtone number. The damping factor (D), called dissipation, is related to the ratio between the energy dissipated during the period of oscillation ($E_{dissipated}$) and the energy stored in the system (E_{stored}).

$$D = \frac{E_{dissipated}}{2\pi E_{stored}}$$

This technique measures the adsorption of each components in real time without the need of any labelling on an adequate support (quartz crystals). Four measurements in parallel are possible in the QCM-D machine – that permits to have internal controls and different conditions to test in parallel. The drawback of the technique is the upper estimation of the mass adsorbed to the quartz since it is not possible to uncouple the mass of the molecule to the mass of the solvent within the film.

Fluorescence recovery after photobleaching (FRAP)

This technique has been used to measure the mobile fraction and the diffusion constant of a fluorescent streptavidin (SAv-Atto565) bound to mobile SLB and carrying HS chains. We hypothesized that if chemokines cross-link the HS chains the lateral mobility of the SAv-Atto565 would been affected. FRAP measurements were performed with a confocal laser scanning microscope (LSM 700, Zeiss, Germany) with a plan-apochromat 63x/1.4 oil immersion objective and a fully opened pinhole (1 mm diameter). We first bleached a central zone of the image with a radius of 10 mm through exposure for approximately 20 s to high laser intensity. The fluorescence recovery, due to lateral diffusion of bleached and unbleached SAv-Atto565 was monitored through acquisition of post-bleach images over a period of typically 10 min. The images acquired were then analyzed by a custom-made algorithm (Kuhnle 2007) implemented in Matlab (MathWorks, MA, USA). This model has two independent fitting parameters, namely the size and diffusion constant of the mobile fraction. These were computed through global minimization of the root-mean-square differences between numerical predictions and all post-bleach profiles.

Spectroscopic ellipsometry (SE) technique was used to obtain the information on the dried mass. SE measures the changes of the reflected light that passes through the sample and hits a detector, in p(Kuhnle 2007)articular of the ellipsometric angles Ψ and Δ. These parameters measure the amplitude and the phase shifts of the parallel

and perpendicular components of the polarized light to the plain of incidence (Fujiwara H. 2007, Migliorini, Weidenhaupt et al. 2018). The film thickness (d_f) and the refractive index (n) of the film are extracting after robust modeling of the angles Ψ and Δ obtained at different wavelengths. Thanks to the Feijter's equation (1) the surface mass density (here also called surface density = Γ) can be calculated:

$$\Gamma = \frac{d_f(n - n_0)}{dn/dc}$$

Where n_0 is the refractive index of the ambient and d_n/d_c the refractive index increment of the molecules in the film.

Finally, SPR measures variations of the refractive index in close proximity (up to ~300 nm) of a sensing surface.
The increase in mass associated with a binding event causes a proportional increase in the refractive index, which is observed as a change in response unit (RU) as well described in (Tang, Zeng et al. 2010). SPR is generally used to measure the association binding affinities between two molecules.

Biolayer Interferometry technique (BLI) is an emerging technique, first described by ForteBio in 2005, which uses interferometry with white light to characterize molecule–molecule interactions. It relies on the reflective property of white light passing through glass fibers and directed towards two interfaces: (i) between the glass fiber and the functionalized surface (ii) between the functionalized surfaces and the solution. The reflected light from these two interfaces generates constructive or destructive interferences that are recorded by a spectrometer. When a molecule in the solution binds to the end of the biosensor, this generates a shift to the interferometer profile. BLI correlates the spectral shifts with the change in thickness (nm) of the add-layers (Do, Ho et al. 2008) and permits to measure kinetic constants (k_a, k_d, K_D) with high precision and reproducibility when biosensors are carefully regenerated to prevent analyte rebinding to the sensor. Comparable results on peptide-antibodies and protein-protein binding kinetics with SPR (Biacore) have been reported (Abdiche, Malashock et al. 2008, Kamat and Rafique 2017). An advantage with respect to SPR is the possibility to reach **high throughput screening of more molecules at the same time since BLI offers a unique high throughput platform** without the limitation of microfluidics and with the possibility to **recover samples and reuse them for another assay**. The main drawback of this technique is a lower sensitivity compared to SPR; indeed, the binding of peptides to the sensors is beyond the sensitivity of the technique (Abdiche, Malashock et al. 2008);